An Implantable Intracranial Volume System For Hydrocephalus Therapy

BY

SUKHRAAJ S. BASATI
B.S., University of Illinois at Chicago, 2005

THESIS

Submitted as partial fulfillment of the requirements
for the degree of Doctor of Philosophy in Bioengineering
in the Graduate College of the
University of Illinois at Chicago, 2011

Chicago, Illinois

Defense Committee:

Andreas Linninger, Chair and Advisor

John Hetling

Terry Layton

Ali Alaraj, Neurological Surgery

Marc Del Bigio, University of Manitoba

PREFACE

The past few decades have seen an acceleration of implantable sensors and systems to improve disease monitoring and treatment. Unfortunately in hydrocephalus, a disease where cerebrospinal fluid (CSF) accumulates within the ventricular system of the brain, optimal diagnostic and treatment options remain limited.

My interest in hydrocephalus originates as a patient of the disease. Growth of a pilocytic astrocytoma within the fourth ventricle resulted in obstructive hydrocephalus 10 years ago. I was, and still am unhappy with the method of monitoring CSF accumulation. The therapy consists of a catheter implanted into the CSF-filled region to drain excess fluid. In 1952 a passive pressure-regulated valve system was invented that drains fluid when intracranial pressure exceeded a set value. Surprisingly this technology is still implemented in patients worldwide even though it has limitations.

This thesis proposes and validates a method to improve diagnostic options available. The method involves applying an electric field and measuring voltage potentials at different spatial locations. Changes in fluid volume result in altered distributions of the electric field. The outcome of this thesis is a device for monitoring CSF accumulation as well as the design for an implantable system.

I am grateful to my advisor Prof. Linninger who has guided me over the years, and also my committee members whom I have consulted with on various aspects of the project. The work presented in this thesis would not be possible without their support. Members from the laboratory of product and process design (LPPD) are acknowledged for their assistance. Work performed from Timothy Harris and Bhargav Desai as a result of an NSF sponsored Research Experience for Undergraduates program is greatly appreciated. Their work contributed in peer-reviewed publications.

SUMMARY

The volume measurement principle is based on the high electrical conductivity ratio between brain tissue and CSF. Changes in the fluid volume correlate to changes in the distribution of an induced, local electric field. This concept, also known as the impedance technique, is first tested *in-silico* on reconstructed brain geometry for finite element analysis. Simulations are performed to obtain design decisions such as catheter diameter and electrode placement. Once the design decisions were chosen, the sensor was fabricated in a scalable procedure.

The sensors are designed with an internal catheter as a pathway for volume control. In a scaled down rat-size sensor, a dicing saw is used to create 75 μm holes in a 500 μm outer diameter polyimide tube. Platinum/iridium wires are passed through and connected to the outer cylinders. The instrumentation is designed using commercially available integrated circuits. Two systems are presented: A short-term system for continuous monitoring, and a long-term battery-operated wireless circuit with microcontroller implementation. The sensor and electronics are characterized in bench-top models prior to animal experimentation. Two novel models construed of agarose and silicone gel emulate various properties of brain tissue. Calibration experiments are performed to provide voltage-volume relationships.

An acute animal model of hydrocephalus to validate the volume measurement principle is demonstrated. Hydrocephalus was induced in 3 week rats by kaolin injection. 28 days post-induction the sensor was implanted into the lateral ventricles and a CSF shunting/infusion protocol was completed. While future research of long-term volume monitoring is necessary, these results indicate that volume monitoring is feasible for clinical cases of hydrocephalus.

TABLE OF CONTENTS

CHAPTER **PAGE**

LIST OF TABLES

TABLE PAGE

LIST OF FIGURES

FIGURE PAGE

I. INTRODUCTION

Summary

Efficient design of implantable medical diagnostics is rapidly becoming an area of research and development due to the aging population, cost of healthcare, and unanswered scientific questions. Diagnosis of hydrocephalus remains a costly and intensive procedure for thousands of patients each year. Hydrocephalus is the result of cerebrospinal fluid accumulation within the brain ventricles. Each year catheter systems are implanted in patients with this disease, which can be for acute drainage of fluid or a chronic implanted shunt. The therapy is based on a pressure differential in order to drive fluid flow out of the system. Elevated intracranial pressure (ICP) is used as a diagnostic for the disease. There is much room for improvement as evidenced by the high failure rates and high number of surgical revisions. There are many causes of shunt failure such as obstruction, over/under-drainage, and mechanical failure. This thesis presents a diagnostic system for patients suffering from cerebrospinal fluid accumulation using the impedance technique for volume monitoring. The translational aspect of this work is that electrodes and electronics can be added to existing shunt systems. The outcome of this work may also lead to improved therapy for patients suffering from this disease.

A. Motivation

Hydrocephalus is a central nervous system disease in which cerebrospinal fluid (CSF) accumulates within the intracranial ventricular system. In the United States, slightly more than 1 in 1,000 births is affected by hydrocephalus. It is one of the most common birth defects and afflicts more than 10,000 babies each year in the U.S [1]. The only clinically approved treatment consists of fluid diversion, and most patients are treated with either a pressure regulated shunt or endoscopic third ventriculostomy (ETV). Regulated shunting systems consist of one way valves based on pressure, while ETV is a

surgical procedure to create alternate fluid pathways. Methods to treat this disease are discussed later. With the advent of CSF shunting procedures, there has been a decline in neurological deficit and death. However, shunt failure is common. Following initial shunt insertion, the failure rate by 1 year post-implantation is 25 to 40% [2]. The primary reason for shunt failure is obstruction, followed by over-drainage/under-drainage. Because intracranial pressure depends on body position, shunts often over drain leading to slit-ventricle syndrome. 6-12 % of shunted children develop slit ventricle syndrome. These statistics indicate a need for improved monitoring and treatment design.

A.1. Cerebrospinal fluid flow

The design of improved treatment for this disease requires a basic understanding of CSF flow pathways. Historical research into CSF dynamics resulted in the bulk flow theory, where the production of CSF in the choroid plexus region of the ventricles was measured. Reabsorption was observed through the subarachnoid space [3]. CSF experimental data was acquired by injecting dye into the ventricular systems of animals and determining fluid pathways histologically [4]. Radiotracers injected into the arterial supply led to the measurement of human CSF production rate of 0.3 mL/min and absorption rates [5]. Imaging techniques allowed for real-time measurements of fluid flow which indicated that complex geometry of the ventricular system permits high fluid velocities in regions with smaller diameter, such as the aqueduct of Sylvius. While the bulk flow theory has resulted in improved treatment for the majority of patients, many clinical cases are not treatable. For example, older patients may develop normal pressure hydrocephalus (NPH) where CSF accumulates yet the intracranial pressure (ICP) remains low. Researchers now postulate that CSF absorption also occurs throughout the brain capillary network [6-7], which may allow for intracranial pressure to reduce.

Our group has developed extensive mathematical models to describe the phenomena between blood, CSF, and brain tissue [8-10]. These models incorporate patient-specific geometry to account for and predict complex fluid flow patterns seen by CINE-MRI. Figure 1 highlights the CSF flow pathway implemented in these models.

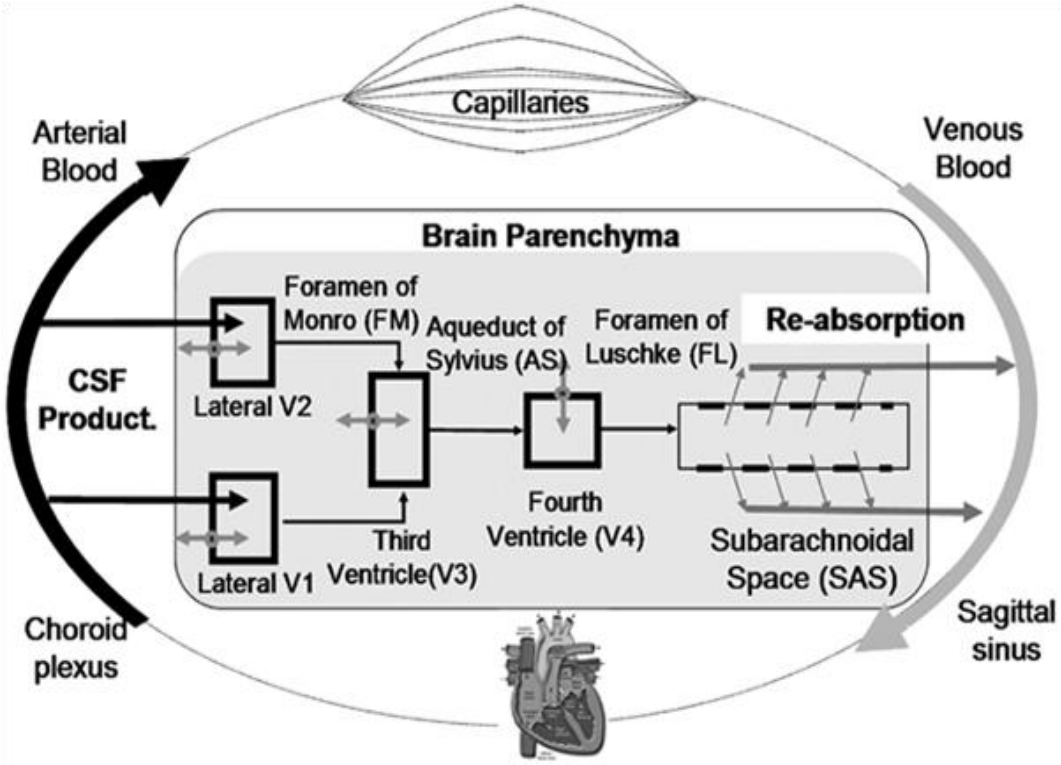

Figure 1. CSF flow pathway throughout intracranial system.

Hydrocephalus is often characterized as communicating or non-communicating where the latter indicates an obstruction in the fluid pathway. Non-communicating hydrocephalus is a result of a tumor, for example, that blocks the flow of CSF. Treatment in this case involves surgical removal of the tumor, which allows fluid to drain. Communicating hydrocephalus, or chronic disease state, has been difficult

to understand and treat. A simple explanation for fluid accumulation is impeded CSF absorption through the arachnoid granulations [11]. Fluid accumulation in a single region of a communicating network implies that a pressure gradient exists. However, our group was the first to show that the pressure gradient between the subarachnoid space and the ventricles is low in a communicating hydrocephalus experimental dog model [12]. A recent observation during hydrocephalus progression in older patients is a decrease in brain tissue compliance coupled with *continuous pulsatile deformation*, which results in fluid accumulation over long periods of time [13-14].

Recently there have been efforts to understand the production and absorption of CSF at a cellular level. Aquaporin channels are responsible for the transport of water across cellular membranes. It has been found that aquaporin-4 (AQP4) receptors are responsible for the intracranial active transport of water, which may play a role in hydrocephalus [15-17]. AQP4 density is largest at the parenchyma and major fluid compartment boundaries. Experimental models with AQP4 null mice showed a high correlation of edema. While it is assumed that the pattern of aquaporin expression is similar to humans, more research needs to be completed in order to translate to clinical research.

A.2. Treatment of Hydrocephalus

In the early 20th century, neurosurgeons started to create alternate fluid pathways - a procedure known as third ventriculostomy for CSF to drain in non-communicating hydrocephalic patients. This procedure is still used today for treatment. A slit is made in the membrane of the third ventricle allowing fluid to drain into the subarachnoid space or fourth ventricle. The treatment is effective for patients where the removal of the obstruction is not possible or where the flow pathway is nonexistent; for example, patients with aqueductal stenosis or tumors. An endoscope is used during surgery for visualization.

In 1949 a pressure-regulated valve system was invented by Frank Nelson as a treatment [18]. This first generation design was integrated into the shunt catheter and allowed for CSF to drain when pressure was above a specified level. Four decades later, the second generation of shunting systems emerged consisting of magnetically-adjustable pressure settings [19]. These systems allowed for clinicians to adjust pressure settings non-invasively using external magnetic fields. Since then second generation valve systems have included anti-siphon or gravitational valves.

Investigators have proposed several methods to assess the functionality of the shunt such as microfabricated intracranial pressure sensors [20-21], (Codman ICP Microsensor, Codman MA). Engineers have also developed external flow monitors to gauge to fluid flow through the shunt (ShuntCheck, NeuroDx Development PA). Improper flow is an indication of possible obstruction. The National Institutes of Health (NIH) has funded research to develop biofilm dispersion catheters to reduce infection (Agile Sciences, NC). The majority of these systems are still under development in animal models of hydrocephalus. While an anti-bacterial impregnated catheter is commercially available (Codman Bactiseal, Codman MA), it does not reduce shunt infection [22]. However it has been shown to reduce infection for external ventricular drainage systems [23-24].

A.3. Limitations of existing treatment

Methods for treating hydrocephalus have not changed significantly over the last 50 years. Most patients are treated with either a pressure shunt or endoscopic third ventriculostomy. Unfortunately, many shunt revisions are necessary over the course of a patient's life [1]. In a randomized evaluation of treatment efficacy, shunt obstruction was shown to be the main necessity for shunt revision, accounting for 31% of total surgeries. Over-drainage was 5% of surgical cases [25]. Pressure regulated shunt treatment is also completely ineffective for patients with normal pressure hydrocephalus (NPH) [26].

In older patients normal pressure hydrocephalus (NPH) may develop [27].While data on NPH is limited, admissions of clinically diagnosed NPH patients range from 0 - 5%. Even though there is an inconsistent clinical definition, acute shunting has proven to be effective for 30-50% of patients, with 50-70% requiring secondary surgery [28]. Daily pressure changes, coupled with the small pressure seen in NPH, can cause over-drainage resulting in excess CSF removal causing subdural effusions or hemorrhage. No devices currently exist to continuously monitor and treat these patients.

The functional basis for the existing therapy is the relationship between intracranial pressure and volume (P-V). Experimental measurements of pressure with volume infusion confirmed the nonlinear pressure-volume hypothesis [29]. Volume infusion and subsequent pressure monitoring is a technique still used to determine the compliance of brain tissue. The accuracy is questionable however because it fails to describe NPH patients or patients with abnormal compliance.

Shunts implanted for extended periods of time may become invaded by choroid plexus tissue [25, 30]. In addition, improper shunt placement impairs functionality, invariably causing long-term problems [31]. Surgical revisions are very dangerous for patients on top of being costly and time-consuming. A novel design by other researchers assesses flow in the shunt to evaluate possible occlusion [32] and whether revision is necessary.

Because intracranial pressure depends on body position, pressure shunts often over drain leading to slit-ventricle syndrome [33-34]. Toy magnets have been shown to disrupt adjustable shunt settings [35]. 6-12 % of shunted children develop slit ventricle syndrome due to over-shunting [36]. In a survey of pediatric neurosurgeons who routinely implant shunts into hydrocephalic children, the majority of them expressed their inability to prevent slit ventricle syndrome [37].

The hospital cost of treating this disease is astonishing. In 1997, 2000, and 2003 hospitals spent on average *$1.4 - 2.0 billion* on CSF shunt-related admissions for pediatric patients [38]. Shunt-related

revisions accounted for half of all admissions and a total of 242,000 hospital days. For endoscopic third ventriculostomy (ETV), hospitals spent up to $500,000 [17] on successful and failed ETV surgeries. The assessment of ventricular drainage in a hospital setting is via medical imaging techniques such as magnetic resonance imaging (MRI) or computed tomography (CT), which is a time consuming and costly process.

There have been several different approaches for monitoring and treating hydrocephalus such as the commercially available flow based shunt system (Orbis-Sigma valve, Integra). This system allows clinicians to assess proper function of the catheter. Another commercially available device uses a variable pressure shunt, which can be adjusted in an outpatient setting using external magnetic fields (Strata Valve, Medtronic). However, at a 2010 hydrocephalus meeting, many clinicians and patients expressed dissatisfaction with the devices due to its sensitivity to any magnetic field, and the frequent need for revisions [39].

There has also been an interest in incorporating wireless intracranial pressure (ICP) sensors within shunt systems. These micro-electric mechanical systems (MEMS) devices are still under development, and would provide readings proximal and distal to the valve system. As early as 1986, researchers proposed using pressure sensors for hydrocephalus monitoring and therapy [40-41]. Researchers have also proposed microfabricating shunt valves [42] and integrating these into the catheters in order to address mechanical failure. However, state-of-the-art devices still do not address the main limitations with shunt treatment. Therefore, a novel approach to monitor and treat this disease is proposed.

B. Novel Therapy Design

The main limitation of the existing treatment is pressure correlation with the disease state. Increased intracranial pressure may not indicate CSF accumulation. There is also a growing consensus within the

neurosurgical community that volume as opposed to pressure monitoring may provide improved treatment modality, as noted in an NIH-sponsored workshop in 2007 [43]. Therefore, active volume monitoring coupled with a feedback control system as a novel therapy is proposed in this thesis. A volume sensor will actively control a pump to maintain desired CSF levels. Figure 2 illustrates the novel therapy design. Frame A shows the sensor implanted into the ventricular system and frame B shows the electronics and control elements. An increase in fluid volume will result in activation of the micro-pump to maintain CSF volume levels.

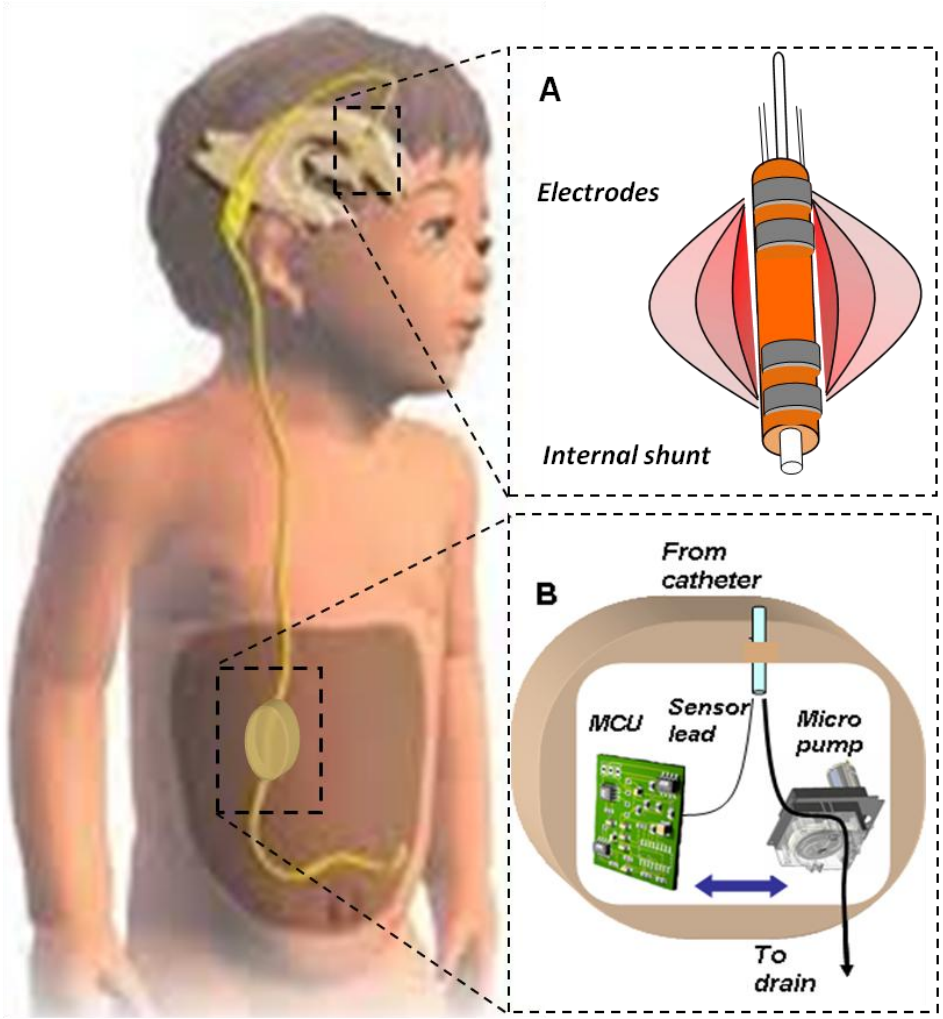

Figure 2. Novel therapy design for hydrocephalus. Frame A shows the volume sensor implanted into the ventricular system, while frame B shows the electronics and micro-pump control system.

B.1.Specific Aims

The hypothesis tested in this thesis is that volume measurements of CSF are feasible with use of an impedance based volume sensor. Integration of electrodes with existing shunt devices will allow for a translational design. This system may act as a crucial diagnostic tool for clinicians and researchers. The technology can be illustrated in Figure 3, where the dashed box indicates the volume monitor. The specific aims of this thesis are:

Specific Aim 1. Design and simulation of an impedance based volume sensor

Prior to trial and error with the volume monitoring technique, simulations are shown for preliminary feasibility. Stacks of images are used to create three-dimensional models for finite element simulations. Case studies consist of human and rat simulations with the volume sensor in cases of hydrocephalus. Catheters with ring electrodes are designed on a reconstructed brain meshes in order to determine design constraints as well as maximize sensitivity of the system.

Specific Aim 2. Battery operated microelectronics design and fabrication with wireless capabilities

The next phase of this thesis details the fabrication of the volume sensor consisting of platinum/iridium ring electrodes. Sensors of 500 μm outer diameter are fabricated with an internal shunt as a pathway for fluid flow. Explanation of the instrumentation follows. Microcontroller implementation allowed for RF transmission of volume measurements as well as power control for battery operation. The implantable unit is designed with surface mount technology for power and size reduction. The entire system is designed to fit inside a biocompatible housing intended for long-term animal studies.

Specific Aim 3. Volume monitoring validation in bench-top and animal models of hydrocephalus

In order to validate the device functionality, the device is tested rigorously on two different bench-top brain models. Two models were designed which emulated the various properties of brain tissue. Once the instrumentation and sensor were optimized on bench-top models, an animal model of hydrocephalus is developed to test the volume monitoring technique. An acute surgery was performed on a hydrocephalic animal to drain CSF out of the ventricles. Simultaneously, the sensor was implanted into the ventricular system. Measurements were coupled with dynamic imaging of ventricular volume reduction via x-ray imaging with contrast injection.

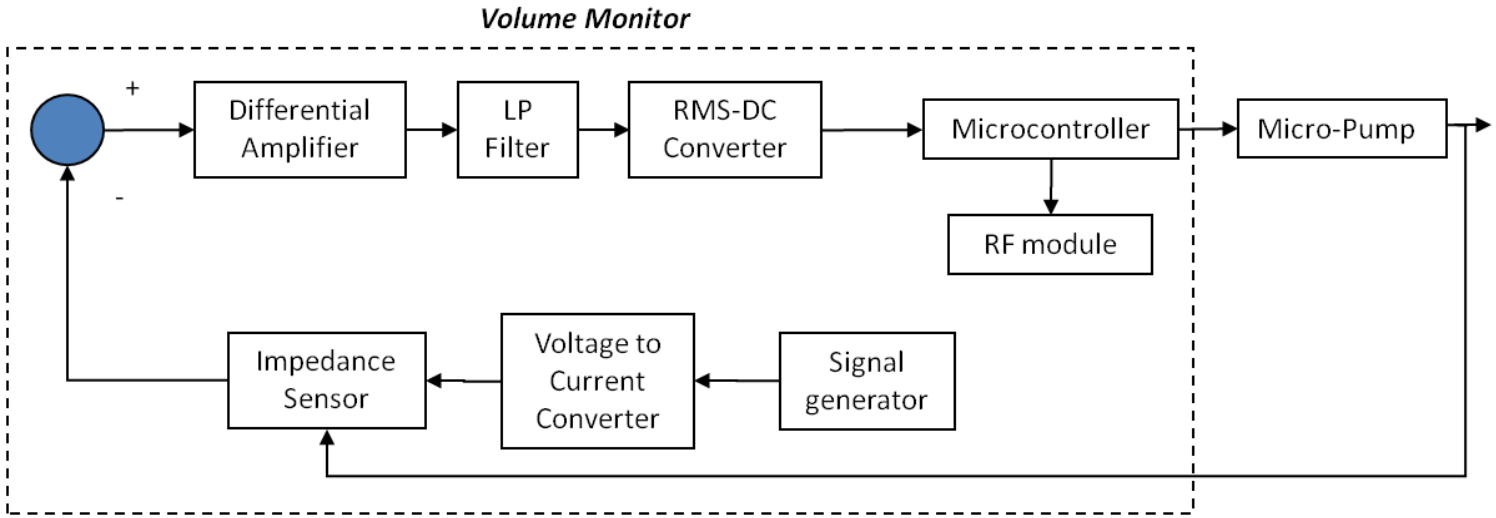

Figure 3. Block diagram for hydrocephalus therapy. The diagnostic volume monitor developed in this thesis is illustrated as the box with the dashed lines.

C. Significance

In the U.S., slightly more than 1 in 1,000 births is affected by hydrocephalus. Hydrocephalus is one of the most common birth defects and afflicts more than 10,000 babies each year in the U.S. [1]. There are also 70,000 discharges a year from hospitals within the U.S. with a diagnosis of hydrocephalus [44]. The primary treatment for hydrocephalus is CSF shunting, and current shunts have a high failure rate. In a large series of children the failure rate was 50% over five years. In adults the reported complication rate is up to 35% [1].

While the past five decades have lead to very sophisticated and costly pressure shunts, overall patient outcomes have not improved significantly. *Also, pressure shunt effectiveness is not a function of device cost*. A recent study of 195 Ugandan children showed no significant differences in patient outcome between those who received an inexpensive Chhabra shunt ($35 US dollars), or the more expensive Codman-Hakim Micro Precision Valve shunt ($650) [45]. Regardless of pressure shunt design, the principle of pressure shunting fails in cases of normal pressure hydrocephalus. Furthermore, pressure shunts can lead to slit-ventricle syndrome and cause CSF under- or over-drainage due to pressure variations due to body position or activity. **Moreover, the cost of ventricular shunt implants amount to a staggering $1 billion a year in the U.S. alone [1].** These statistics show a clear need for improvement. An entirely new approach is necessary for proper maintenance of childhood and adult hydrocephalus.

II. IMPEDANCE-BASED VOLUME SENSOR DESIGN AND SIMULATION

Summary

In medical device development, the application of generic devices for novel therapies is often based on trial-and-error. In order to minimize the time to market a new therapy, devices must be re-designed to optimize performance and assess feasibility. This chapter presents various sensor configurations simulated on finite element models to assess performance and predict experimental outcome. The mathematical model consists of reconstructed brain and ventricle meshes for *in-silico* sensor design. Design decisions such as interelectrode spacing, surface area, and number of electrodes are followed by microfabrication, which results in cost-effective scalable sensors. Two case studies are presented on human and rat models of hydrocephalus. At the end of this chapter, a design for human patients based on finite element simulations is presented. The process for a novel measurement technique presented in this chapter may reduce trial and error involved with improved treatment options for patients.

A. Background

Cerebrospinal fluid (CSF) properties for the assessment of hydrocephalus are currently obtained using imaging techniques such MRI or CT. On a two-dimensional single imaging plane of the brain, clinicians compare the length of the frontal horn of the lateral ventricles with the length of brain tissue, known as the frontal horn index. This two dimensional analysis allows for the assessment of fluid accumulation. CSF volume can be computed for a more rigorous analysis of accumulation by reconstructing many images into a three-dimensional object.

Imaging analysis of CSF accumulation has many limitations such as the high cost of continuous monitoring, and a finite resolution. On a 3T machine, the voxel size is not less than 1 mm^3. An MRI with a stronger magnet results in a higher resolution; however they are not used practically. *Low*

resolution does not allow for measurements of pulsatile deformation, which are an indication of brain compliance. An analog volume sensor that monitors volume can provide dynamic monitoring and high sensitivity, which can be increased by design parameters and instrumentation.

A.1. Measurement Theory

The volume measurement system proposed in this thesis is an implementation of the impedance technique that was developed for tomography [46-51]. In impedance tomography, low intensity electric fields are applied to surface electrodes, and voltage potentials are recorded at various spatial locations. The difference in the electrical properties of tissue distributes the electric vector field in a non-uniform manner. An inversion algorithm is then applied to calculate the impedance distribution [52]. Eq. (1) represents ohm's law in a three dimensional volume where $\vec{J}$ is the electric current density $\left(A/m^2\right)$, $\vec{E}$ is the electric vector field $\left(V/m\right)$, and σ is the electric conductivity $\left(1/ohm \cdot m\right)$. Eq. (2) substitutes the gradient of the scalar voltage potential field with an electric vector field, $\vec{E} = \nabla V$. By observing current continuity, eq. (3) the impedance can be found by inverting experimental measurements of voltage. This equation, readily solved using finite element analysis, can also be derived by applied steady state to Maxwell's first equation (not shown).

$$\vec{J} = \sigma \cdot \vec{E} \tag{1}$$

$$\vec{J} = \sigma \cdot \nabla V \tag{2}$$

$$\nabla \cdot \left(\sigma \cdot \nabla V\right) = 0 \tag{3}$$

When an electric vector field is applied to a tissue with non-homogenous conductivity values, the electric field has a non-uniform distribution. The impedance technique observes dynamic disturbances to the distribution of an induced electric field, which is a result of conductivity change. Accurate measurements of fluid volume require the conductivity of the surrounding tissue to be sufficiently different from the conductivity of the fluid in the cavity. Then the detected voltage drop is a function of the fluid filled space. Dynamic volume increases can be detected as changing voltage drops across the measurement electrodes. Figure 4 shows a simulation of the distribution of an electric vector field applied to ring electrodes of a catheter. Boundary conditions consist of a normal current flux applied to electrode 1, and potential ground on electrode 2. The computational mesh consists of a fluid region with conductivity of CSF ($\sigma = 1.13\ S/m$).

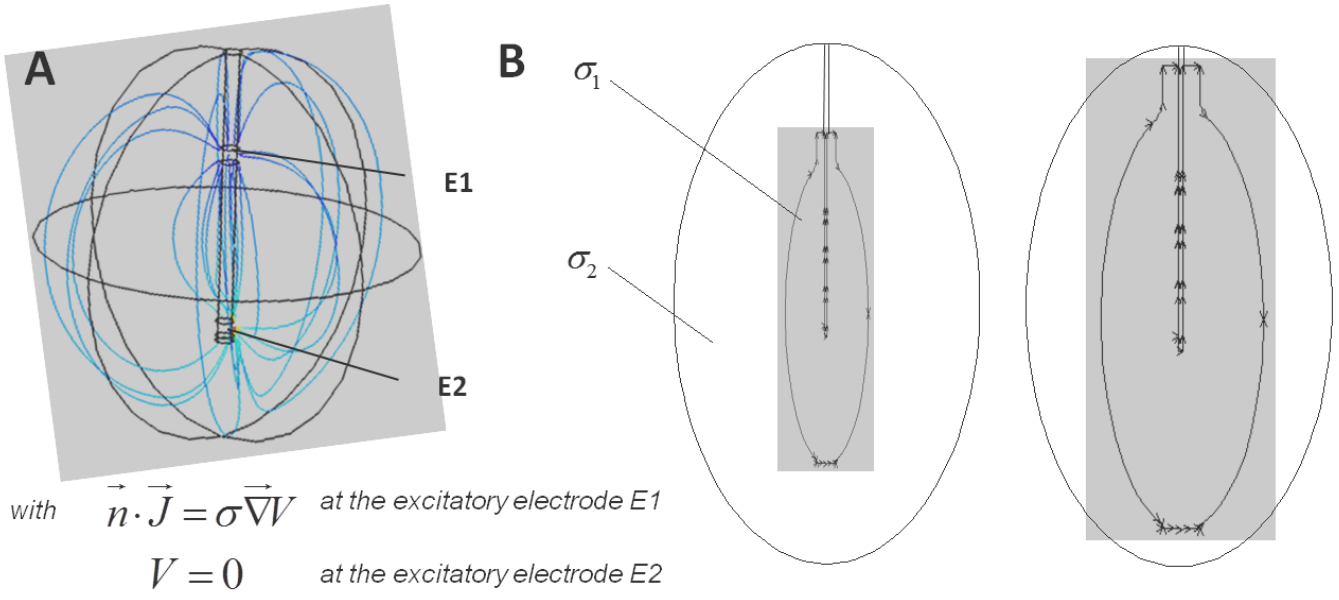

Figure 4. Distribution of an induced electric vector field on a catheter with ring electrodes. A three dimensional simulation is shown in frame A. Frame B shows 2 models with different cavity size.

Volume can be calculated by predetermined voltage drop - volume relationships during calibration experiments or by eq. ((4). This equation calculates the volume of CSF-filled ventricles, V_f, related to the measured voltage difference, ΔU, with α, a calibration factor; σ_{csf} the specific conductivity of CSF; L, the distance between the electrodes; I, the current emitted; G_{brain}, the conductance of brain tissue; and G_{CSF}, the conductance of CSF.

$$V_f = \alpha \cdot \sigma_{csf} \cdot L^2 \cdot \left(G_{CSF} - G_{brain}\right) = \alpha \cdot \sigma_{csf} \cdot L^2 \cdot \left(\frac{I}{\Delta U} - G_{brain}\right) \quad (4)$$

The relationship between the steady-state solution to Maxwell's equation and the diffusion equation is apparent. Application of the diffusion equation for the simulation of intracranial drug transport has been extensively used by our laboratory [53-54], where the anisotropic properties of the brain tissue were obtained using diffusion tensor imaging. Similarly, an electrical conductivity tensor can be implemented for the precise distribution of an induced electric field within the brain [55-56].

A.2. Previous Work

The impedance technique has been applied to measure changes in lung compliance [49, 57], thoracic imaging [58-59] blood stroke volume [60-61], breast imaging to detect cancer [62], tissue characterization [63-65], and intracranial blood flow to estimate neuron electrical activity [66-68]. Most devices consist of externally applied electric fields for non-invasive monitoring. Signals are applied to surface electrodes placed on the skin, and voltage potentials are recorded similarly. An ex-vivo approach may seem feasible for external monitoring of CSF accumulation; however it is not practical for many

reasons such as the non-conductivity of bone. Also, the strength of the field reduces as a function of distance; therefore high field strengths with high precision amplifiers must be used due to large patient sizes. Measurement artifact can be introduced due to daily motion, which makes external monitoring of CSF accumulation using the impedance technique infeasible.

An inversion algorithm is sometimes applied to calculate the impedance map, or to determine the distribution of impedance from an induced electric field. This may be important in determining local volume changes around portions of the catheter. Inversion may also be applied to determine the location of the poles of an electric field. For example, in electroencephalography (EEG) source localization, the inversion of voltage potential, eq. (3), is performed to determine the source of electrical activity recorded from surface electrodes. Technical limitations of the inversion process limit the accuracy of the impedance and source localization. Inversion is typically performed using a generic computational mesh, which limits the accuracy of the solution. Current efforts in this research area consist of using precise anatomical meshes with anisotropic conductivity regions [69-70], which may provide accurate distribution of impedance and the location of source potentials.

There are *in-vivo* systems for measuring dynamic changes in blood volume such as the cardiac conductance catheter. This device, not approved for clinical use, implements the impedance technique on four or more ring electrodes on a catheter that is implanted into the cardiac ventricle [71-73]. An electric field is applied and voltage potential is recorded along the length of the catheter, which allows for an estimation of volume. There has been much research dedicated to this area of research. Researchers have found that the calibration curves used to convert voltage into volume have an error caused by leakage current into the cardiac muscle [73]. Several researchers have improved the calibration curve; however these sensors cannot be used for measuring CSF accumulation because the tissue properties are vastly different. Also, the calibration curves are entirely dependent on the

placement of the electrodes. The electrode spacing is not optimal for high sensitivity of CSF accumulation. Currently available cardiac conductance catheters have a minimal interelectrode spacing of 3 mm.

A.3. Chapter Outline

The chapter aims at computer aided sensor design for maximum sensitivity of volume measurements and is organized as follows. Section two will introduce a computer-aided sensor design methodology for predicting the sensor response supported by state-of-the-art medical imaging data. Section three will present the computational results on two case studies with different species as a function of different design parameters. The discussion in section four suggests recommendations for future simulations for optimal sensor design. The chapter closes with conclusions.

B. Computer-Aided Sensor Design Methodology

The simulated performance of a volume sensor under the pathological disease state of hydrocephalus is a specific contribution introduced for the first time. Progressive ventricular enlargement caused in acute stages of hydrocephalus was reconstructed from MRI. Critical sensor parameters such as catheter placement, inter-electrode distance, catheter diameter, electrode surface area, and number of measurement electrodes were simulated with finite element analysis of the electric fields induced in the cerebrospinal fluid and the brain parenchyma. Figure 5 shows the method used to design and fabricate the sensor. The novel design process is effective in detecting design flaws, diagnosing deficient device accuracy or excessive sensitivity disturbance than traditional design based on trial-and-error. In this thesis, design and fabrication is demonstrated on a rat hydrocephalus model followed by a clinical design and fabrication.

B.1. Previous Design Methodologies

A new application of a catheter with ring electrodes requires design specifications such as electrode placement, surface area, diameter, etc. Custom fabricated sensors can be manufactured; however the design is often based on intuition. There are researchers who perform simulations for optimization of design specifications, which are application-specific. Researchers of deep brain stimulation suggest specific electric field orientation and magnitude based on simulations [74-75]. Their suggestions have led other researchers to microfabricate MEMS electrodes [76]. Researchers of the cardiac conductance catheter have suggested optimal electrode placement for higher sensitivity to volume measurements during the cardiac cycle [77-78]. Using a similar approach, the design of a sensor for CSF volume measurements with patient-specific geometry is presented.

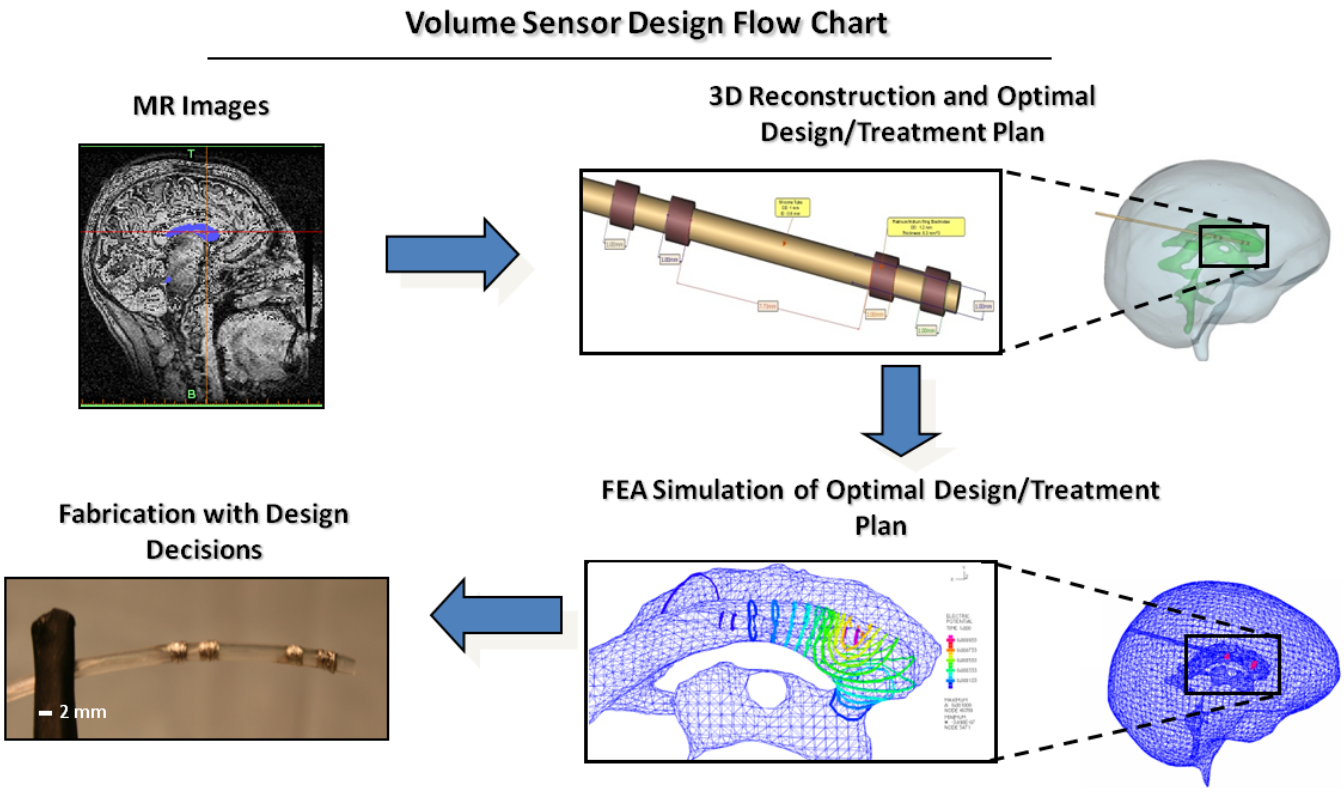

Figure 5. Computer assisted design of a volume sensor for hydrocephalic patients.

B.2. Finite Element Simulations using Species-Specific Geometry

Imaging techniques such as MRI or CT allow visualization of internal structures in axial, sagittal, or coronal planes. These images are then combined into a single stack that is used for three-dimensional reconstruction. Points between each image delineating boundaries are interpolated resulting in a surface mesh. Reconstructed volumes were partitioned into sub-volumes using a grid generator (Gambit, Fluent, Inc.). The discretization step typically generated 550,000 tetrahedral elements for the CSF-filled spaces and 600,500 elements for the parenchyma in each stage of hydrocephalic rats. Volume meshes are calculated over which the partial differential equation is solved over each element. Volume was calculated using MIMICS reconstruction software (Materialise, Belgium). This software creates tetrahedron elements within the volume mesh. Our lab has extensively used this approach for simulations of CSF flow [79], drug delivery [80], and intrathecal CSF dynamics [81]. The advantage of this approach is that realistic simulations predict experimental and clinical observations. Models are exported into finite element software (ADINA, MA) for simulation of the volume sensor. Equation (5) was solved in each element of the mesh, which typically consisted of at least 30,000 elements. The electrical conductivity of the CSF was 2.0 S/m, while brain was modeled as 0.2 S/m. The models were generated by subtracting the sensor mesh from the ventricle and brain mesh. Boundary conditions were then applied on the resultant faces which were the outer surface of the electrodes.

$$\sigma\left(\frac{\partial^2 V}{\partial x^2}+\frac{\partial^2 V}{\partial y^2}+\frac{\partial^2 V}{\partial z^2}\right)=0 \qquad (5)$$

B.3. Case Studies of Volume Sensor Performance

Even though at the early stages of the project, an assessment of the expected sensor performance and positional dependence in real human brain geometries was desired. To realize this assessment

without harm to patients, a rigorous finite element analysis of the induced fields of different sensor configurations on real patient ventricular models was performed. The computations helped optimize sensor design parameters for best performance in hydrocephalus humans. Frame A of Figure 6 shows normal ventricular spaces in a 32 year old normal subject. An image of a fully developed hydrocephalic brain is shown in Frame D. It was obtained from a 62 year old patient suffering from communicating hydrocephalus. The images were reconstructed using image reconstruction tools. The ventricular sizes were determined using a snake algorithm where T1-weighted volume images were converted to milliliters. These brain images were used as accurate representations of the computational domain for finite element analysis. Models for intermediate ventricular sizes to simulate the transition of pathological stages B, C, and D with ventricular sizes of 42, 75, and 160 mL respectively were also created (not shown). For the brain geometry of each of the disease states, finite element models according to eq.(5), with equal geometrical dimensions and electrical properties of the sensor, CSF, and brain tissue are given in Table 1. Triangular meshes were used with an average of 59,568 elements for each stage. The proper mesh size was determined by trial and error to obtain mesh independent simulation results. A current source of 0.88 A/m^2 was applied to an outer electrode pair to produce a current of 25 μA. To emulate different sensor configurations, the potential difference at the surface of the measurement electrodes positions B and C were calculated. Although anisotropic conductivity tensor, σ, was not applied using DTI methods, here the electrical conductivity of the brain tissue was assumed to be isotropic and homogenous with a mean value of $\sigma = 0.172\, S/m$. The CSF conductivity was set at $\sigma = 2.01\ \ S/m$. The conductance predictions correctly reflect the trend in size changes from normal ventricular size to hydrocephalus. The ventricular size change from 25 cc to 250 cc in hydrocephalus incurred a conductance change from 1 S to $1.45\,S$. The rigorous computations also

allowed an estimation of leakage current into the brain tissue. In the normal subject, leakage was also determined to be less than 5 μA or less than 20% of the input current.

Table 1. Boundary conditions and material properties used for computer simulations using Finite Element Analysis.		
Condition	Gel Phantom Cavity	Human Brain Hydrocephalus
Neumann $\vec{n} \cdot \vec{J} \in S_{A.D}$	$\vec{n} \cdot \vec{J} =$ 16.66 A/m^2	$\vec{n} \cdot \vec{J} =$ 0.88 A/m^2
Dirichlet $V = S_{B,C}$	$V = 0$ V	$V = 0$ V
Brain Tissue Conductivity	0.172 S/m	0.172 S/m
CSF Conductivity	2.01 S/m	2.01 S/m

The sensor performance can be compared to the MRI volume accuracy. The resolution in the horizontal and vertical direction in MR images is limited by a voxel size of typically 1 x 1 x 1.5 mm in a 3T GE Sigma scanner (GE Medical Systems, Milwaukee, WI). For the lateral ventricles, this MRI resolution is estimated to cause a volumetric variance of at least ± 0.276 mL, or ± 3.6 % of its size. The prototype volume sensor variance was 8%, which was obtained by comparing measured to calculated volumes. This preliminary error is not much larger than the best state-of-the-art MRI technique. However, MRI scans are not practical for an on-line treatment. The sensor accuracy could further be improved with *(i)* higher gain amplifiers, *(ii)* more measurement electrode pairs, and *(iii)* optimal placement of excitatory electrodes along the full length of the cavity. The simulation approach would provide a systematic tool to address these improvements.

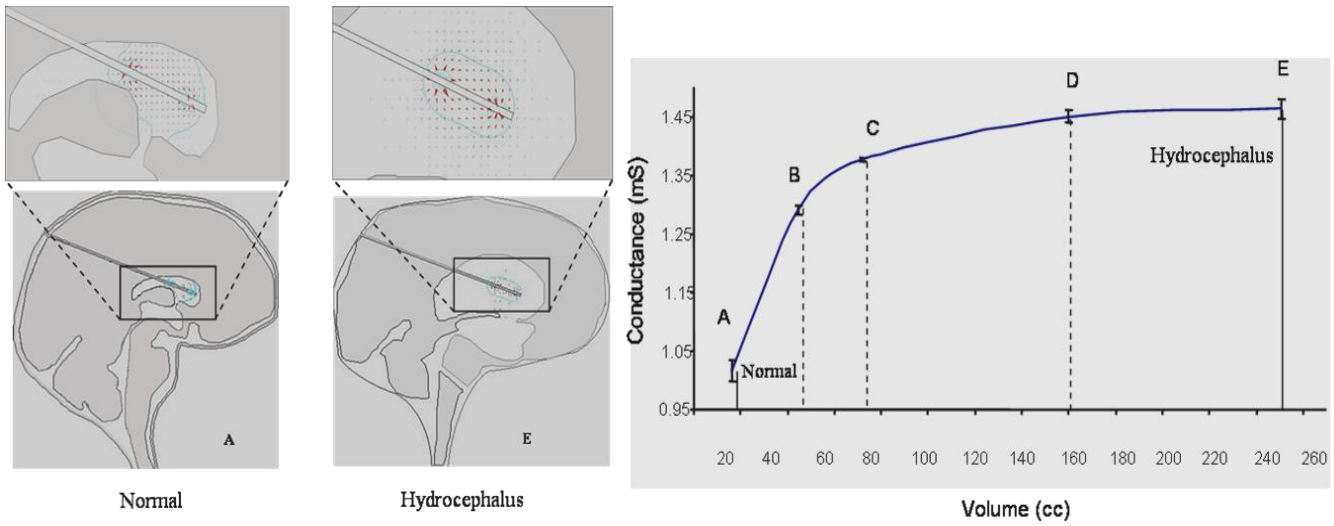

Figure 6. Case Study of conductance changes during the transition of hydrocephalus. The sizes of the intermediate stages B-D (not shown) were artificially created by interpolation to emulate transitions from normal to hydrocephalus. The projections of volume changes were taken as size changes of the lateral ventricle with known volumes of the normal and hydrocephalic lateral ventricle. The simulations were repeated five times with different sensor positions located between 1 – 5 mm away from the central axis. An 8 fold increase from normal size correlates with our experimental and simulated analysis.

The positional dependence of the sensor within simulated human lateral ventricles was also addressed. In repeated simulations, electrodes were displaced from the center towards the ventricular walls. For five different positions of 1 mm displacements from the actual center to the superior and inferior ventricle wall, the simulations gave similar volume readings with a variance of less than 2%. As a general trend, it was observed that the conductance decreased when the sensor moved closer to the wall due to an increase in leakage current. However, these changes were modest due to the high electrical contrast between CSF and human brain tissue. Overall, the sensor position detecting the ventricular CSF space is only mildly dependent on the position; therefore a sensor placed in a human subject who maintains normal activities is expected to be sufficiently insensitive to the sensor position inside the ventricle.

C. Sensor Simulation Results

C.1. Clinical Volume Sensor Case Studies

The previous section presented results from a two-dimensional steady state simulation. The result of two dynamic case studies performed with a sensor is now presented. These multi-physics simulations implemented time-dependent pressure boundary conditions applied to the boundary of the ventricles. Displacement was solved for every face of an element simultaneously with equation (5) in each time step. The volume of the ventricles expanded as pressure increased over each time step. The first case study consisted of obtaining the potential on the boundary of the ventricle to estimate leakage current of the sensor. The resultant electric potential on the boundary of the ventricles did not exceed 1 mV , which is below the threshold for neuronal stimulation. The simulation is shown in frame A of Figure 7. The second case study consisted of placing the measurement electrodes along 3 different locations along the length of the catheter in order to maximize sensitivity. The excitatory electrodes locations remained fixed. Voltage difference between the measurement electrodes was integrated over the surface. Because the relationship between voltage and volume is non-linear, more than 1 different sensitivity region was necessary. Sensitivity is defined as the slope of the voltage-volume relationship. Frame B shows that the largest measurement electrode distance produces the highest sensitivity.

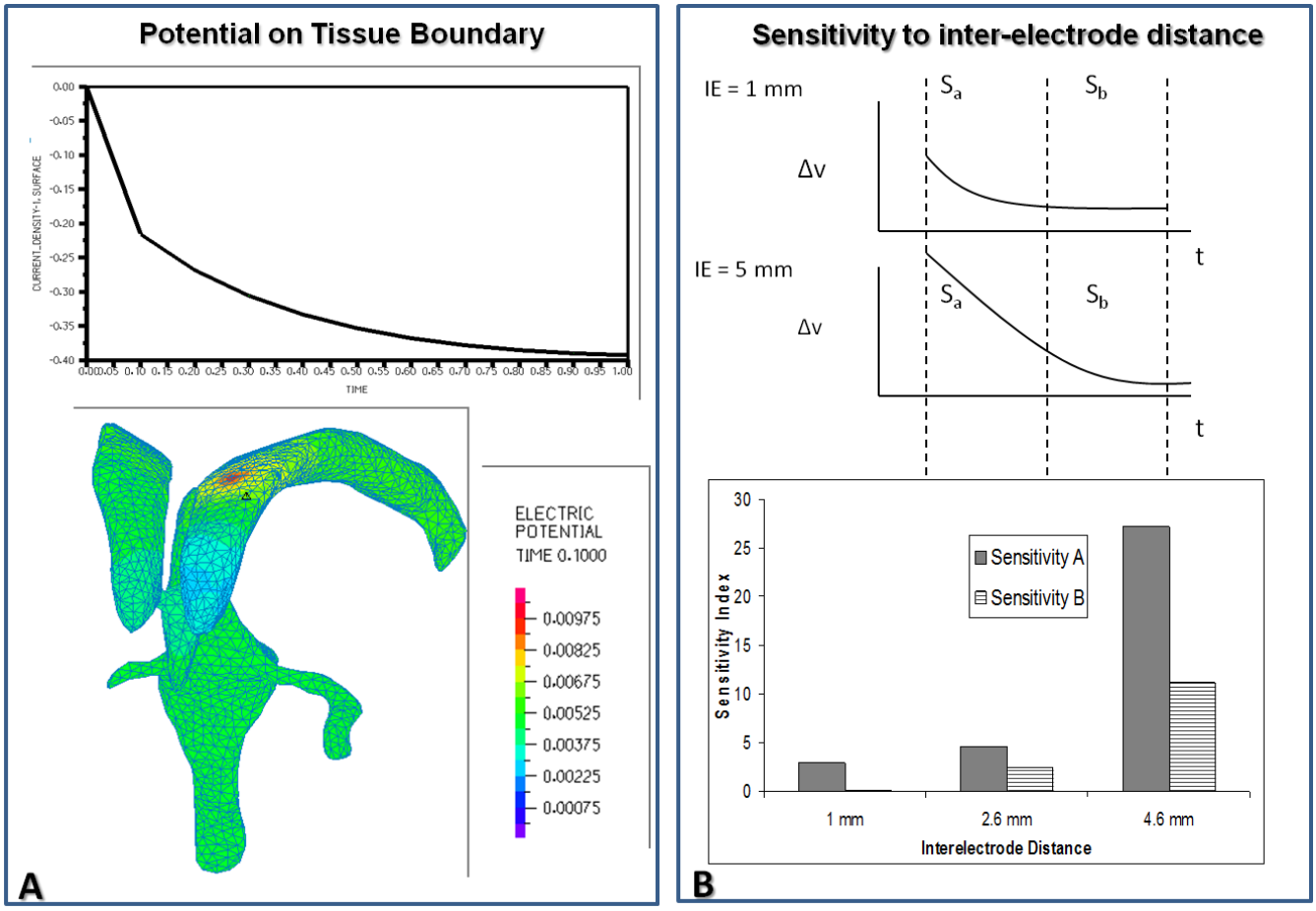

Figure 7. Case studies with dynamic simulations in a normal human patient. Frame A shows the electric potential on the boundary of the ventricles. Frame B shows the result of 3 different inter-electrode distances.

C.2. Sensor Design for Rat Hydrocephalus Model

Animal validation of the novel monitoring system was necessary prior to clinical trials. Therefore simulations on an animal hydrocephalic model were performed for experimental design and prediction of outcome. A 3 week old weanling rat induced with hydrocephalus emulates ventricular expansion of that in human infants [82-83]. MR images during the progression of hydrocephalus and the three-dimensional reconstructions are shown in Figure 8, which highlight the ventricles in green and brain parenchyma in yellow. T2-weighted MRI images from Sprague Dawley rats made hydrocephalic

via cisternal kaolin injection were obtained from Dr. M.R. Del Bigio from the Department of Pathology at the University of Manitoba. Mimics *image reconstruction* software was used to create exact geometrical representations of the three-dimensional rat ventricular system, subarachnoid spaces and brain parenchyma. Extreme ventricular enlargement can be seen with the rat hydrocephalus model.

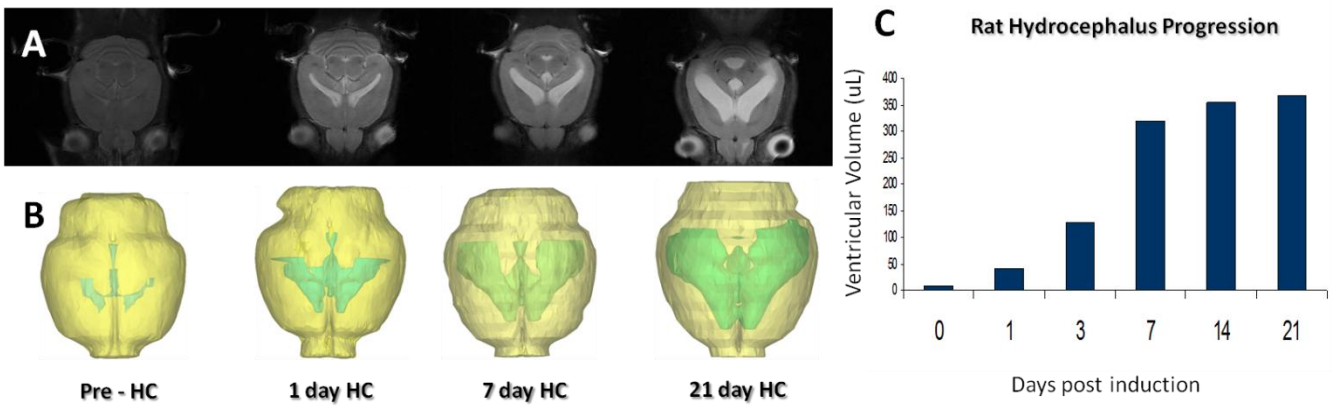

Figure 8. Ventricular enlargement in a hydrocephalic rat model. In frame A, MR images are showing the progression of ventricular enlargement starting with a pre-HC rat on the left. In frame B three-dimensional reconstructions outlining the ventricles (green) and brain (yellow) are shown. Frame C shows calculations of ventricular volume.

A steady-state simulation in a 21-day hydrocephalic rat is shown in Figure 9, which shows the electric vector field distributed throughout the brain and ventricles in frame C. The outcome of the HC rat simulation was design decisions for the sensor fabrication provided in Table 2. The maximum diameter for the sensor to fit inside the ventricles is 500 µm, with an electrode spacing of 1 mm. Our simple cost-effective fabrication procedure allowed for validation of the monitoring technique in hydrocephalic animals.

Table 2. Computer-aided sensor design properties implemented in fabrication process.				
Catheter Length	Inter-electrode Distance	Applied Current Density	Catheter Diameter	Number of Electrodes
10 mm	1 mm	0.1 A/m^2	0.5 mm	4

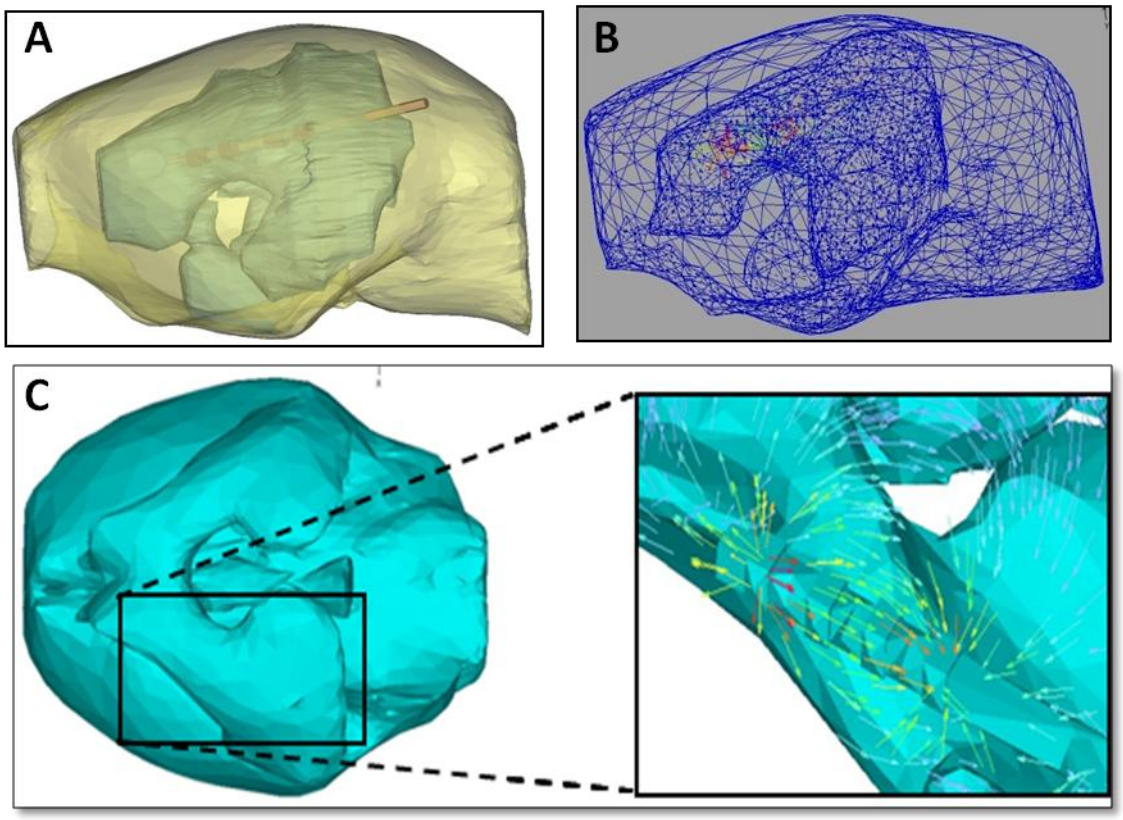

Figure 9. Simulation of a volume sensor implanted in the ventricles of a 21 day hydrocephalic rat. Frame A shows the three-dimensional model, while frame B shows the mesh and boundary conditions. Frame C shows the simulated electric field in the ventricles.

D. Discussion

In classical biological research, there is a tendency to perform design optimization directly on animal models in an iterative trial and error process. Parameters are improved in several stages, scaling up from small animals to larger ones until a device or treatment for humans has been generated. Modeling of distributed systems accelerated the scaling procedure and design decisions typically achieved with animal experimentation. In this chapter, the implementation of these design decisions to fabricate a ventricular volume sensor was discussed.

The proposed catheter was integrated into a computer model to predict ideal sensor measurements according to Maxwell's equations. The geometric and electronic properties of the proposed volume sensor were integrated with a computational model for the brain geometry. The potential field induced inside the ventricular spaces by the sensor's excitatory electrodes was predicted by solving Maxwell's equations over the computational domain. The *in silico* model was used as a virtual laboratory to test different catheter parameters such as spacing and position. The simulations helped maximize device sensitivity and catheter position with respect to the enlarging ventricles. Once ideal sensor parameters were determined using computer simulations, the sensor was fabricated with microfabrication techniques.

The rigorously simulated performance and optimization of a micro-electronic volume sensor under pathological disease states of the brain was a specific contribution introduced for the first time. Reconstructed three-dimensional models of the progression of ventricular enlargement were used for finite element simulations of the impedance based volume sensor. The main advantage of performing this work is that *a priori* knowledge about the relationship between voltage and volume was obtained, providing a comparison between the experimental measurements demonstrated in the following chapters and simulations.

E. Conclusions and Significance

An in-vivo measurement of the disease progression in hydrocephalic rats with computational methods to find the key parameters of a rat ventricular volume sensor was demonstrated. Systematic testing to determine whether the sensor would provide sufficiently accurate voltage measurements for all size ranges and ventricular shapes expected during hydrocephalus was demonstrated. This computer-aided approach accelerated the design process without resorting to numerous trial-and-error animal experiments by allowing for a selection of properties crucial for sensor performance.

Two case studies were demonstrated. Measurement electrode spacing was varied and a higher sensitivity to volume change was achieved when electrodes were 4.6 mm apart in the clinical simulation. An additional case study consisted of solving for the potential on the surface of the ventricles in order to estimate leak current. This systematic device development process advances the knowledge gain in each level, thus rendering the animal testing procedure more effective.

The comparison of actual ventricular sizes obtained from the reconstructed rat images and the simulated ventricular volume measurements from electric field simulation allowed for a prediction of expected measurement error. It also enabled experimentation with the effect of sensor parameters on sensor accuracy *in silico*. After rat sensor specifications were obtained, fewer rat experiments were needed to validate the predicted sensor performance. Experimentally determined properties were incorporated into the model. Sensor prototypes with simulated specifications and their validated performance with bench-top experiments are described in the next chapters.

III. SENSOR AND INSTRUMENTATION FABRICATION

Summary

Sensors for medical applications require reliable electronics in order to function correctly and efficiently. Inefficient design may lead to incorrect interpretation of the phenomenon under study, due to signal attenuation. Also, large power consumption may drastically reduce battery life. This chapter presents instrumentation design and fabrication for CSF volume monitoring. An acute system where measurements sent to Labview is described in detail, followed by the design of an implantable version that utilizes a microcontroller. The microcontroller conveyed a byte of data to an RF transmitter synchronized to a receiver. In order to prolong battery life and reduce drift, the electronic unit was designed to function for 10s over one hour which is sufficient for CSF volume monitoring. This was achieved by implementing a duty cycle with the microcontroller for power regulation. The novel instrumentation design was first tested on a circuit breadboard, followed by computer layout and fabrication using surface-mount technology. Characteristics such as current linearity, and wireless range were obtained by calibration with a resistor decade box. The instrumentation presented in this chapter highlights the step-by-step procedure taken in this thesis towards developing an implantable system for volume monitoring in hydrocephalic patients.

A. Sensor Design and Fabrication

The fabrication of an impedance-based volume sensor with an internal shunt for volume control is a specific contribution introduced for the first time. Progressive ventricular enlargement caused in acute stages of hydrocephalus was reconstructed from high resolution MRI. Critical treatment and sensor parameters such as catheter placement, inter-electrode distance, catheter diameter, electrode surface area, and number of measurement electrodes were simulated with finite element analysis of the electric

fields induced in the cerebrospinal fluid and the brain parenchyma. Figure 5 shows the method used to design and fabricate the sensor. The novel design process is effective in detecting design flaws, diagnosing deficient device accuracy or excessive sensitivity disturbance than traditional design based on trial-and-error. In this thesis, design and fabrication is demonstrated on a rat hydrocephalus model followed by a clinical design and fabrication.

A.1. Sensor Fabrication Prior Work

Fabrication of a catheter with ring electrodes is significant for many different clinical areas. For example, stimulation of the auditory nerve in hearing-disabled patients requires a design with a coiled-catheter configuration [84-85]. For these patients, a catheter with a low density of ring electrodes is implanted into the cochlea. Stimulation of pairs of electrodes results in the perception of auditory tones. Deep brain stimulation (DBS) devices also utilize a cylindrical electrode design [86]. These electrodes are implanted into brains of patients with subsequent stimulation. Commercially available devices have been used as a therapy for Parkinson's patients, tremor reduction, and dystonia. The Activa system (Medtronic, MN) has been FDA-approved for Parkinson's patients in 2002 and recently for epilepsy treatment. FDA approval of the technology during the 1980's and the subsequent manufacturing process of catheters with ring electrodes resulted in relatively little change over the years.

Many researchers have proposed utilization of micro-electro mechanical systems (MEMS) techniques for intracranial therapy systems. A planar MEMS electrode array was recently implanted into the temporal bones of cadavers and showed to have the structural integrity required during cochlear implant surgery [87]. MEMS devices for DBS research has gained popularity with researchers able to fabricate a high density of electrodes onto flexible substrates [88], and rigid substrates such as the Utah

electrode array [89]. However, no commercially available devices exist and these new MEMS devices have not been FDA approved.

MEMS fabricated systems for three-dimensional environments is difficult to achieve. In 1 mm^3 volume of brain tissue the neuron density is around 5,000 [90]. These neurons each have different spatial locations requiring a three-dimensional electric field for optimal stimulation. Ergo, a catheter with ring electrodes has a larger volume of electric field distribution. Researchers have been able to microfabricate a three dimensional catheter with ring electrodes using an electroplating process [91]. However the complexity and cost required for the fabrication of these MEMS devices make it impractical for the assessment of a novel volume monitoring technique.

The cost and availability of small integrated circuits has allowed for the electronics of medical devices to undergo vast improvement. Early medical devices required large transistors, or combinations of resistor and capacitor components. The evolution of pacemaker electronics is an example. The first implantable pacemaker was designed in 1959 and used resistors, capacitors, and inductors to form an oscillator and amplifier. This design generated a pulse signal to stimulate cardiac tissue. The next design of pacemakers, circa 1964, incorporated a feedback mechanism to sense the electrical activity of the heart to adjust the pulse sequence [92]. Modern pacemakers use this design and also include a microprocessor and antenna for wireless communications. The electronics of other medical devices such as the cochlear implant (which was developed around 1980), and deep brain stimulation devices (which were recently developed) implement similar technology as the pacemaker. Large efforts are underway for the integration of application specific integrated circuits (ASIC) into medical devices, which are much smaller, and more efficient than existing components. In this thesis, the design of an electronic unit for the volume sensor was done using generic integrated circuits for future design with ASIC

technology. An implantable system was designed; an acute system where the signal was sent to Labview was also created.

A.2. Previous instrumentation design

Similar design criteria were chosen from cardiac conductance catheter research. In the cardiac conductance catheter, the electronics are not designed to be implantable. Therefore, there are no size or power limitations. A single or multiple excitatory signal(s) may be applied to one or two outer electrodes by use of current source(s), whereas multiple signals may be applied for more precise impedance measurements [72]. Current sources are used because impedance changes caused by the electrode/electrolyte interface may affect the excitatory signal magnitude if voltage is applied. The voltage potential is measured on separate electrodes connected to amplifiers with high input impedance, which prevents current from entering. An impedance-based volume sensor should utilize similar design criteria as the cardiac conductance catheter, where more than 20 years of research has been dedicated to [71]. Figure 10 shows a block diagram of the necessary electronic components for an implantable impedance-based volume sensor for CSF monitoring, and a computer-aided design using EAGLE-CAD.

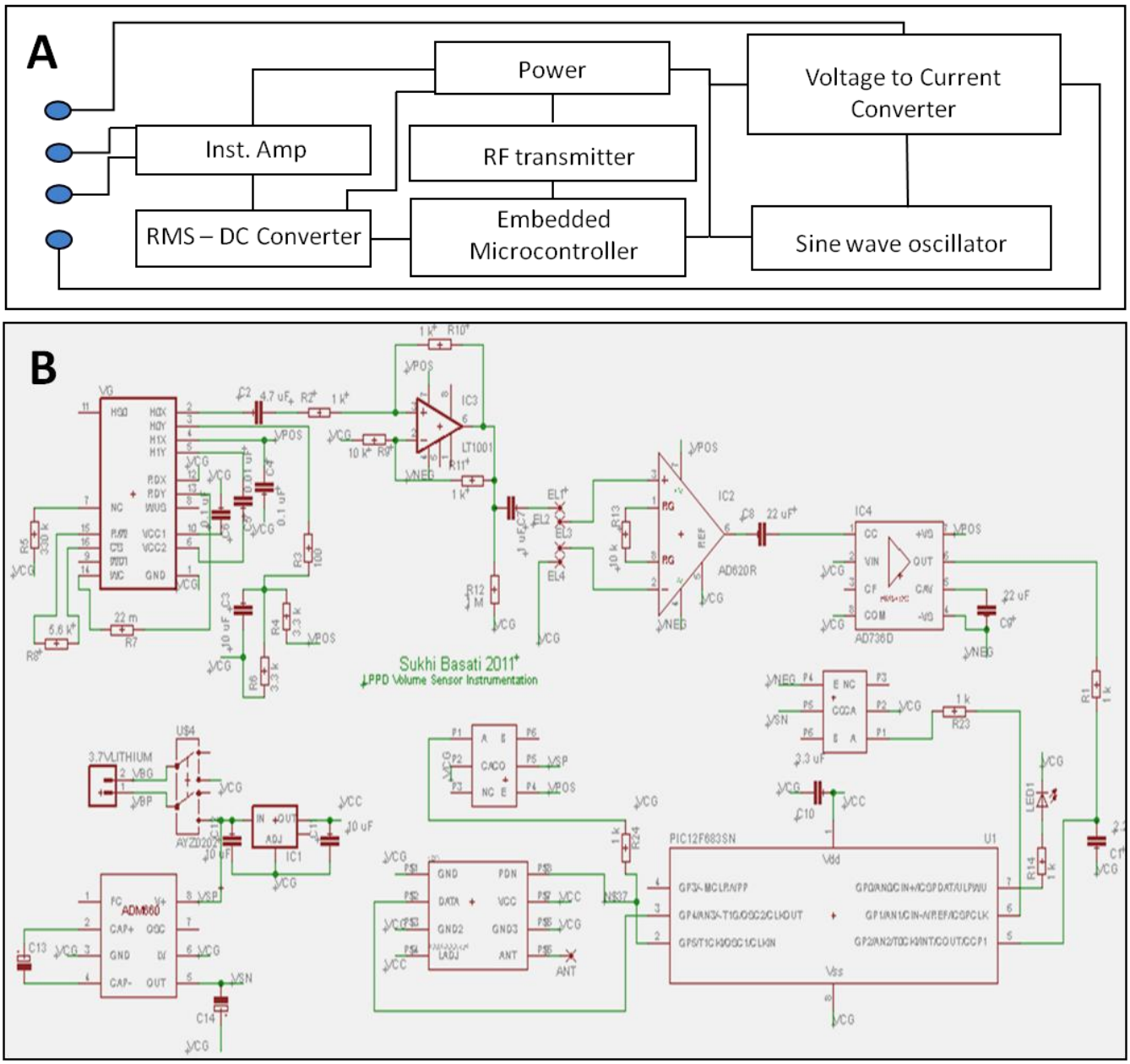

Figure 10. Instrumentation design. Frame A shows a block diagram of the components for a wireless implantable volume monitor, while frame B shows the EAGLE-CAD schematic.

A.3. Chapter Outline

The chapter aims at computer aided sensor design for maximum sensitivity of volume measurements and is organized as follows. Section two will introduce a computer-aided sensor design methodology for predicting the sensor response supported by state-of-the-art medical imaging data. Section three will present the computational results on two case studies with different species as a function of different design parameters. The discussion in section four suggests recommendations for future simulations for optimal sensor design. The chapter closes with conclusions.

B. Fabrication Methodology

B.1. Sensor Fabrication Methodology

In order to reduce the time for FDA approval of a new diagnostic system, the addition of electrodes and subsequent electronics onto existing shunt systems is proposed. A simple, cost-effective fabrication process was chosen to assess the feasibility of volume measurements for hydrocephalus therapy in this thesis. Frame A of Figure 11 shows the steps taken for fabrication. The sensor was fabricated using biocompatible materials, such as a 1 French silicone catheter (330 μm outer diameter), polyimide tubing (127 μm outer diameter), and platinum-iridium electrodes (1.25 mm^2 surface area). First, holes were created in polyimide tubing (frame C) or silicone tubing (frame D) using micro-scissors (World Precision Instruments, FL) under a stereoscopic microscope. Next, copper wires soldered to the platinum-iridium cylinders (Johnson-Matthey Medical, PA) were passed through the slits. An internal shunt was passed through the assembled sensor prior to epoxying the ends for rigidity. 734 silicone sealant (Dow Corning) was applied on the boundary of the electrodes to prevent fluid from leaking into the sensor. Frames B through D show completed sensors. The leads from the sensor were soldered to a polarized nano-connector (Omnetics, MN) which was directly attached to the instrumentation.

Polyimide tubing was chosen as the shunt catheter material due to its rigidity as well as biocompatibility [88, 93-94]. Frame C of Figure 11 shows an entire sensor made of polyimide. Torque of these sensors often resulted in permanent damage. The interface of the silicone sealant and polyimide was also not strong. Often, these sensors could not be re-used in experiments. Therefore, a 1 French silicone catheter was chosen as the sensor housing shown in frame D. Silicone is an FDA approved material for medical implants, and is also currently used in CSF shunt systems. The flexibility of these sensors far exceeded the polyimide-based design and these sensors were also reused in experiments. An internal polyimide shunt was still included, however, to add toughness to the device. Platinum-iridium was chosen as an electrode because it is a common metal used for electrodes due to its inert properties. The impedance at the electrode/electrolyte interface remains constant, which allows for minimal drift.

The impedance-based volume sensor required an excitatory signal and measurement signal applied to independent electrodes. Many researchers of neuronal stimulation use the same electrode as excitatory followed by measurement, whereas other researchers of impedance sensors suggest using two electrodes as excitatory. The current through the electrodes may then be measured, which will give an indication of the impedance. However, separate excitatory and measurement electrodes are optimal for impedance measurements because there are no artifacts. When current is emitted from a source electrode to a return electrode there is no direct transfer of ions across the surface as long as the electrode resembles a polarizable surface. A charge separation layer is created whereby ionic flow in the fluid only completes the current pathway to ground. Therefore, the outer electrodes were chosen as excitatory because the sensitivity is higher due to the disperse electric field distribution.

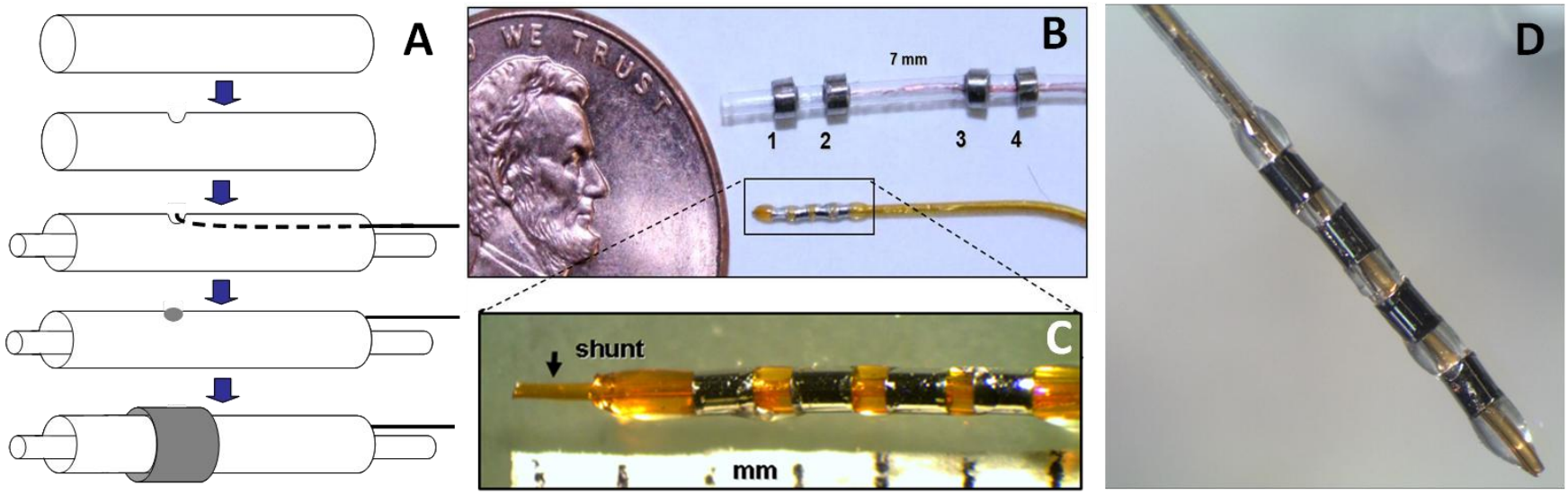

Figure 11. Cost-effective and scaleable fabrication of a sensor for volume measurements in hydrocephalus. Frame A shows the fabrication procedure. Frame B shows two different scaled designs. Frames C and D show a polyimide based sensor and silicone based sensor respectively.

The scaleable fabrication method allows for various diameter sensors illustrated in frame B. In a larger animal model of hydrocephalus, the sensor dimensions can be larger. The surface area of the electrodes should be larger in order to increase the sensitivity of the measurements. These observations were made during the sensor simulations. Also, an increase in the surface area of the excitatory electrodes decreases the electrical current density, which decreases the probability of tissue damage and neuronal stimulation. Tissue growth in chronically implanted shunts obstructs CSF diversion, rendering the treatment ineffective. Therefore, the internal shunt diameter should be larger in order to prevent obstruction at the tip. Additional measurement electrodes can also be included in a larger diameter sensor to map the impedance spectra, which may provide additional information on the state of the treatment modality. These modifications can be readily performed under the simple fabrication method.

B.2. Instrumentation Fabrication Methodology

For a CSF volume monitoring system, the following components were used due to their ease of use and availability of surface mount design. A function generator (XR-2206) was configured for sine wave generation with a frequency of 300 Hz, and peak-to-peak amplitude of 1.5 V with a DC offset of 0. A sine wave signal was chosen to prevent electrolysis at the electrode/electrolyte interface and prevent any charge accumulation. A low frequency was chosen to prevent neuronal stimulation. A high precision amplifier (LT-1001) was used in a Howland current source configuration to convert the voltage into a constant peak-to-peak magnitude current signal. The current output was connected to the distal electrode, while the proximal electrode was ground. This design passes fixed current through variable impedances under a grounded load. The Howland current source was recently acknowledged as an optimal method for neural implants [95].

The measurement electrodes were connected to a high input impedance instrumentation amplifier (AD620) for subtraction and amplification. The instrumentation amplifier subtracted the signal from the two measurement electrodes to measure relative impedance changes caused by fluid volume change. A DC converter (AD736) converted the resultant sine wave into a DC signal, which was representative of the root-mean-square (RMS) magnitude. The RMS calculation was performed in order to reduce any sampling errors caused by the analog-digital conversion. The RMS signal was sent to Labview for acute monitoring using a USB data acquisition device (National Instruments) with a sampling rate of 10,000. The Labview program consisted of an 8^{th} order digital Butterworth filter followed by digital amplification. The data was written to a txt file for off-line analysis.

B.2.1. Implantable System Using a Microcontroller, RF Transmitter, and Battery

An implantable impedance sensor requires a microcontroller unit (MCU) for optimum functionality; however a system without a programmable logic device is feasible. For example the RMS signal could be sent directly to an antenna for signal transmission. The advantages of a MCU include the ease of: programming a duty cycle for power conservation, including additional sensors, and future incorporation of a control system such as a pump. The simplest yet most efficient device on the market is the programmable-in-chip (PIC) microcontroller family. Therefore, a MCU (PIC-12F683) was programmed with analog input for data acquisition and analog output for serial communications. Code was written using MPLAB v8.53 with a built in C-compiler. Table 3 shows the main code of the program written. The code was downloaded with a USB-programmer. The complete code can be found in appendix A.

When the main loop is run, two high outputs are sent to different optocouplers for power control. Since microcontrollers output a small current, Darlington optocouplers were chosen as an interface for

the 30 mA of power drawn by the instrumentation. The third line in the main loop calls the measure_and_send subfunction.

Table 3. Main code of MCU program

```
load header

// initialization
TRISIO=0b00100;                 // configure output and input ports

void main( ) {
    for (;;)                    // run loop indefinitely
        optocoupler 1 = 1;      // positive power control
        optocoupler 2 = 1;      // negative power control
        measure_and_send();     // subfunction for A/D and serial communication
        optocoupler 1 = 0;      // power off
        optocoupler 2 = 0;
        SLEEP;                  // sleep until watchdog timer - programmable
    }
}
```

The measure_and_send subfunction sends a high value to an LED to indicate that the signal is measured and sent. Several microseconds later, the MCU performs analog-digital conversion of the input from the RMS-DC converter. The MCU converts the analog signal to a digital representation and stores it as a byte of information in a register. Then, the MCU sends a synchronization byte to the RF transmitter, which is for strengthening the transmitter-receiver link. The MCU converts the stored measurement data into a serial byte of information by reading every bit and converting it into a high or low signal, which is sent to the RF transmitter (Linx-TX-443-LR). Once the measurement byte is sent, the loop is run 8 more times to ensure that the data is sent properly. Finally, the program exits the subfunctions and returns to the main loop where the MCU enters sleep mode and all electronics are shut off.

Power was applied to the electronic unit by use of a single 7 volt lithium battery (Sparkfun Electronics). The battery was connected to a switched mode capacitor circuit (AD660) in order to generate the negative power required by some of the components. A step down voltage regulator supplied 3.3 V to the microcontroller and RF transmitter.

B.3. Surface Mount Fabrication

Miniaturization of the electronic unit was performed by design using surface mount technology (SMT) on a printed circuit board. Surface mounted components use less power, require less space, and are reliable for long periods of time. Shown in Figure 12 are the top and bottom sides of a printed circuit board with surface mount components. Frames A-B is the design layout using EAGLE-CAD, and frames C-D show the completed electronics for a chronic system. A similar acute unit was used in the bench-top and hydrocephalic animal measurements of fluid volume.

With completion of the sensor and instrumentation, a prototype for an implantable system is conceivable. The right frame of Figure 12 shows a prototype of the implanted unit consisting of the wireless electronics, battery, sensor, and shunt to drain CSF. Future work consists of testing this unit in bench-top and animal models for long-term volume monitoring.

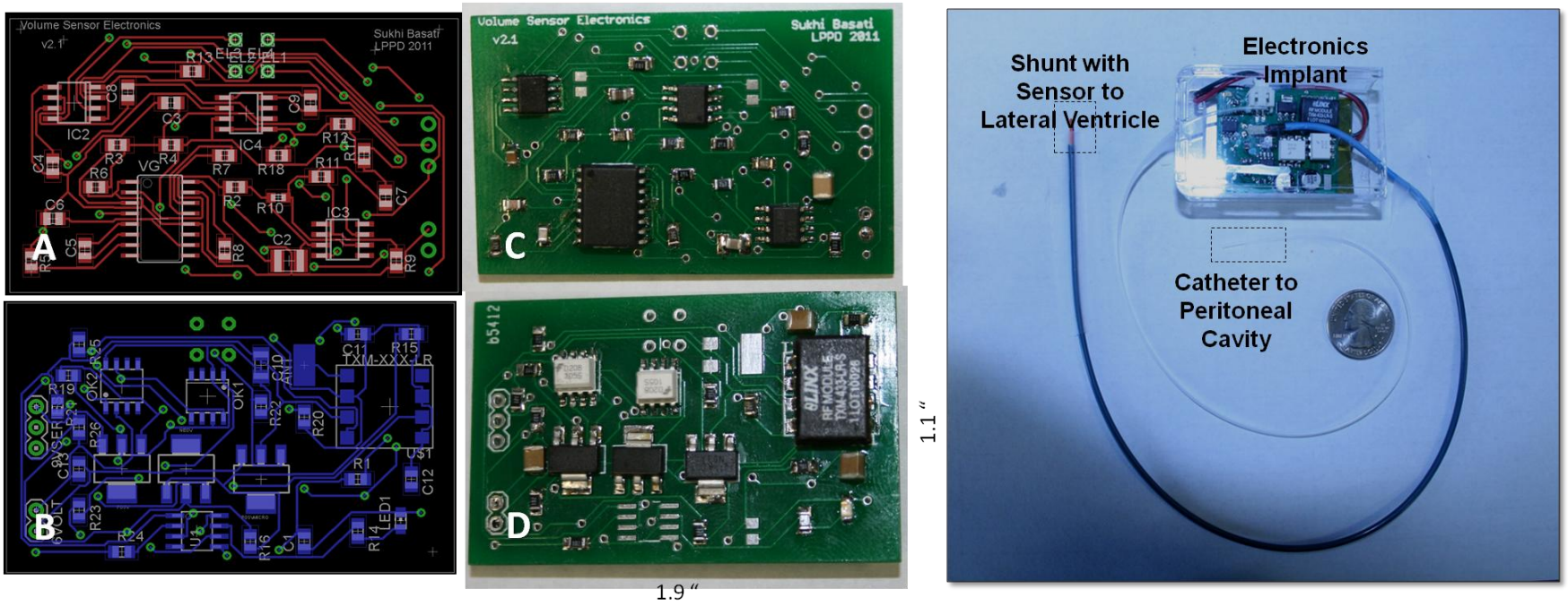

Figure 12. Instrumentation Fabrication and implantable system prototype. Frames A-B shows the component layout on the top and bottom side respectively. Frames C-D shows the fabricated instrumentation. The figure on the right shows a prototype implantable system for volume monitoring.

C. Sensor and Instrumentation Results

C.1. Sensor Characteristics

Implanted medical devices that emit or record electrical signals must undergo rigorous analysis of the interface between the electrode/electrolyte. Impedance changes, caused by charge depletion, tissue coverage, or wire detachment, may cause the resultant signal magnitude to be different than intended. Electrical impedance spectroscopy (EIS) is a test performed to characterize the interface between the electrode/electrolyte. This test consists of a three-electrode setup where current is applied between two, and voltage potential is recorded in the electrode under study. Rigorous EIS testing was not necessary for our sensor, because the sensor materials are currently used clinically and the interface between platinum/iridium (90-10%) and cerebrospinal fluid has been well researched. Therefore, the only quantitative study performed with the sensor was drift measurements.

In a series of tests, the interconnect system of each fabricated sensor was attached to the electronics and the sensor was placed into beakers of saline for drift measurements. The analog output from the instrumentation was stored with Labview using a data acquisition card (National Instruments) with a sampling rate of 10,000.

C.2. Instrumentation Characteristics

The performance of the instrumentation with known impedance was important to assess prior to animal experimentation. Electronic characterization was performed on the bench-top using a resistor decade box. Current output magnitude and gain were adjusted in order to maximize sensitivity to volume change by replacing resistors with an SMD rework station (Aoyue Int968). Figure 13 shows the current linearity in frame A with impedance changes using the decade box. The dashed box shows

impedance ranges due to volume change in the lateral ventricles of a hydrocephalic rat. Specific dimensions and conductivity were used to calculate an impedance range of 100-1300 ohms. Frame B of shows a time evolution due to impedance changes.

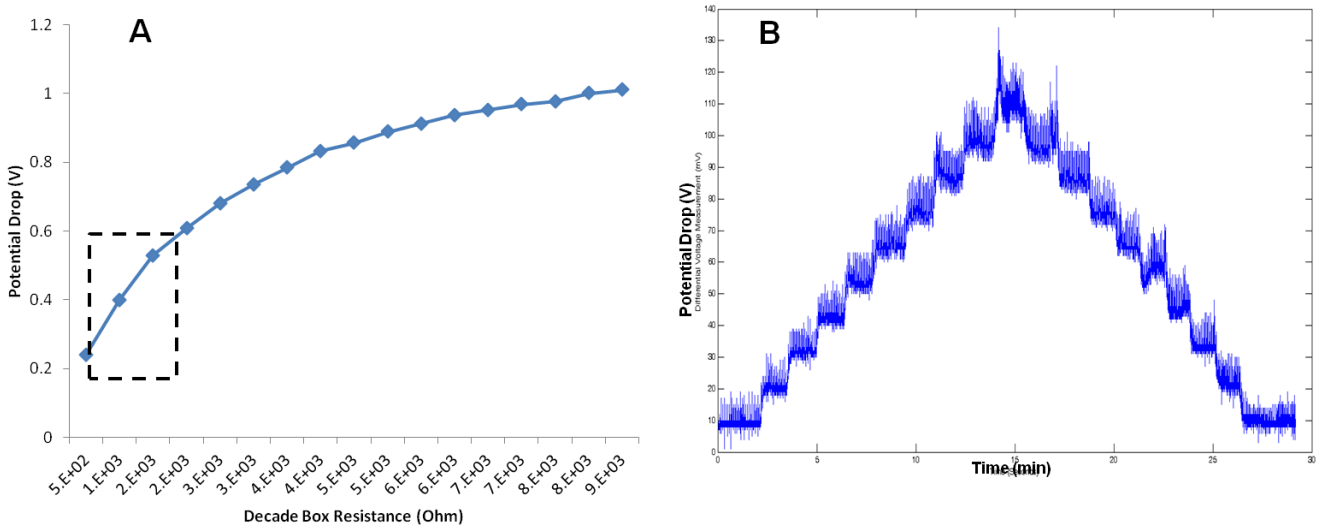

Figure 13. Instrumentation Characterization. Frame A shows the potential drop across a resistor decade box. The dashed region is the impedance change due to 100 µL volume change in the ventricular system. Frame B shows the dynamic potential reading of the dashed region.

D. Discussion

This chapter was devoted towards understanding the electronic design of an implantable diagnostic system for CSF volume monitoring. An acute electronic system was first demonstrated for measurement and analysis using Labview. This system was implemented in the rat hydrocephalic experiments. A long-term system for chronic implantation was also developed with a microcontroller and RF technology. Further development may consist of inductive operation, where a physician holds an

external receiver near the implant that powers the device. The main requisite for this thesis has been to assess the feasibility of volume monitoring.

D.1. Novel Design Decisions

Careful consideration was taken during the design of the implantable unit. Design considerations included *i)* battery operation, *ii)* wireless operation, and *iii)* future micro-pump integration. The unit demonstrated in this chapter implements these choices as well as many novel decisions.

The sleep mode of the MCU is unique in that it allows for the instrumentation to be duty cycled. Therefore, the battery life was greatly enhanced. The production rate of CSF is low enough for periodic measurements. If there was charge accumulation occurring at the electrode interface, the duty cycle will allow for the charge to dissipate. This phenomenon often occurs during continuous signal excitation in fluids. Another unique design decision is the single battery supply of the electronics. An initial design consisted of multiple power sources for the MCU and other integrated circuits, but the size was much larger.

E. Conclusions and Significance

This chapter presented the fabrication of the sensor and electronics required for CSF volume monitoring. The next few chapters demonstrate the feasibility of the sensor and electronics in bench-top and animal models of hydrocephalus.

The significance of custom designed instrumentation is the flexibility in specifications. For instance, pressure transducers and the associated electronics can easily be included to the diagnostic system. Future control elements such as a micro-pump for fluid volume control will interface with the microcontroller. Proportional-integrative-derivative (PID) control schemes, or even adaptive control schemes can also be programmed. Further development of the instrumentation will reduce the size and

power of the electronic unit. Most likely, application-specific-integrated-circuits will be used. These decisions warrant microelectronic knowledge for the design of implantable diagnostic devices.

The sensor fabrication process resulted in 500 µm outer diameter sensors. Several constraints were imposed on the fabrication as a result of the selection of the animal model. Hydrocephalic rats were chosen to assess the feasibility of volume monitoring. Therefore, the maximum spacing between the excitatory and measurement electrodes was 5 mm. Also, the diameter of the catheter was limited to 500 µm. The significance of custom sensor fabrication was that it allowed for novel design decisions such as the internal shunt to be included.

IV. BENCH-TOP CHARACTERIZATION

Summary

Knowledge of intracranial ventricular volume is important for the treatment of hydrocephalus, a disease in which cerebrospinal fluid accumulates in the brain. Current monitoring options involve magnetic resonance imaging or pressure monitors (InSite, Medtronic). However, there are no existing methods for continuous cerebral ventricle volume measurements. In order to test a novel impedance sensor for direct ventricular volume measurements a bench-top model that emulates the electrical properties of the brain and ventricles is presented. In addition, a separate model for the expansion of the lateral ventricles seen in hydrocephalus is demonstrated. To quantify the ventricular volume, sensor prototypes were fabricated and tested with these experimental models. Sensor sensitivity was estimated using the static bench-top model, while fluid was injected and withdrawn cyclically in a controlled manner in the dynamic model where volume measurements were tracked over eight hours. The results from the bench-top models served to calibrate the sensor for preliminary animal experiments. This method of testing new designs on brain phantoms prior to animal experimentation accelerated the medical device design by determining sensor specifications and optimization in a rational process.

A. Background

The ventricular system of the brain is composed of two lateral ventricles, one in each of the hemispheres. Centrally placed are the third and fourth ventricle from which CSF passes into the cerebral subarachnoid space via the foramen of Lushke and foramen of Monroe. In diseases such as hydrocephalus, the ventricular spaces may expand drastically. The lateral ventricles undergo the largest expansion often from 1 mL up to 30 mL, while the third ventricle may grow from 1 to 8 mL. In order to assess the feasibility of volume measurements for hydrocephalus monitoring, a bench-top model mimicking the expansion seen in the lateral ventricles is needed. A full model of the entire ventricular

system is not necessary. Figure 14 shows a three dimensional model of normal and enlarged ventricles reconstructed from human MRI data depicted in the top row. The enlarged ventricles are clearly discernable. The green ellipsoid in the figure shows the dimensions of a brain phantom for testing the volume sensor in this chapter.

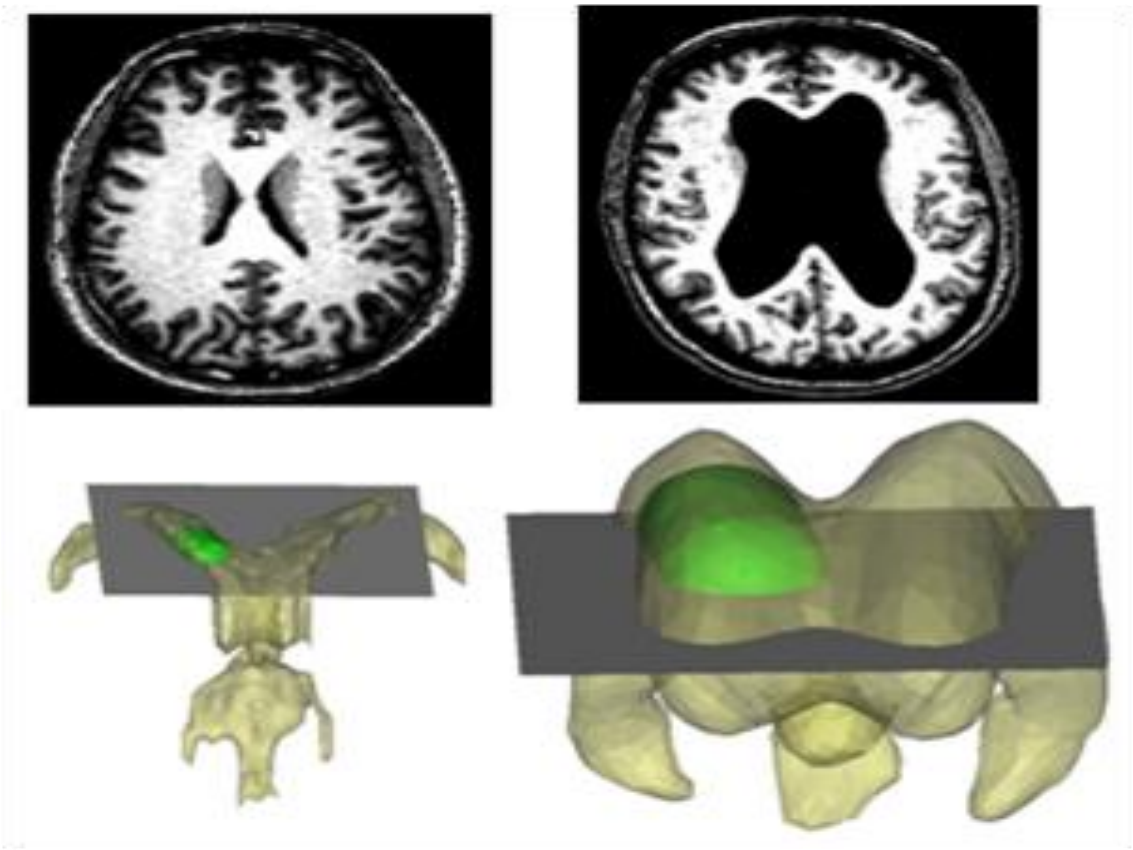

Figure 14. Two dimension MRI and three dimensional reconstructions. Bench-top models with dimensions similar to the green ellipsoid are used to emulate ventricular enlargement.

Medical device development such our novel sensor requires specification and optimization of numerous parameters. That is why testing a prototype design in bench-top surrogates is advisable. Previous bench-top models for the brain have included rigid Plexiglas models of the skull filled with

potassium chloride, or agarose gel models for electrode insertion and drug transport studies. This chapter presents bench-top agarose models with electrical characteristics similar to brain tissue as well as a deformable brain surrogate with properties similar to brain tissue under large dynamic volume expansion. Specifically, the performance of the novel sensor in an expansion of a CSF-filled cavity consistent with the expansion in the clinically relevant size range for hydrocephalus will be demonstrated.

A.2. Chapter Outline

The chapter aims at computer aided sensor design for maximum sensitivity of volume measurements and is organized as follows. Section two will introduce a computer-aided sensor design methodology for predicting the sensor response supported by state-of-the-art medical imaging data. Section three will present the computational results on two case studies with different species as a function of different design parameters. The discussion in section four suggests recommendations for future simulations for optimal sensor design. The chapter closes with conclusions.

B. Bench-top Model Methodology

B.1. Agarose Brain Phantom

In order to test sensor performance in realistic ventricular geometries, surrogate brain phantoms using three-dimensional molds of agarose gel (Sigma Aldrich) were created. These models were designed to match the conductance properties of brain tissue with artificial CSF. By adding salt, the formulation of the gel was adjusted to closely match the electrical conductivity of brain tissue. Molds of different size were created to cover the expected range of ventricular enlargement. For testing human-sized sensors the volume ranged from 2 mL to 16 mL. In this thesis, much work was done on testing rat-sized sensors on agarose models from 20 µL to 100 µL, shown in frame A of Figure 17. Volume ranges

were relevant for lateral ventricle enlargement. Agarose gel is rigid and brittle, thus limiting the possibility to do dynamic deformation tests. The gel also has the tendency to shear and crack under mechanical loads. A brain phantom that emulated dynamic physiological conditions was needed.

B.2. Clinical Dynamic Brain Phantom

Silicone gel was chosen as the dynamic surrogate for brain tissue, because its viscoelastic properties permit large expansion suitable for dynamic deformation tests. Its material strength, such as the shear modulus is similar to those found in humans during in vitro testing. Table 1 lists the elastic modulus of gel as $G_{gel} = 4.7 \times 10^{-3} Pa$, which is similar to that of brain, $G_{brain} = 2.9 \times 10^{-3} Pa$. Due to silicone gel's material properties, it can undergo large deformation without cracking or disintegration. Additionally, the dielectric property of silicone gel is critical in order to permit the distribution of an induced electric field for impedance measurements. Another advantage is its transparency, which allows for quantification of the boundary displacement.

Table 4. Comparison of phantom properties and brain tissue.

Property	Agarose Gel	Silicone Gel	Brain Tissue (Grey Matter/White Matter)
Elastic modulus	5.3 – 14 kPa	4.68 x 10^{-3} Pa [96], [97]	2.87 x 10^{-3} Pa [96], [98]
Density	.06 g/ml	.97 g/ml	1.05 g/ml [99]
Dielectric Strength	58	2.85	58.2 [100]

A realistic model was created with a ventricle-shaped cavity surrounded by silicone gel. This was achieved by using a reverse cast of the model using clay. This cast was then coated with a 1/16” layer of paraffin. The shape of the inner cavity was made to match that of a normal human ventricle of about 4 cm3 in volume. A paraffin ventricle-shaped solid was then formed on the end of a 1.5 mm polyethylene inlet tube. This tube and ventricle solid was suspended within the bounds of the reverse cast. The ventricle shell was then created with silicone dielectric gel (Dow Corning Sylgard 527 A & B). After the gel had set, the entire cast and gel was placed into boiling water in order to dissolve the reverse cast paraffin wax, leaving behind only the ventricular gel cavity.

Figure 15 shows the gel model and a schematic of the volume expansion induced by injection of artificial CSF. The dynamic, deformable ventricle model was expanded by injection and withdrawal of artificial CSF using a programmable pump (New Era Pump Systems Inc). In the human brain, cerebrospinal fluid is produced at a typical rate of 0.3 mL per hour. Therefore, this production rate was selected for fluid injection and withdrawal. Realistic ventricular volume changes were matched in the range of ±10 mL.

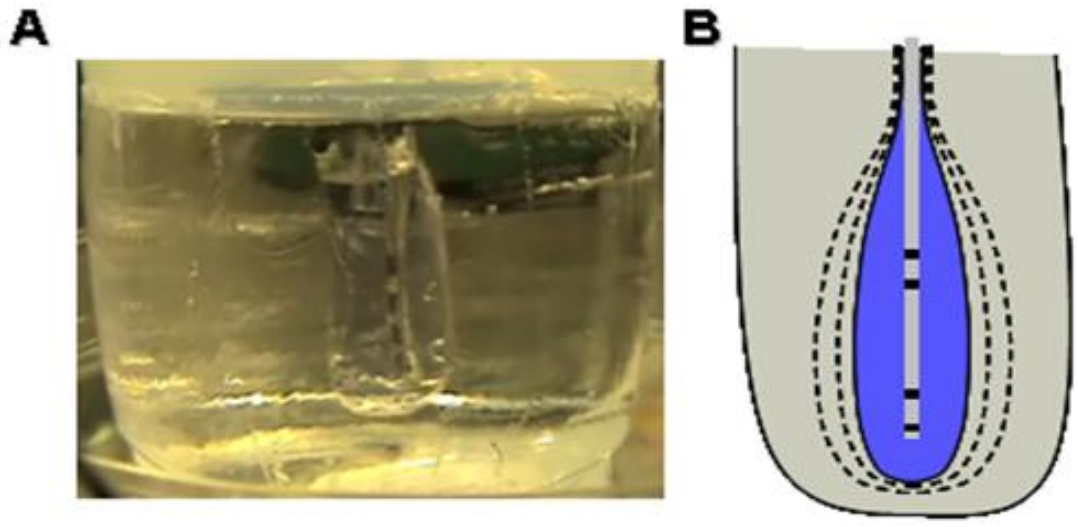

Figure 15. Dynamic brain phantom and experimental setup. A schematic showing the CSF-filled space and boundary with the gel is depicted in frame B.

B.3. Rat-sized Dynamic Brain Phantom

Dynamic testing of a bench rat-sized sensor was performed with a detachable silicone balloon (DSB) (Boston Scientific). The DSB is an artificial embolization device for selective, acute, focal endovascular occlusion of blood vessels when used in conjunction with standard percutaneous catheterization techniques. The balloon was attached to an 18-gauge needle by first drilling a hole onto the plastic needle hub above where the syringe locks onto the needle hub. The sensor was correspondingly threaded through this hole and up and out of the barrel of the needle. A MultiPro Dremel was used to cut the needle and shorten the barrel for our application. The barrel was cut horizontally and sanded down to prevent damage of the sensor. After the sensor was threaded through the barrel the next step was to use 5-minute Loctite epoxy to seal the hole. After the sensor had been threaded through the needle, the detachable silicone balloon (DSB) was then fixed to the end of the dulled needle. The DSB was modified by removing the self-sealing silicone valve that rests inside the

elastomer. Epoxy was then used to seal the connection between the silicone balloon and the barrel of the needle. Testing was done with air and saline to ensure that leaks were not present in the model. The third step in preparing the model was to add a 5 French angiography catheter onto the other side of the needle hub across from the inlet of the sensor. The tip of a syringe was used to epoxy the catheter into place. Saline was added or removed by a Harvard Apparatus syringe pump at 30 µL/min to control the volume in the balloon model. A completed model is shown in Figure 16.

Figure 16. Completed Silicone Balloon Model. The sensor is visible inside.

C. Bench-top Model Experimental Results

C.1. Dynamic Volume Expansion

Figure 17 frame C illustrates the wide range of volume expansion the dynamic human ventricular model was capable of performing. Ventricular volume from hydrocephalic patients can increase 30 times the normal size. Similarly, the model is also able to expand up to ten times the base volume. For volume increases beyond that limit, the model sheared near the fittings with the sensor. Therefore expansions beyond 30 mL were not performed.

C.2. Calibration of Sensor for Volume Output

To convert measured voltage values to volume, a relationship between volume and time was created in calibration experiments using the brain phantoms. This procedure related voltage and volume for each individual sensor. An exponential decay was used to closely approximate the voltage-volume relationship.

Figure 17 frames B and D shows the calibration curve plotted in MATLAB. Equation (6) was then used to convert subsequent voltage measurements into calculated volume, with the fitted parameters: $\alpha=1.23$, $\beta=2.9$, $\gamma=573$, and $\delta=.43$.

$$Volume=\alpha\cdot e^{-\beta\cdot voltage}+\gamma\cdot e^{-\delta\cdot voltage} \qquad (6)$$

While the dynamic measurements were used to assess the tracking capabilities in a human-sized gel phantom, we needed to assess the performance of the rat sized sensor. Therefore, we also performed measurements in agarose brain phantoms. Frame B of Figure 17 shows the results of a calibration curve with the rat sized sensor.

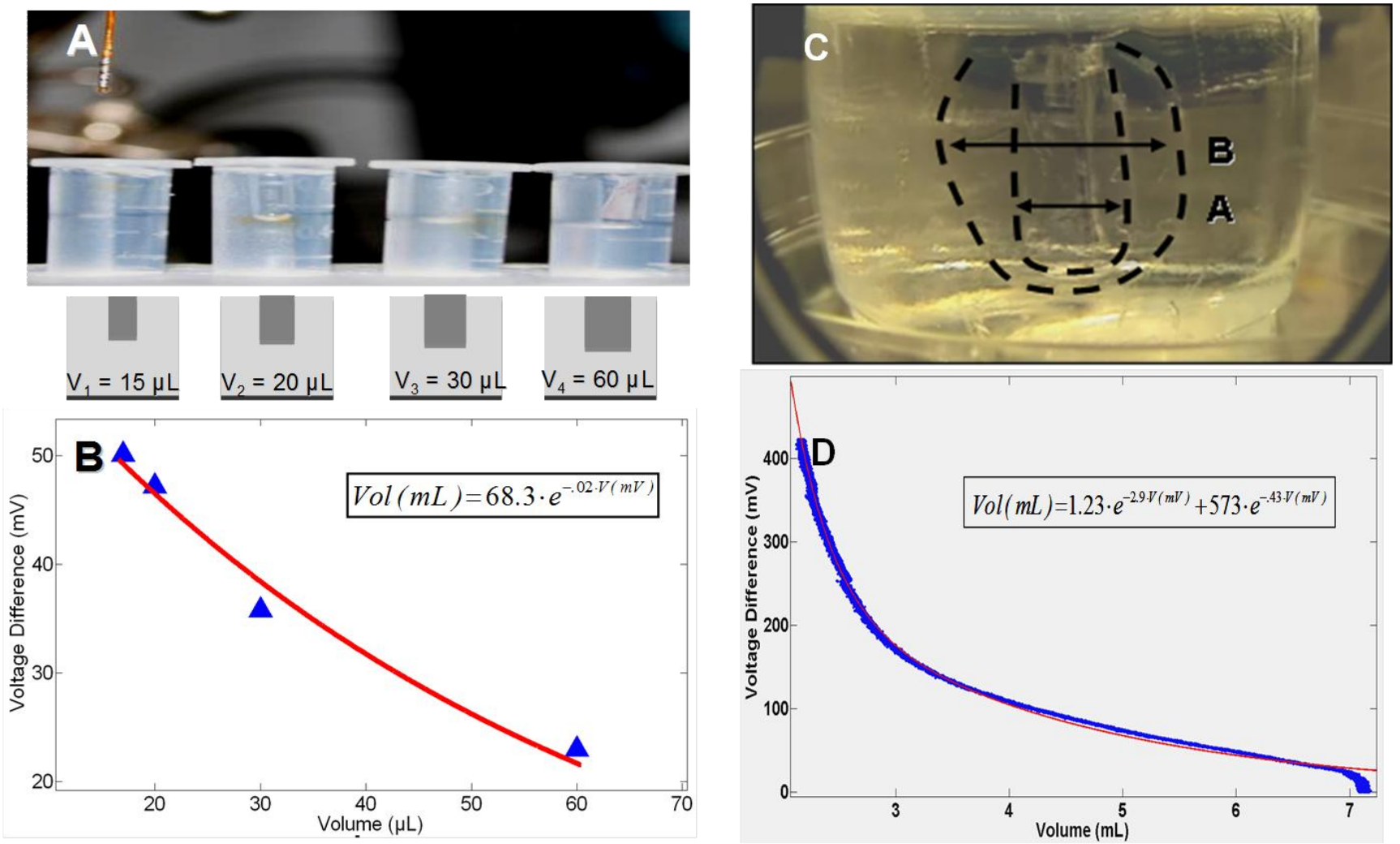

Figure 17. Two different bench-top models used to test prototypes. Frame A illustrates placing the rat-sized sensor in cavities of different volume in agarose gel. Frame B shows the calibration curve used to convert subsequent measurements into volume. Frames C and D show the dynamic response with the human-sized sensor.

The DSB model allowed for expansions seen in animal models of hydrocephalus. The initial volume of the balloon was 13 µL. Volume expansion was capable up to 1000 µL but this was typically not performed. Experiments with 90 µL of fluid addition and removal were performed. Line pressure was measured with a Transpac disposable pressure sensor (ICU Medical, CA). Real-time measurements were obtained using Labview. The data was sampled at a rate of 10,000 samples per second, with a low-pass 8^{th} order Butterworth filter applied. Frame A of Figure 18 shows the voltage-volume relationship. Validation of the volume calculation technique can be seen in frame B of Figure 18, which shows converted volume and actual volume in the balloon model, with pressure shown in frame C.

Dynamic pressure and volume was recorded in the balloon model. Appendix B shows the volume sensor voltage measurements with pressure shown below. The compliance of the balloon was observable due to the small dynamic increase in pressure as volume was reduced.

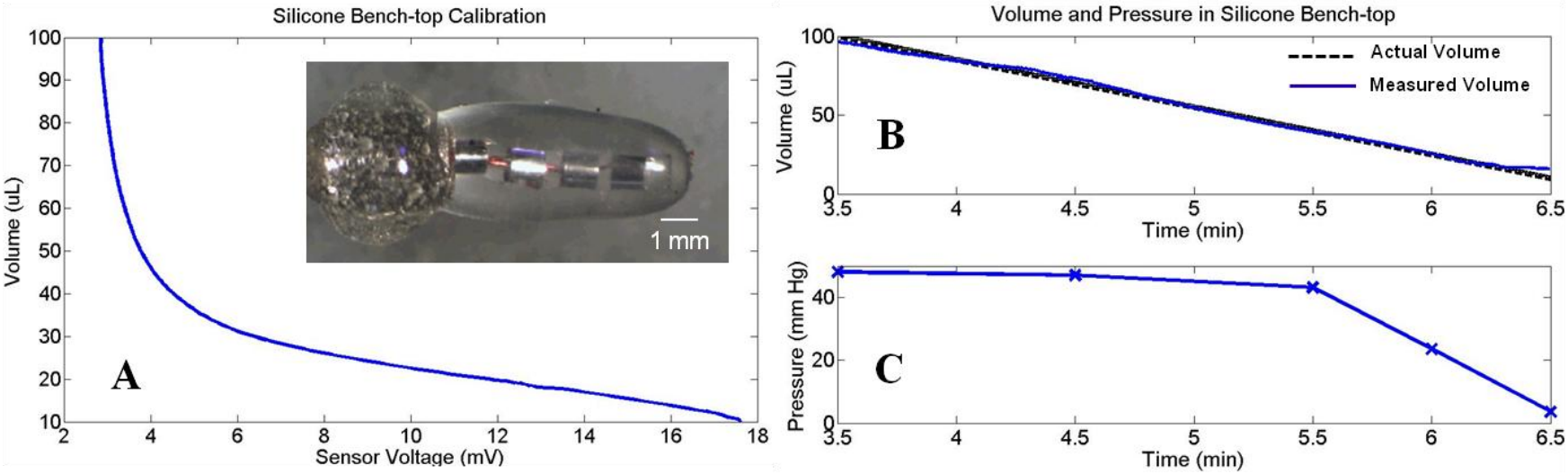

Figure 18. Silicone balloon calibration experiment. The sensor is placed in a silicone balloon whose size can easily be manipulated by adding fluid through a syringe pump shown in frame C. A comparison of frames A and B show a slight increase in pressure while volume decreases, which indicates independence of pressure and volume.

C.3. Dynamic Volume Measurements under Cyclic Conditions

In order to test the sensitivity of the sensor for the purpose of tracking ventricular volume dynamically, controlled volume changes were performed in the brain surrogate. These experiments allowed for an accurate comparison between the actual volume and the sensor reading. To test the dynamic tracking capabilities of the sensor, a triangle function for expanding the surrogate cavity size was programmed using a syringe pump. After specifying an increase and decrease cycle, total system volume remained constant over time; the peak volume addition was 10 mL.

Figure 19 shows a volume reading measured by the sensor as a function of time. Ten cycles were averaged and plotted using MATLAB. The maximum standard deviation was ±1.6 mL. The largest deviation occurred during the peak of the cycle as expected. One period of fluid injection lasted six hours in order to emulate CSF clearance.

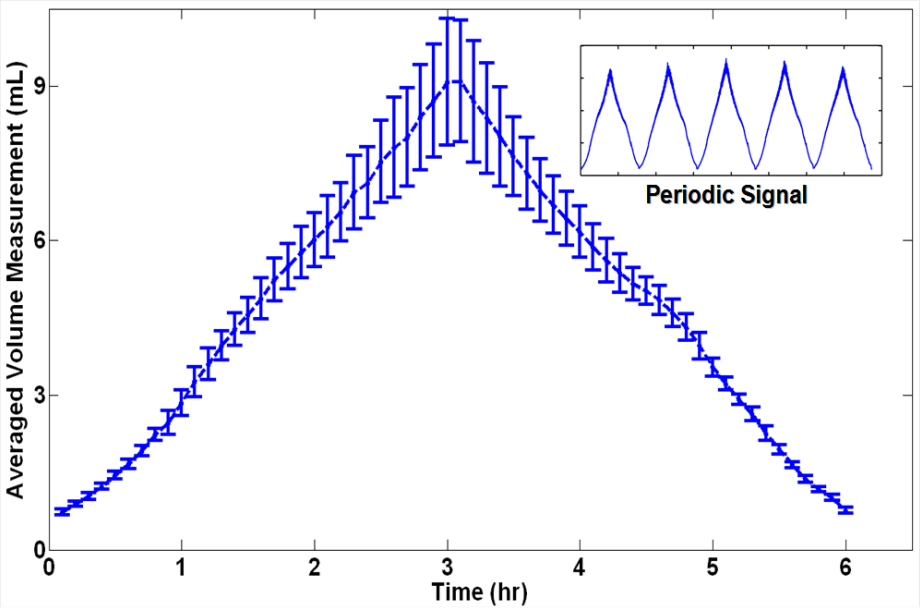

Figure 19. Cyclic volume injection. The tracking capabilities of the sensor are shown in a bench-top test. Fluid is injected cyclically into the brain phantom with a period of 6 hours over 48 hours of experimental duration. The voltage measurements are converted to volume from calibration curves, and averages over ten cycles are displayed with error bars. The top inlet shows five cycles over 24 hours.

Due to the large volume change in hydrocephalic patients, the measurement range of the sensor was an important parameter. The unsaturated range for the sensor was found to amount to 10 mL. In the scaled-down sensors, the saturation range decreased due to the smaller dimensions and distances between the electrodes.

C.4. Brain Phantom Measurements with Independent Variation

In order to assess the independence of additional variables other than volume, experiments were performed with the rat sized brain phantom. The variables consisted of varying diameters, variation in cavity depth with a controlled diameter, artificial saline in comparison to real CSF recovered from surgery, sensor performance in the brain phantom and varying distance from cavity, and positional dependence within cavity. Figure 20 shows the experimental design of variables studied where *V* indicates cavity volume, *d* represents sensor position, σ represents conductivity, and *h* represents cavity height.

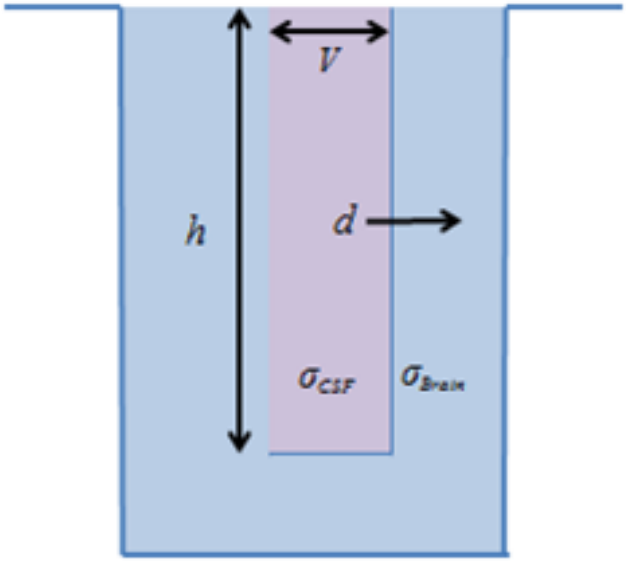

Figure 20. Parameter assessment with agarose brain phantom. The dependency of variables with brain phantom was assessed. The sensor was placed in different configurations and measurements were obtained.

To measure diameter alteration (*V* in Figure 20), four cavities were created in every trial: each with a slightly different diameter. The exact volume of NaCl in each cavity was measured using a syringe. After this, LabView was used to record voltage measurements.

Cavity height (*h* in Figure 20) was measured in a parallel, but opposite, format. In this set of experiments diameter was fixed in all of the trials. Multiple trials were completed in which a different diameter to be fixed was chosen and then depth was varied. Measurements with deeper cavities were slightly higher than comparable shallow cavities. This may be because distortion of the electric field may occur with extra NaCl in a deeper cavity, which increases the measurements. As the cavity dimensions increase, there was a general trend for the voltage to drop. Keeping a depth constant and increasing the diameter, in turn, gave a decreased voltage reading. An example of this reading is shown in appendix C.

Different salt solutions of varying concentrations were produced for signal comparison with rat CSF conductivity (σ in Figure 20). Each solution was placed in identical Eppendorf tubes filled to the same level as the cerebrospinal fluid. The test tubes were held in place by a solid support, and a stereotactic frame was employed. Readings were then measured in an identical position inside each cavity for a 20-second period of time to ensure a steady-state result. The contents of each test tube were mixed prior to each trial to ensure a homogeneous solution in which the solutes remain mixed. Voltage readings when in CSF matched most closely to the .08% NaCl solution. The results are in appendix C.

A problem during surgery with rats is the placement of the sensor. Implantation error into the ventricles was understood by measuring the sensor response when inside brain tissue. Plastic polystyrene test tubes, filled with agarose gel and a .08% NaCl solution were used to prepare these

models. The sensor response was measured in millimeter partitions away from the edge of a distal cavity. Cavities had a controlled depth for each trial, but different diameters were tested. The region closest to the cavity was important to note because these readings show that measurements were lower. Readings, shown in Figure 21, stabilize at about 4 mm away from the edge of the cavity. There was an increase in voltage 7 mm away from the cavity, but that may be due primarily to electric field alteration. It was clear from prior experimentation that when the sensor was placed in the center of cavities with different volumes, the voltage changes. However, the sensor performance was not predictable when placed in the brain tissue. The results show that when the sensor is placed between 1 and 2 mm away from the cavity edge, the cavity still influences a change in the voltage measured.

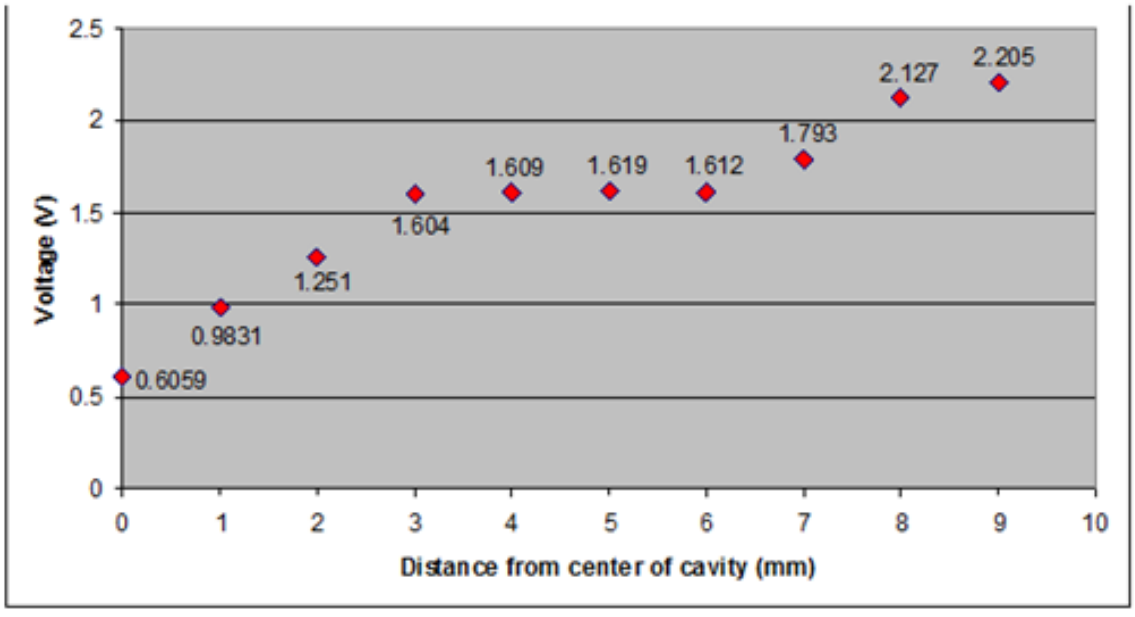

Figure 21. Sensor displacements within brain phantom.

Figure 22 shows readings in the center with various volumes. Each line represents a certain distance away from the cavity. The average is the sensor measurement directly inside the cavity. The next line, "1 mm away avg.", shows that it also follows the same slope as the original line. The slopes due to the change in volume indicate similar change in voltage for each of the sets of data. At 2 mm away, there is still a change in resistance. At 2 mm away from the cavity, the sensor was not able to effectively measure voltage of the cavity.

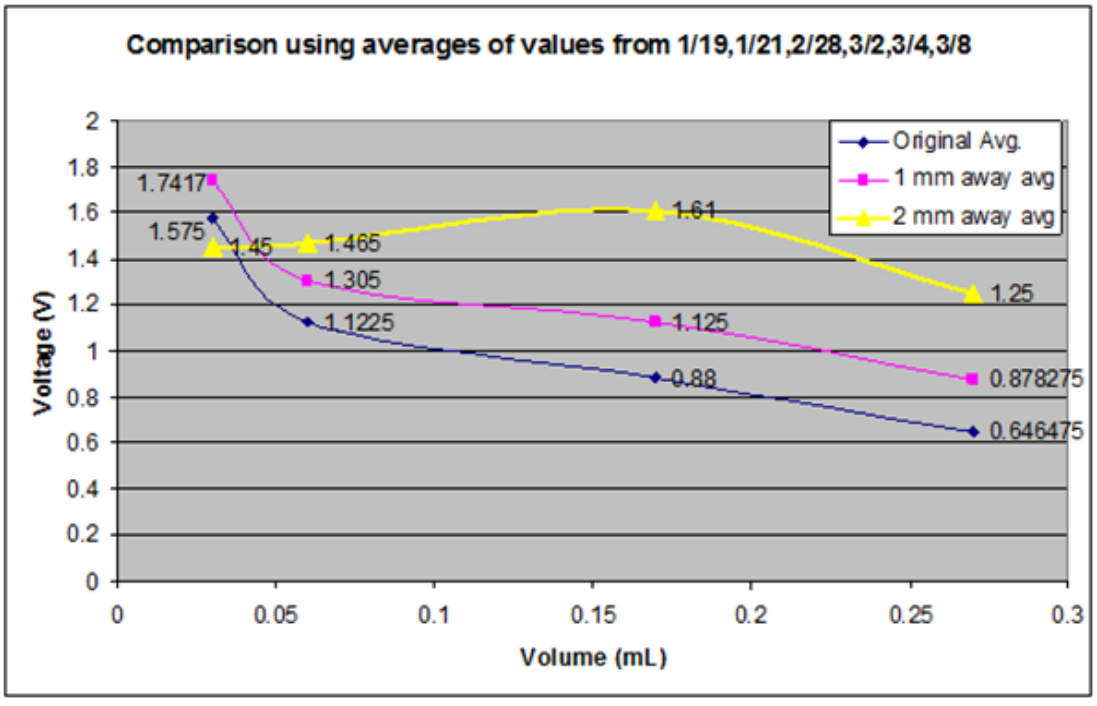

Figure 22. Sensor displacements as a function of volume.

The final variable studied was sensor positional dependence. A sweep within the cavity from left wall to right wall at a constant height was done using a stereo-tactic frame to analyze changes in measurement based on the relative position of the sensor. In addition, the same sweep was also done in 1 mm steps using the stereo-tactic frame.

D. Discussion

The clinical dynamic models presented in this chapter were satisfactory in replicating realistic lateral ventricle expansions. Even for long cycle durations of several hours, volume measurement tracked precise size changes consistently. The size changes permitted to assess the expected accuracy of the sensor under clinical conditions where large deformation of the brain tissue allows up to 30 mL of CSF to accumulate in the frontal horns. The dynamic models were approximations to the clinical expansion of the ventricles; therefore, this model does not match the complex deformation patterns seen in humans. The frontal horns of the lateral ventricles enlarge the most, while the third and fourth ventricles enlarge minimally. The model mimicked the volumetric expansion in the frontal horns of the lateral ventricle, but did not maintain physiological shape seen in human patients. During cyclic loading, the sensor provided precise measurements in the small volume range. When in the small volume range of 1-4 mL, the standard deviation between cycles was less than 1 mL. The variances at large volumes were acceptable because the sensor could also be used for treatment of enlarged ventricles. This sensor could then be used passively and only turned on at a regular interval to track the patient's disease.

The DSB model was used to test rat-sized sensors prior to animal experimentation. The error between measured volume and actual volume was obtained.

The bench-top models allowed us to test various sensor design parameters such as inter-electrode distances, electrode surface areas, and location of measurement electrodes. The calibration of the sensor

and optimization of instrumentation parameters such as output current, filter design, and gain were also performed on the bench-top model. Preliminary measurements in an animal model are shown in the following section as a method to validate the relationships observed at the bench-top.

This article demonstrated the feasibility and sensitivity of fluid volume measurements in a dynamic brain phantom. Various gel models exist; however, our silicone gel brain surrogate permits dynamic sensor testing under conditions of realistic size expansion and cyclic loading. The expansion that occurs in the lateral ventricles of the brain due to hydrocephalus was emulated using a dielectric, viscoelastic material. The surrogate model established a protocol for testing novel devices under simulated disease states. The parameters of the microfabricated sensor system such as gain, sensitivity, and saturation could be optimized on the bench-top, before animal experimentation to reduce trial-and-error as well as unnecessary animal suffering. This process of microfabrication, testing in brain phantoms followed by animal validation is expected to provide new innovative volume monitoring options for hydrocephalic patients.

E. Conclusions and Significance

For development of the intracranial volume sensor, two sets of bench experiments on models of the brain were performed. The first model type consisted of a static-agarose model. This model allowed us to match the electrical properties of the brain and CSF. The second model consisted of a dynamic model, which demonstrated maximum sensitivity with volume change. Silicone is an insulator; therefore there is no leakage current.

Not only did the bench-top models provide calibration curves for the animal measurements, but they allowed for optimization of the instrumentation. This approach for testing novel diagnostic devices prior to animal or clinical trials is invaluable.

V. ANIMAL VALIDATION OF VOLUME MONITORING FOR HYDROCEPHALUS

Summary

This chapter presents measurements with the volume sensor in an animal model of hydrocephalus. Intracranial compliance has been postulated to change during hydrocephalus; however, experimental data about the evolution of intracranial pressure and ventricular volume is limited due to the lack of available monitoring techniques. In this chapter, intracranial fluid volume using impedance sensors simultaneously with pressure transducers in hydrocephalic animals are tested. Line pressure was measured via a disposable Transpac pressure transducer. Bench-top calibration experiments provided relationships in the 10 to 150 μL volume range. Hydrocephalus was induced in weanling rats by kaolin injection into the cisterna magna. At 28 days post-induction, the sensor was implanted into the lateral ventricles and a shunting/infusion protocol was performed acutely. Implant location was confirmed via x-ray imaging with iohexol contrast. Results suggest that tissue compliance throughout the intracranial system is affected by the hydrocephalic state. The significance of this work stems from the lack of brain compliance research for cases of hydrocephalus. The overall clinical application is to provide alternative monitoring options for hydrocephalic patients. Future work includes testing a chronic or long-term volume monitoring system.

A. Introduction

The dynamics of ventricular enlargement remain elusive to researchers of hydrocephalus, a disease where cerebrospinal fluid (CSF) accumulates in the ventricles. In normal pressure hydrocephalus (NPH), the observable CSF flow pathway remains open yet the ventricles remain enlarged despite normal intracranial pressure (ICP). This leads to an initially elevated intracranial pressure within the ventricles while the volume expands. In a canine model of hydrocephalus we showed a small transmantle pressure gradient observed in animals whose ventricles enlarged [12] while other

researchers contend that a high pressure gradient exists [101-102]. A reduction in CSF reabsorption caused by a decrease in vascular compliance may also cause the ventricles to enlarge with low intracranial pressure [11, 103]. There has also been evidence that lymphatic drainage of CSF is hindered in animals which may result in CSF accumulation [104]. Other researchers have shown an intracranial pressure (ICP) amplitude difference in normal and idiopathic NPH patients, which suggests a decrease in tissue compliance [105].

The exact pathophysiology of hydrocephalus is likely caused by the aforementioned observations. A reason for the multitude of speculated mechanisms is that there are few available tools to measure the dynamic properties of brain and CSF. Therefore, few experimental data are available to support different hypotheses. Recently, CINE-MRI has been used to obtain quantitative information on pressure, velocity, and volume during the cardiac cycle [79]. Researchers have also developed innovative systems such as the capacitive ICP sensors [106] or the micro-valves for shunts [107], however there are currently no devices to continuously monitor volume directly. The only available option for researchers to *chronically* obtain data on intracranial dynamics is via pressure transducers.

A.1. Previous Rat Hydrocephalus Research

In the weanling rat hydrocephalic model, sterile kaolin clay is injected into the cisterna magna. This method of inducing hydrocephalus has been experimentally shown to block the reabsorption of CSF, which causes extreme ventricular enlargement [108]. It also closely approximates the type of ventricular expansion seen in human infants [82]. Much research has also been done with this animal model in relating structural and behavioral changes as the disease progresses [83, 109]. Histological measurements show a reduction in ventricular size after shunt treatment in hydrocephalic weanling rats [110]. In a recent study, acute ICP measurements were obtained in an infusion protocol with

hydrocephalic rats [111]. In this chapter, acute measurements with volume and pressure measurements in an animal model of hydrocephalus as a first step towards understanding compliance and a novel monitoring system is presented.

A.2. Chapter Outline

In this chapter, volume and pressure measurements are validated in an animal model of hydrocephalus as a first step towards understanding dynamic properties of brain tissue. The chapter is organized as follows. Volume sensor and hardware setup are described first, followed by *in-vitro* calibration with bench-top models. The induction of hydrocephalus and the *in-vivo* experiment are described next followed by imaging confirmation of the sensor implant. The results section provides dynamic volume and pressure data with measurement error followed by the conclusions section.

B. Methodology

B.1. Experimental Methodology

The volume sensor consists of a catheter with several pairs of ring electrodes. Many commercial devices with similar designs exist. However, the size constraints posed by the hydrocephalic rat model do not allow for their use; the outer diameter of most commercially available devices is typically 1 mm, whereas sensors to fit inside hydrocephalic rat ventricles are required. The enlarged ventricles allow for an assessment of the technique with simple fabrication. A stack of MR images was obtained to create a three dimensional representation. Axial slices of the rat brain were obtained pre-induction and 1, 3, 7, 14, and 21 days post induction of hydrocephalus. Sensors were then designed using the CAD module in MIMICS (Materialise, Belgium) noting the electrode distance and catheter diameter.

In order to fabricate the sensor, holes were drilled in a 1 Fr diameter silicone tube using a dicing saw at the Nanotechnology Core Facility at the University of Illinois of Chicago. Wires were then passed through these holes to nano-connectors (Omnetics, MN) which lock the sensor to its instrumentation. The wires protruding from the hole were bonded to platinum/iridium cylinders (Johnson-Matthey Medical, PA), to create catheters with ring electrodes. A smaller diameter polyimide tube was inserted as a shunt. The tip of the shunt catheter was beveled to ensure that the brain tissue did not cave in during insertion. Silicone sealant was applied on the boundary of the catheter to seal the gap space. The total outer diameter of our device shown in frame B of Figure 23 did not exceed 600 µm.

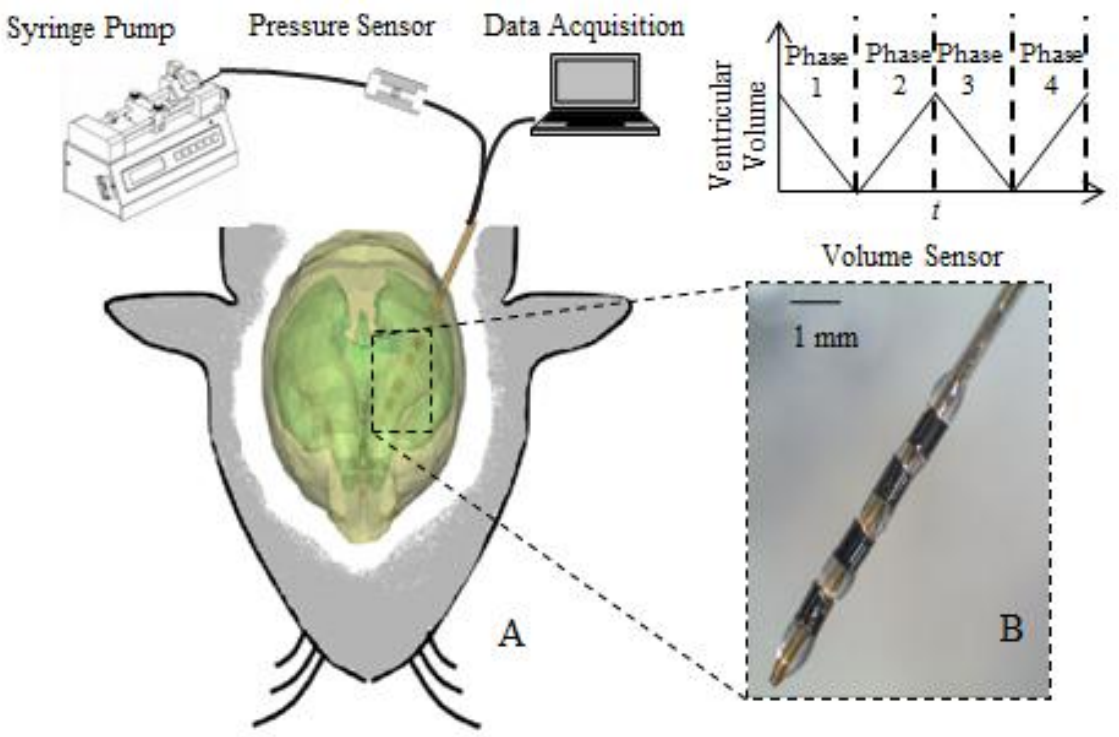

Figure 23. Volume and pressure measurement protocol. A volume sensor is implanted into the lateral ventricles of a hydrocephalic rat. An acute procedure consisting of shunting and injecting is performed using a syringe pump. Volume and pressure is recorded dynamically 10,000 times per second.

B.2. Brain Phantom Calibration

Sensors were tested in brain phantoms and silicone balloon models prior to animal testing for calibration. The brain phantom consisted of 0.02% NaCl / 0.6% agarose gel in order to exactly match brain tissue: CSF electrical conductivity ratio of 12:1 [50]. The volume in the brain phantom ranged from 15 µL to 150 µL. Measurements were obtained by repeatedly placing the sensor in four cavities of the gel, which were chosen to cover the ventricular volume range in normal to hydrocephalic rats. The known relationship between voltage and volume was used to calculate CSF volume in the animal model.

B.3. Acute Rat Surgery

An acute experiment was designed which consisted of removing excess CSF from the ventricles of a hydrocephalic rat. The outcome was to measure dynamic volume change. Frame A of Figure 25 shows an image of the surgical procedure in a 28 day hydrocephalic rat. Animal experiments were approved by the Animal Care and Use Committee at the University of Illinois at Chicago. Animals were weighed prior to induction of hydrocephalus and regularly throughout the experimental endpoint. 15 three-week old Sprague Dawley rats were injected with 20 µL of 25% w/v sterile kaolin suspension into the cisterna magna using a 26 gauge needle. The necks of the animals were flexed in order to expose the atlanto-occipital membrane. Proper implant into the cistern magna was confirmed when a "pop" was felt during injection. Buprenorphine was administered prior to recovery. The animals were allowed to recover from anesthesia and were closely monitored after injection. Weights of kaolin-injected animals were compared to the weights of control animals; kaolin-injected animals exhibiting qualitative retarded weight gain, dome-shaped head and gait instability were considered hydrocephalic [112], and hydrocephalus was quantitatively verified post-mortem. The weight and score of hydrocephalus assessment are shown in Figure 24. The surgical protocol is described in detail in appendix D.

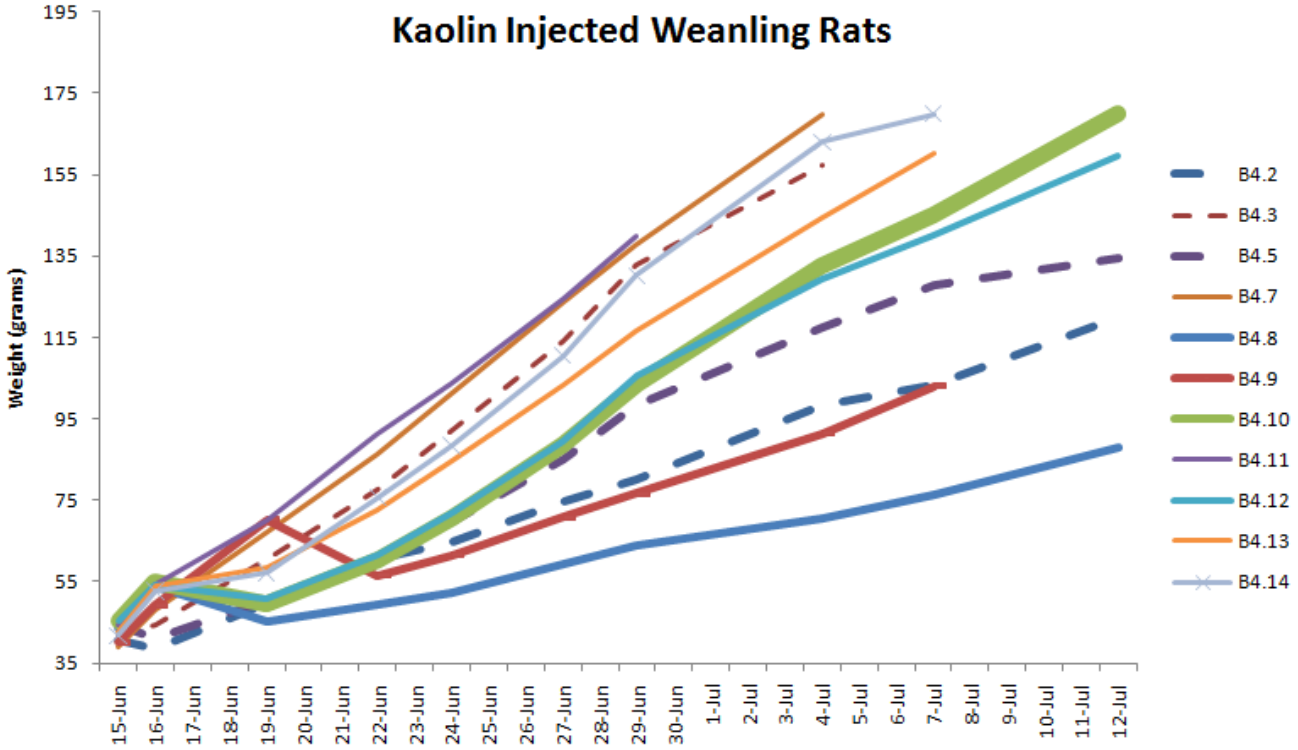

Figure 24. Weights of kaolin-injected rats. The thickness of the line represents the assessment of hydrocephalus via visual observation of dome-shaped head and gait instability.

Four weeks following the induction of hydrocephalus in the rats, the sensor was implanted and measurements during shunting and infusion were obtained. In each hydrocephalic rat, a burr hole was made and the sensor was stereotaxically implanted in the lateral ventricle 8.0 mm anterior, 1.5 mm medial, and 4.0-6.0 mm ventral to lambda [113]. Dental cement was applied over the burr-hole to prevent fluid leakage. A shunting/infusion protocol was performed with rates similar to normal rat CSF production of 3-5 µL/min [114]. This was done in order to match physiological parameters. In the protocol, CSF was first shunted at 3 µL/min for 10 minutes, then infused at 6 µL/min for 15 minutes, then shunted at 3 µL/min for 15 minutes, and finally infused at 30 µL/min for 4 minutes to observe a

rapid volume change. Rates were maintained with a syringe pump (Harvard Apparatus). Immediately following the experiment, the animals were sacrificed, and brains were fixed in 10% formalin.

B.4. X-ray with Contrast Imaging

X-ray with contrast injection was performed in one hydrocephalic and one non-hydrocephalic animal to assess the location of the implant, as well as to discern ventricle integrity during implantation. X-ray imaging with contrast was recently suggested for clinical diagnosis of occluded ventricles [115]. 60 µL of 250 mg/mL iohexol contrast agent was injected through the shunt, and an x-ray imaging system (Philips Integris V3000) was used. Two-dimensional dynamic images were obtained at a frame rate of 0.5 frame/second at the highest resolution of 100 µm per pixel. Frame B of Figure 25 shows the last frame with the sensor, ventricles, and skull outlined. Three-dimensional images were also obtained using the rotational arm of the X-ray machine; however the resolution was of poor quality for reconstruction.

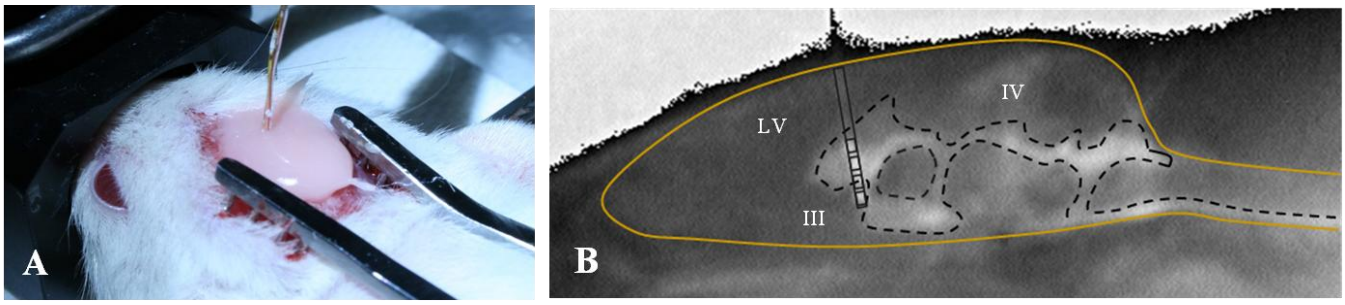

Figure 25. Surgical sensor placement. The surgical procedure implant is shown in frame A, while frame B shows an x-ray with contrast injected into the hydrocephalic animal. The sensor and ventricular system are outlined by a dashed line. The skull is outlined in a solid line for better visibility.

C. Results

Three dimensional models show a 3000% increase of CSF volume within the ventricles of a weanling hydrocephalic rat. At 14 days post induction of hydrocephalus, 300 µL of CSF is present

within the ventricular system. At 21 days, the ventricles contain up to 340 µL of CSF. According to the computer-aided sensor design, a 600 µm outer diameter sensor with a total electrode distance of 5 mm is sufficient to fit inside the enlarged ventricles of a 28 day hydrocephalic rat. The lateral ventricles were chosen to implant the sensor because the surface area of that region is larger than any other part. They also expand the largest during hydrocephalus. Therefore, it was presumed to be the most compliant region of the brain and permissible for acute CSF volume change.

C.1. Sensor Measurements in Hydrocephalic Animals

Voltage measurements from the volume sensor due to sequential shunting and infusion in hydrocephalic rats are shown in Figure 26. Each column represents a subsequent procedure. Run 1 consisted of first shunting the HC animals at 3 µL/min for 10 minutes in order to reduce CSF volume. The next procedure, run 2, consisted of infusing CSF back into the ventricles at a slightly higher rate of 6 µL/min for 15 minutes in order to confirm sensor functionality. Run 3 consisted of shunting CSF from the ventricles at a rate of 3 µL/min for 15 minutes in order to assess the measurement similarity from the first run. The last run consisted of high flow rate infusion, 30 µL/min for 4 minutes. Prior to the shunting and infusion protocol, drift measurements were obtained during hardening of the dental cement. Drift was minimal and was less than 2% of the voltage measurement. Results were plotted using MATLAB with a moving average filter. The data sampled was continuous; sample points were reduced in order to observe the general trend. During sensor implantation in one animal, bleeding occurred which affected the sensor measurements, shown in row two of Figure 26. Calibration was applied to each dataset in order to convert the measurements into relative volume. The average and standard deviation (N=4 animals) from the hydrocephalic animals are plotted in Figure 27.

C.2. Volume and Pressure Measurements

Calibrated volume is plotted with pressure in Figure 29 to understand the dynamics of shunting and infusion. In the infusion runs 2 and 4, the volume sensor did not detect the full amount of fluid injected from the syringe pump. The pressure measurements in these two runs also do not match data published recently on ICP measurements with acute infusions [111]. The incorrect measurements may be due to CSF leakage through our burr hole. Despite rigorous efforts to seal with dental cement a minute amount of fluid may have leaked into the gap space.

C.3. Statistics of Measurement

Measurements of CSF volume reduction for the assessment of treatment efficacy must maintain high accuracy. The actual volumes during shunting hydrocephalic rats are plotted against the measured volume for shunting and infusion. The Pearson correlation coefficient during the CSF shunting (run 1, 3) were (R^2= 0.99, 0.98) respectively with an error of 12%. CSF infusion (run 2, 4) were less accurate with an error of 75%; however the Pearson correlation coefficient of (R^2= 0.97, 0.98) respectively, is acceptable for monitoring CSF accumulation. The difference in the recorded error between CSF infusion and drainage is related to the fact that CSF infusion into hydrocephalic ventricles was associated with CSF leakage around the implanted sensor. This is further confirmed by the relationship of the recorded pressure and volumes infused (runs 2, 4 Figure 29) where there is unexpected plateau of the pressure as volume continued to be infused, a phenomena that can only be explained by CSF leakage around the sensor, resulting in plateau of the pressure recorded as well as lack of change of the volume recorded.

The Bland-Altman method allows for a comparison of measurement data with the "gold standard" [116]. The difference between the two volumes is plotted as a function of the average of the two volumes per time. A Bland-Altman plot was generated using MATLAB for run 1. Figure 28 shows

that the mean difference between the sensor measured volume and volume controlled using a syringe pump was 4.6 µL. The code is provided in appendix E.

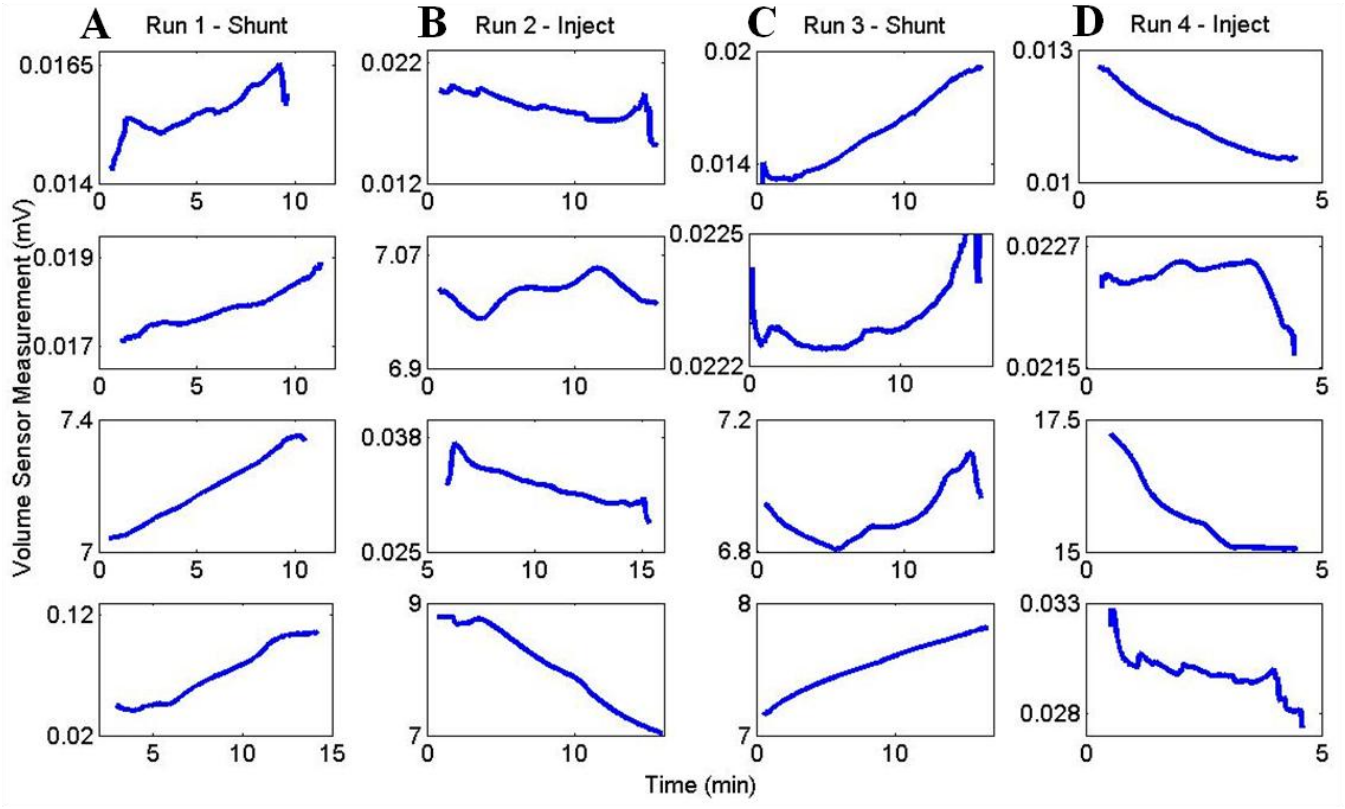

Figure 26. Sensor voltage measurements in hydrocephalic animals (N=4). Each column represents sequential experiments consisting of first shunting the HC animal. Afterwards an infusion was performed which is shown in the second column followed by shunting. The last experiment consisted of high flow rate infusion in column four.

15 animals were intra-cisternally injected with kaolin. 6 animals were removed from the study due to severe neurological impairment caused by possible brain stem injury or intra-ventricular hemorrhages. Out of the remaining animals, 5 animals displayed signs of hydrocephalus, which was confirmed post-mortem. Figure 31 shows cross-sections of a normal rat in frame A, while frames B-F show rats with increasing severity of hydrocephalus. Gross enlargement of the ventricles with compression of cortex adjacent to the ventricles was observed. The ratio between the length of the mantle and the lateral ventricle was measured.

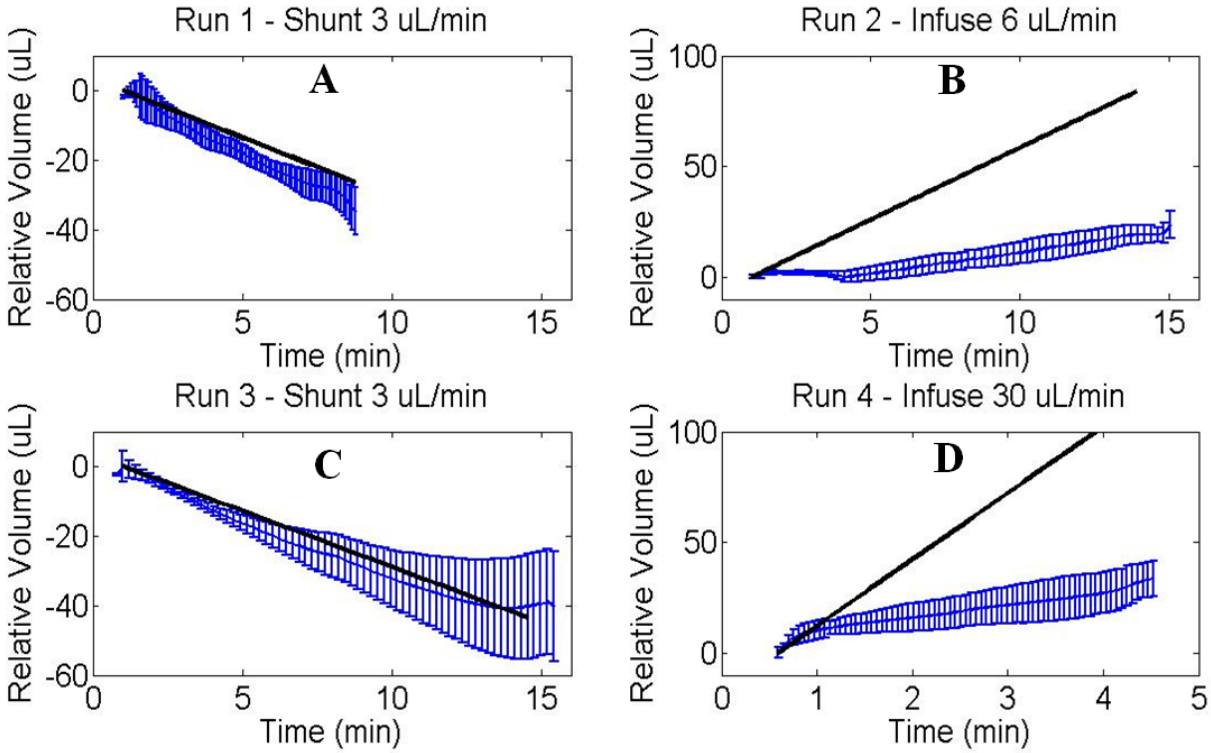

Figure 27. Average volume measurements in hydrocephalic animals. A sequential series of shunting and infusion experiments were performed in 28 day hydrocephalic rats. Frames A-D shows measurements with the impedance-based volume sensor. The volume removed using the syringe pump is shown as the solid line.

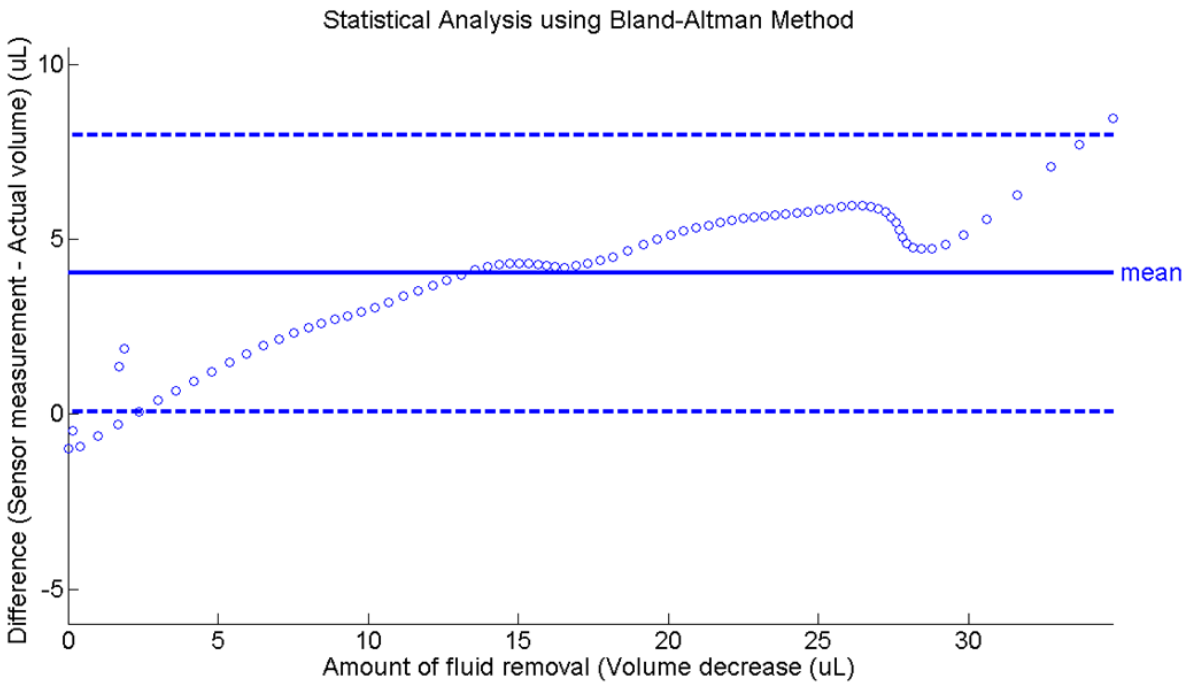

Figure 28. Bland-Altman plot in run 1 of the sensor measurements. Volume was removed using the syringe pump. The mean value of 4.6 µL represents the error.

C.4. Two Dimensional and Three Dimensional Rotational Imaging

The x-ray imaging with contrast technique allowed for an assessment of ventricular shape after implantation. A burr-hole created in a hydrocephalic skull immediately resulted in CSF leakage. Therefore, the shape of the ventricles was in question during the shunting/infusion protocol. Measurements were also obtained during imaging; however the electrical conductivity of iohexol altered the measurement and results are not shown. During imaging the infused iohexol traveled down spinal CSF more rapidly than the ventricle expanded. Each individual animal may have a different hydrocephalic state; therefore the intracranial dynamics may be slightly different.

The feasibility of performing three-dimensional volume reconstruction was performed with the Philips V3000 system. Frames A and B of Figure 30 show the highest resolution achievable with the

system. The dashed box in frame A represents the iohexol-filled balloon with 10 µL volume. An outline of the ventricular system of a hydrocephalic rat infused with iohexol is shown in frame B.

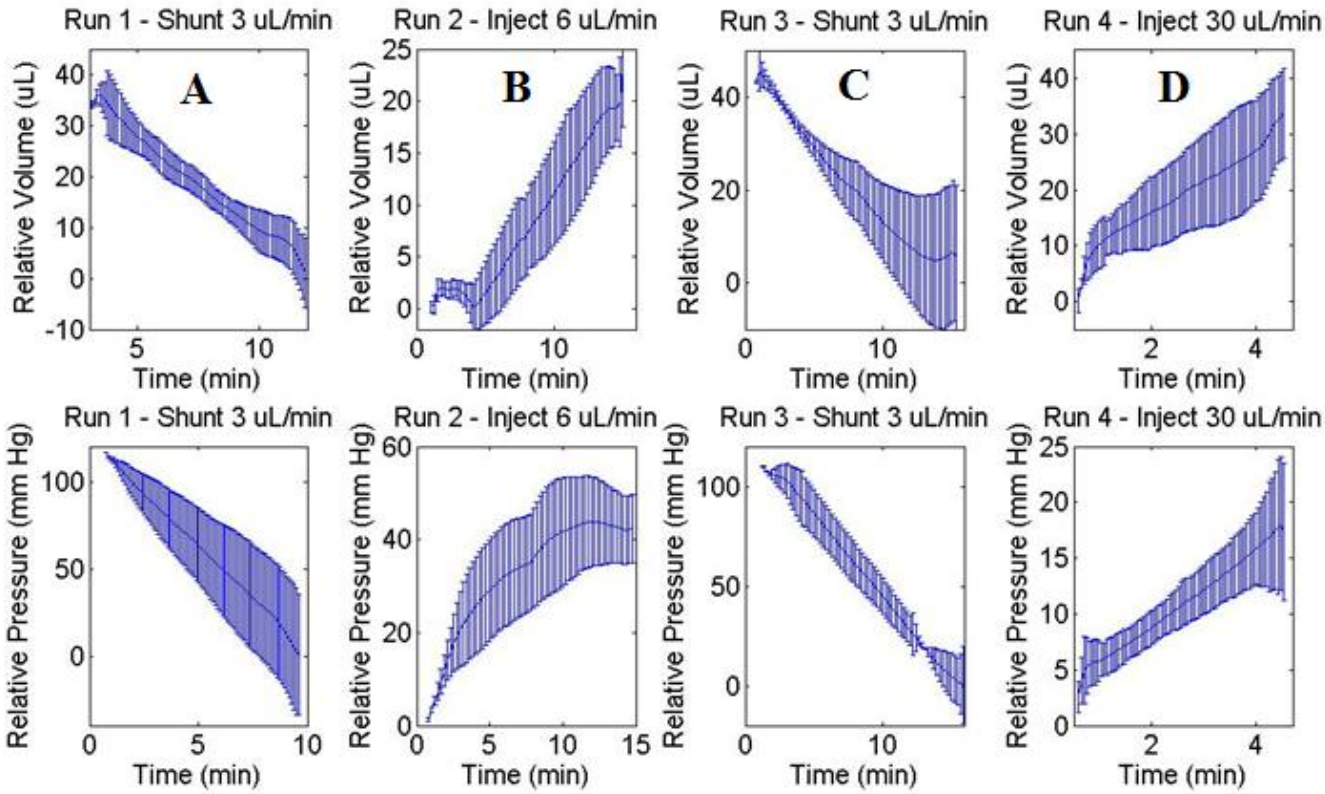

Figure 29. Volume dynamics measured during four sequential shunting/infusion protocols (frames A-D). The pressure measurements are plotted below.

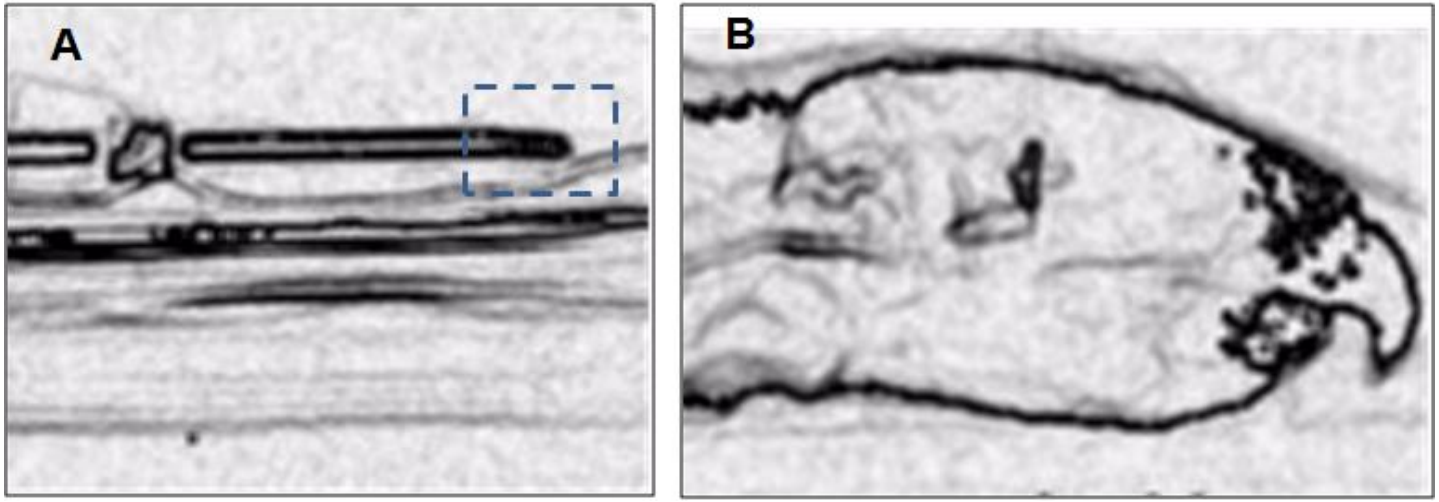

Figure 30. Two dimensional images obtained during three dimensional rotational scanning. The balloon model is shown in frame A while frame B shows the outline of the ventricular system when iohexol was infused through the shunt at 3 µL/min. Darkened regions correspond to attenuation of the x-ray or iohexol-mixed region. The low resolution did not allow for accurate three dimensional reconstructions.

D. Discussion

The experiments demonstrate dynamic measurements of CSF volume and pressure in a hydrocephalic animal. CSF volume was controlled from the ventricles of a hydrocephalic rat using a syringe pump, while local intra-ventricular volume and pressure were recorded. The volume sensor was designed and fabricated using computer aided design principles on three-dimensional reconstructions of the rat brain. Acute measurements of volume and pressure change were performed as a first step towards understanding compliance changes in hydrocephalus.

D.1. Volume Sensor Accuracy

The sensor measurements due to shunting at similar CSF production rates are precise. The sensor detected 30-35 µL of volume change in run 1, which is comparable with the 30 µL of volume removed using the syringe pump. In run 3, the sensor detected a 25-45 µL volume change due to shunting 45 µL of CSF.

The shunting and infusion procedure and dynamic measurements of intracranial volume and pressure have not been performed to the best of our knowledge. When CSF volume was controlled, a fixed rate was used; therefore the voltage-volume relationship obtained in the calibration experiments was implemented. The calibration experiments were performed using simple geometry; therefore local relative volume changes are plotted. Future experiments consist of performing a three-dimension imaging reconstruction of the ventricles before and after shunting to offset the calibration curve. This may improve the accuracy of the measurements and also allow for absolute volume as opposed to relative volume change.

The electrical conductivity ratio between CSF and brain tissue is 12:1 in the normal state [117]. However, the conductivity of CSF and brain tissue during hydrocephalus may change. This alteration

may be caused by hemorrhage, and some researchers have shown that protein concentration levels change during hydrocephalus [118]. While the water content of brain tissue has been measured under normal and pathological conditions [119-120], the changes in electrical conductivity of CSF during hydrocephalus have not been. However the change in conductivity values should not be larger than the measurement change due to large volume expansion; therefore this is not expected to alter the measurements.

When an acute shunting procedure is performed at different stages of hydrocephalus the properties of the brain tissue may lead to unusual outcomes. The high incidence of shunt failure warrant further study of CSF removal rate, tissue compliance, and volume change. Future experiments will use larger animal models with a chronic, wireless volume-pressure monitoring system. These measurements, coupled with high-resolution MR imaging may allow for long-term compliance studies of brain tissue.

The outcome of this chapter is a validation method to measure dynamic volume and pressure in hydrocephalic rats. Two phenomena were observed: CSF volume can be controlled acutely from the ventricles of a hydrocephalic rat and the local dynamic volume and pressure changes can be recorded. The methodology consisted of surgically implanting a sensor, and simultaneously recording volume and pressure measurements. Volume was controlled using a shunting/infusion protocol with a syringe pump. The induction of hydrocephalus via kaolin-injection was confirmed post-mortem. Future work involves measuring volume change in a hydrocephalic animal using implanted sensors and implanted electronics with wireless capability.

Volume and pressure monitoring is intended to provide tools for researchers of hydrocephalus where compliance research as well as shunt efficacy are concerned. These dynamic measurements will provide alternative monitoring and treatment options for patients of hydrocephalus.

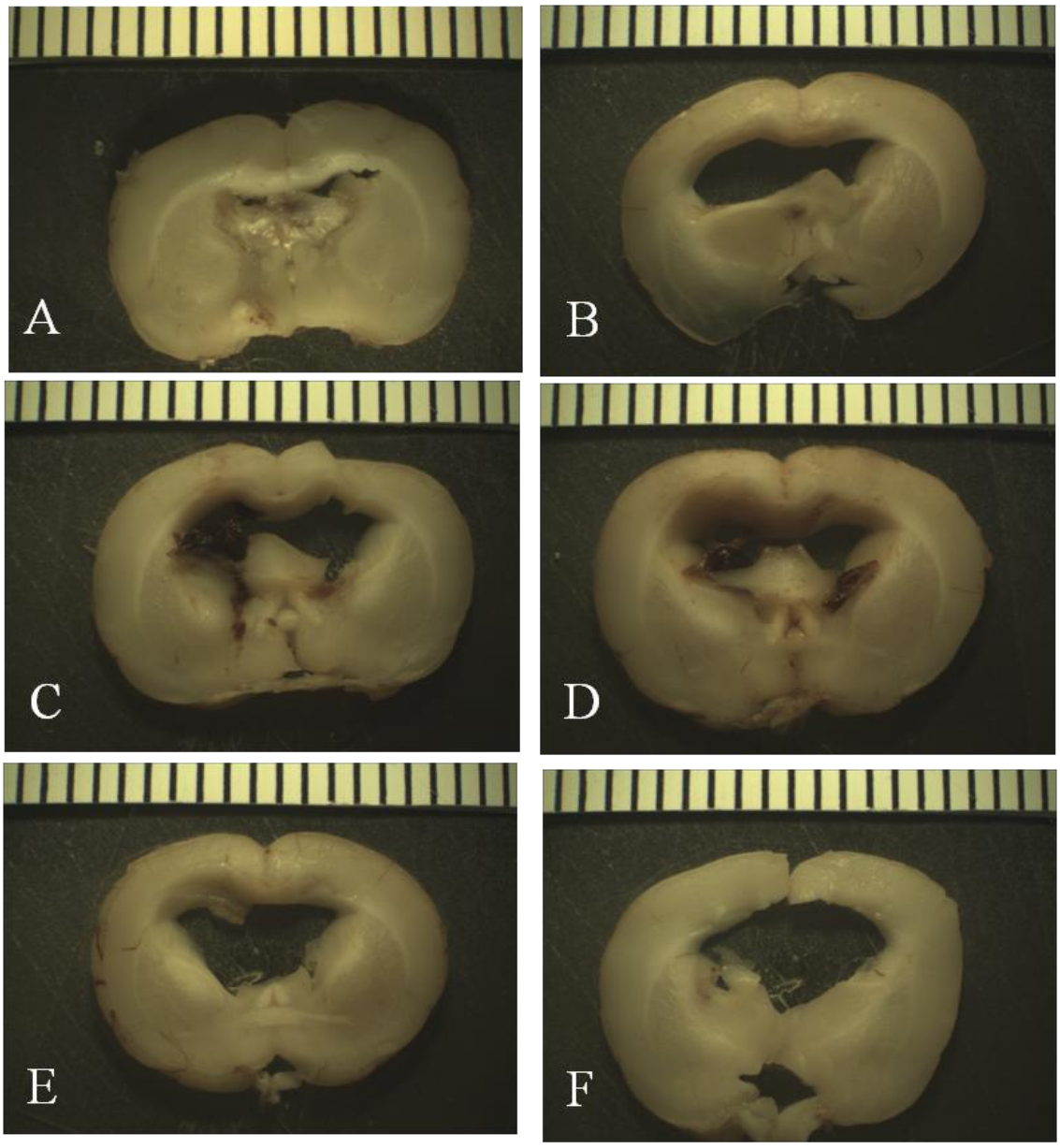

Figure 31. Cross sections of hydrocephalic rats ranging in severity shown in frames B-F. Frame A is a normal rat.

E. Conclusions and Significance

The current clinical treatment for patients with hydrocephalus involves placing a catheter inside cerebral ventricles to shunt CSF. Many problems occur related to treatment such as over-drainage and the need for shunt revisions. Pressure regulated shunts are ineffective for patients with normal pressure hydrocephalus (NPH). Daily pressure changes, coupled with the small pressure seen in NPH, can cause over-drainage resulting in excess CSF removal causing subdural effusions or hemorrhage. There are innovative systems such as the commercially available flow based shunt (Orbis-Sigma valve, Integra). Another commercially available device can be adjusted using external magnetic fields (Strata Valve, Medtronic). However, at a 2010 hydrocephalus meeting in Cleveland, many clinicians and patients expressed dissatisfaction due to its sensitivity to magnetic fields, and the frequent need for revisions [39]. Even toy magnets have been shown to disrupt adjustable shunt settings[35]. 6-12 % of shunted children develop slit ventricle syndrome due to over-shunting[36]. In a survey of pediatric neurosurgeons who routinely implant shunts into hydrocephalic children, the majority of them expressed their inability to prevent slit ventricle syndrome[37]. Researchers have developed pioneering systems such as the capacitive ICP sensors[106] or the micro-valves for shunts[107], however there are currently no devices to continuously monitor volume directly.

VI. CONCLUSIONS AND FUTURE WORK

Summary

This thesis proposes and validates a CSF volume monitor for hydrocephalus therapy based on the impedance technique. Specifically, the design, simulation, fabrication, bench-top calibration followed by animal validation of the device was demonstrated. The premise is that such a system can simply be added to existing shunting systems for improved diagnosis. Analogously, an engineering approach chosen for hydrocephalus therapy is the application of closed-loop feedback systems. Feedback systems typically incorporate sensor input to assess the state and to devise a suitable response to maintain a desired set-point [121]. For volume monitoring to be implemented into existing shunt systems as a translational device, inclusion of electrodes onto the catheter with microfabricated electronics is proposed. In this final chapter, the significance and contributions are outlined followed by a description of future work, consisting of feedback control mechanisms.

A. Contributions of this thesis

In the U.S., slightly more than 1 in 1,000 births is affected by hydrocephalus. Hydrocephalus is one of the most common birth defects and afflicts more than 10,000 babies each year in the U.S. There are also 70,000 discharges a year from hospitals within the U.S. with a diagnosis of hydrocephalus. The cost of ventricular shunt implants amount to a staggering $1 billion a year in the U.S. alone. These statistics show a clear need for improvement.

The main contribution of this thesis is the feasibility of volume measurements specifically for hydrocephalus monitoring. While important for diagnostic and shunt efficacy, the technology also has the potential for an improved understanding of the pathological state. For example, recent evidence suggests that brain tissue compliance is a significant indicator of patient status in hydrocephalus [122].

Compliance can be inferred from the volume-pressure relationship. Therefore, a catheter system to measure pressure and volume continuously may provide insight into the mechanisms of hydrocephalus.

Currently, the assessment of ventricular drainage in a hospital setting is via expensive medical imaging techniques such as MRI or CT. Scanning is a time consuming and costly process, which raises treatment cost for hydrocephalus. Repetitive exposure of x-rays via CT scans to assess shunt functionality also raises the concern of patient safety. Therefore, a monitor that displays information about the volume and pressure can eliminate the need for imaging.

This thesis focuses on three aims: (i) design and simulation of an impedance based volume sensor, (ii) battery operated microelectronics design and fabrication with wireless capabilities, and (iii) volume monitoring validation in bench-top and animal models of hydrocephalus. Further development may consist of advancing the instrumentation and sensor design, while the groundwork for such a system has now been rigorously defined. The specific contributions of this thesis are as follows.

Design and Simulation. An approach to optimize the sensor performance was demonstrated *in silico*. The purpose of these simulations was to provide key design decisions of the sensor. For instance, if a sensor with random placement of electrodes were used in experimental work, the results may not indicate high sensitivity to volume measurements. Knowledge gained from these simulations produced expected outcome in the experimental work. The groundwork for future simulations was arranged by reconstructing ventricular volumes during the progression of hydrocephalus. This approach for treatment design has not been performed elsewhere. Case studies were performed with a human patient and a rat with hydrocephalus. The outcomes provided sensor design decisions such as electrode placement and maximal catheter diameter which were passed for fabrication.

Sensor and Electronics Fabrication. An advantage of self-fabricating sensors over outsourced-fabrication is knowledge gain for additional inclusion of transducers. For instance, strain gauges at the tip or side of the sensor can be readily included in our devices. Sensor prototypes were fabricated in a cost-effective, scaleable manner. Minimal outer diameters of 500 μm were achieved, which is much smaller than most commercially available catheters. The novel fabrication process also allowed for an inner shunt to be included for CSF removal. Design and fabrication of the instrumentation satisfied requirements of the diagnostic device such as duty cycling, wireless transmission and microcontroller implementation. Uses of a microcontroller allow for future implementation of additional transducers and even control elements such as a micro-pump for volume control. These may be included onto existing shunting systems.

Bench-top Characterization and Calibration. The bench-top models are invaluable in assessing the feasibility of novel technology. Most new ideas are tested on the bench-scale prior to animal or clinical trials. Two bench-top models were implemented which consisted of static and dynamic responses. The electrical conductivity ratio between CSF and brain tissue was maintained with the agarose model and the dynamic expansion similarly seen in the physiological system was emulated with the silicone model. Both of the models were used for testing the volume sensors for calibration and validation.

Animal Validation. The novel system was validated in an animal model of hydrocephalus. An acute surgical procedure of shunting followed by infusion experiment was designed. Controlled CSF shunting *in-vivo* with hydrocephalic rats resulted in precise and accurate sensor measurements (R^2=0.98). The shunting runs resulted in only 12% error between measured volume and actual volume as assessed by a Bland-Altman plot. A secondary outcome consisted of a confirmation that both volume and pressure decrease during CSF shunting and increases during infusion. Hydrocephalus was confirmed with imaging as well as post-mortem. These results indicate that volume monitoring is feasible for clinical

cases of hydrocephalus. While long-term measurements of CSF volume are necessary, the acute experimental designed allowed for rapid validation of the technique.

There is a consensus in the neurosurgical community that volume measurement is one of the most promising options to improve prognosis for hydrocephalic patients. The deliverables in this thesis consist of a) bench-top validation of the volume monitoring technique and b) continuous volume measured during shunting and infusing CSF for the first time in hydrocephalic animals.

B. Future Work

The main focus of this thesis is validation of the volume monitoring technique for hydrocephalus. While the wireless unit was not tested in bench-top or animal models, future work will consist of additional development of the hardware for long-term monitoring and biocompatibility studies. Another future development includes the use of an actuator such as micro pump for volume control. The feedback with volume sensor may achieve a precise level of CSF diversion without over- or under-drainage.

In prior work completed, an envisioned feedback treatment was implemented conceptually to demonstrate the feasibility of maintaining desired fluid volume with the help of feedback based on dynamic volume sensing [123]. A simple on-off control scheme was successful in restoring desired setpoint volume in response to CSF accumulation disturbance. In the experiment, CSF was inserted by a second pump to emulate pathological CSF accumulation causing hydrocephalus. Although the actual volume exhibited some fluctuation due to the simplicity of the control scheme, the sensor performed satisfactorily. The oscillations in the tracking response can be reduced easily by implementing more advanced control schemes.

While the inclusion of an actuator for control is developed, an immediate clinical device is envisioned as a result of this thesis. Frame A of Figure 32 shows an image of the sensor implanted into the ventricles of a hydrocephalic rat, while frame B shows a potential clinical system. In this application, the efficacy of an external ventricular drainage system could be monitored.

The sensor fabrication technique presented in this thesis may not be optimal for long-term implantation; therefore the sensor may be fabricated from a company with existing FDA-approval. The fabrication of ring electrodes onto catheters has been explored for various other clinical applications mentioned in chapter 3 such as cochlear implants, and deep brain stimulator electrodes. This industrial collaboration may also reduce the time for clinical trials due to the proven biocompatibility of the materials and methods used.

The electronics may be further miniaturized by companies with ASIC fabrication capability. Many medical device fabrication companies are exploring the feasibility of radio frequency identification (RFID) coupled with medical sensors. These systems typically do not include a battery supply and are powered through an inductive link by a RFID reader. The signal components presented in this thesis could be powered through the inductive link established by the RFID reader, and perform the volume measurement. Such a clinical system would enable physicians to establish functionality of shunt treatment during hospital visits.

The device will also be made ready for long-term measurements in larger animal models of hydrocephalus. Larger animal models of hydrocephalus such as the rabbit, or dog model allow for size constraints similar to human cases. The rat model presented in this thesis is too small for an implanted monitor and control system. The electronics would not fit. Collaboration with external surgeons to

implant the microfabricated device into larger animal models may be performed in order to increase our understanding of this pathological state and devise better treatment strategies.

In 1997, 2000, and 2003, there were on average 39,000 admissions, 400,000 hospital days, and $1.4 - 2.0 billion spent on pediatric hydrocephalus care nationwide [38]. Shunt-related revisions accounted for half of all admissions and a total of 242,000 hospital days. The mean length of stay for pediatric patients with shunt related admissions is 4.9 days, with an average cost of $40,000 to replace hydrocephalic shunts. An implanted system that actively monitors shunt function as well as provide volume control options is expected to decrease the number of revisions; fewer revisions mean an estimated reduction of 2-3 hospital days. In the first year of chronic of hydrocephalus treatment this cost reduction would save each hospital $7.2 million per year [1].

This thesis closes with the prospect of obtaining improved knowledge of hydrocephalus as well as assessing treatment efficacy. There is currently no method to measure ventricular volume expansion except for MRI, which is impractical for continuous monitoring or integration with intelligent shunting systems. However, dynamic volume monitoring would provide invaluable observations towards a better understanding of the pathophysiology of the disease.

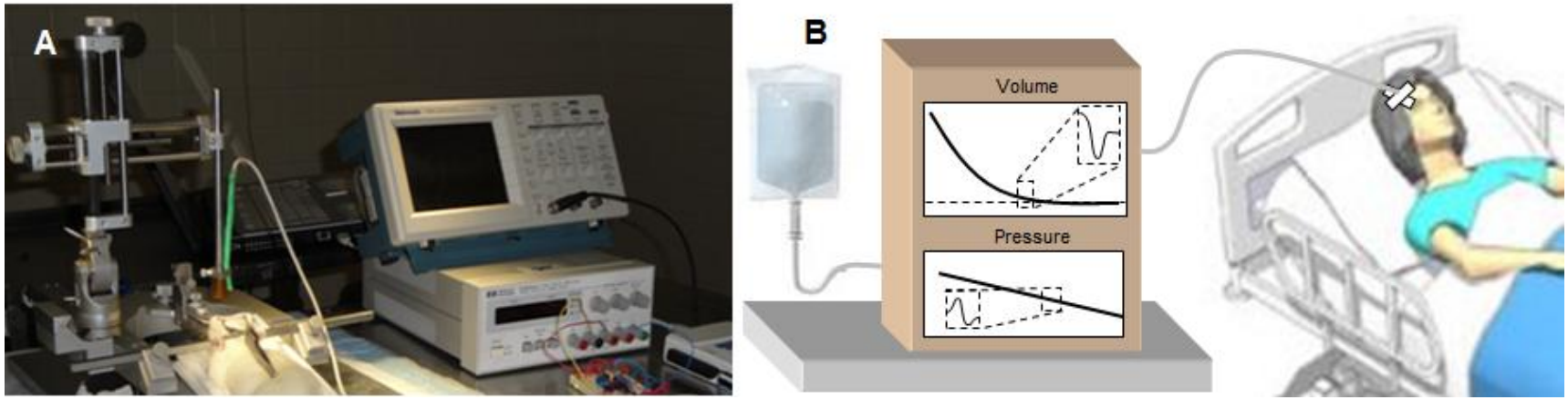

Figure 32. Future design of bedside system. A sensor implanted into the lateral ventricles of a hydrocephalic rat is shown in frame A while frame B shows a potential clinical application as a monitor for an external ventricular drainage system.

VII. REFERENCE LIST

[1] R. V. Patwardhan and A. Nanda, "Implanted ventricular shunts in the United States: the billion-dollar-a-year cost of hydrocephalus treatment," *Neurosurgery,* vol. 56, pp. 139-44; discussion 144-5, 2005.

[2] S. Tuli*, et al.*, "Risk factors for repeated cerebrospinal shunt failures in pediatric patients with hydrocephalus," *J Neurosurg,* vol. 92, pp. 31-8, Jan 2000.

[3] D. Greitz, "Radiological assessment of hydrocephalus: new theories and implications for therapy," *Neurosurg Rev,* vol. 27, pp. 145-65; discussion 166-7, Jul 2004.

[4] A. Aschoff*, et al.*, "The scientific history of hydrocephalus and its treatment," *Neurosurg Rev,* vol. 22, pp. 67-93; discussion 94-5, Oct 1999.

[5] T. H. Milhorat, "Choroid plexus and cerebrospinal fluid production," *Science,* vol. 166, pp. 1514-6, Dec 19 1969.

[6] D. Greitz, "Cerebrospinal fluid circulation and associated intracranial dynamics. A radiologic investigation using MR imaging and radionuclide cisternography," *Acta Radiol Suppl,* vol. 386, pp. 1-23, 1993.

[7] D. Greitz and J. Hannerz, "A proposed model of cerebrospinal fluid circulation: observations with radionuclide cisternography," *AJNR Am J Neuroradiol,* vol. 17, pp. 431-8, Mar 1996.

[8] A. A. Linninger*, et al.*, "Cerebrospinal fluid flow in the normal and hydrocephalic human brain," *IEEE Trans Biomed Eng,* vol. 54, pp. 291-302, Feb 2007.

[9] A. A. Linninger*, et al.*, "Pulsatile cerebrospinal fluid dynamics in the human brain," *IEEE Trans Biomed Eng,* vol. 52, pp. 557-65, Apr 2005.

[10] A. A. Linninger*, et al.*, "A mathematical model of blood, cerebrospinal fluid and brain dynamics," *J Math Biol,* vol. 59, pp. 729-59, Dec 2009.

[11] A. A. Linninger*, et al.*, "Normal and hydrocephalic brain dynamics: the role of reduced cerebrospinal fluid reabsorption in ventricular enlargement," *Ann Biomed Eng,* vol. 37, pp. 1434-47, Jul 2009.

[12] R. D. Penn*, et al.*, "Pressure gradients in the brain in an experimental model of hydrocephalus," *J Neurosurg,* vol. 102, pp. 1069-75, Jun 2005.

[13] M. Czosnyka*, et al.*, "Age dependence of cerebrospinal pressure-volume compensation in patients with hydrocephalus," *J Neurosurg,* vol. 94, pp. 482-6, Mar 2001.

[14] P. K. Eide and E. Kerty, "Static and pulsatile intracranial pressure in idiopathic intracranial hypertension," *Clin Neurol Neurosurg,* vol. 113, pp. 123-8, Feb 2011.

[15] A. D. Skjolding*, et al.*, "Hydrocephalus induces dynamic spatiotemporal regulation of aquaporin-4 expression in the rat brain," *Cerebrospinal Fluid Res,* vol. 7, p. 20, 2010.

[16] L. Paul*, et al.*, "Expression of Aquaporin 1 and 4 in congenital hydrocephalus rat model," *Neurosurgery,* Nov 25 2010.

[17] T. Tourdias*, et al.*, "Aquaporin 4 correlates with apparent diffusion coefficient and hydrocephalus severity in the rat brain: a combined MRI-histological study," *Neuroimage,* vol. 47, pp. 659-66, Aug 15 2009.

[18] D. C. McCullough, "A history of the treatment of hydrocephalus," *Fetal Ther,* vol. 1, pp. 38-45, 1986.

[19] S. Hakim, "Considerations on the physics of hydrocephalus and its treatment," *Exp Eye Res,* vol. 25 Suppl, pp. 391-9, 1977.

[20] K. E. Richard*, et al.*, "First clinical results with a telemetric shunt-integrated ICP-sensor," *Neurol Res,* vol. 21, pp. 117-20, Jan 1999.

[21] J. S. Kroin*, et al.*, "Long-term testing of an intracranial pressure monitoring device," *J Neurosurg,* vol. 93, pp. 852-8, Nov 2000.

[22] R. Ritz*, et al.*, "Do antibiotic-impregnated shunts in hydrocephalus therapy reduce the risk of infection? An observational study in 258 patients," *BMC Infect Dis,* vol. 7, p. 38, 2007.

[23] C. Hayhurst*, et al.*, "The impact of antibiotic-impregnated catheters on shunt infection in children and neonates," *Childs Nerv Syst,* vol. 24, pp. 557-62, May 2008.
[24] S. Muttaiyah*, et al.*, "Efficacy of antibiotic-impregnated external ventricular drain catheters," *J Clin Neurosci,* vol. 17, pp. 296-8, Mar 2010.
[25] J. M. Drake*, et al.*, "Randomized trial of cerebrospinal fluid shunt valve design in pediatric hydrocephalus," *Neurosurgery,* vol. 43, pp. 294-303; discussion 303-5, Aug 1998.
[26] U. Meier*, et al.*, "Course of disease in patients with idiopathic normal pressure hydrocephalus (iNPH): a follow-up study 3, 4 and 5 years following shunt implantation," *Acta Neurochir Suppl,* vol. 102, pp. 125-7, 2008.
[27] R. Caruso*, et al.*, "Idiopathic normal-pressure hydrocephalus in adults: result of shunting correlated with clinical findings in 18 patients and review of the literature," *Neurosurg Rev,* vol. 20, pp. 104-7, 1997.
[28] J. A. Vanneste, "Diagnosis and management of normal-pressure hydrocephalus," *J Neurol,* vol. 247, pp. 5-14, Jan 2000.
[29] A. Marmarou*, et al.*, "A nonlinear analysis of the cerebrospinal fluid system and intracranial pressure dynamics," *J Neurosurg,* vol. 48, pp. 332-44, Mar 1978.
[30] P. C. Whitfield*, et al.*, "Safe removal of retained ventricular catheters using intraluminal choroid plexus coagulation. Technical note," *J Neurosurg,* vol. 83, pp. 1101-2, Dec 1995.
[31] U. W. Thomale*, et al.*, "Perforation holes in ventricular catheters--is less more?," *Childs Nerv Syst,* vol. 26, pp. 781-9, Jun 2010.
[32] Z. Czosnyka*, et al.*, "Posture-related overdrainage: comparison of the performance of 10 hydrocephalus shunts in vitro," *Neurosurgery,* vol. 42, pp. 327-33; discussion 333-4, Feb 1998.
[33] C. E. Johanson*, et al.*, "Multiplicity of cerebrospinal fluid functions: New challenges in health and disease," *Cerebrospinal Fluid Res,* vol. 5, p. 10, 2008.
[34] W. Serlo*, et al.*, "Classification and management of the slit ventricle syndrome," *Childs Nerv Syst,* vol. 1, pp. 194-9, 1985.
[35] R. C. Anderson*, et al.*, "Adjustment and malfunction of a programmable valve after exposure to toy magnets. Case report," *J Neurosurg,* vol. 101, pp. 222-5, Nov 2004.
[36] H. L. Rekate, "Shunt-related headaches: the slit ventricle syndromes," *Childs Nerv Syst,* vol. 24, pp. 423-30, Apr 2008.
[37] A. L. Albright, "Hydrocephalus shunt practice of experienced pediatric neurosurgeons," *Childs Nerv Syst,* vol. 26, pp. 925-9, Jul 2010.
[38] T. D. Simon*, et al.*, "Hospital care for children with hydrocephalus in the United States: utilization, charges, comorbidities, and deaths," *J Neurosurg Pediatr,* vol. 1, pp. 131-7, Feb 2008.
[39] A. Watanabe*, et al.*, "Overdrainage of cerebrospinal fluid caused by detachment of the pressure control cam in a programmable valve after 3-tesla magnetic resonance imaging," *J Neurosurg,* vol. 112, pp. 425-7, Feb 2010.
[40] W. H. Ko*, et al.*, "Intracranial pressure telemetry system. I. Hardware development," *Biotelem Patient Monit,* vol. 8, pp. 131-50, 1981.
[41] A. M. Leung*, et al.*, "Intracranial pressure telemetry system using semicustom integrated circuits," *IEEE Trans Biomed Eng,* vol. 33, pp. 386-95, Apr 1986.
[42] H. J. Yoon*, et al.*, "Micro devices for a cerebrospinal fluid (CSF) shunt system," *Sensors and Actuators A: Physical,* vol. 110, pp. 68-76, 2004.
[43] M. A. Williams*, et al.*, "Priorities for hydrocephalus research: report from a National Institutes of Health-sponsored workshop," *J Neurosurg,* vol. 107, pp. 345-57, Nov 2007.
[44] J. H. Piatt and M. Cosgriff, "Monte Carlo simulation of cerebrospinal fluid shunt failure and definition of instability among shunt-treated patients with hydrocephalus," *Journal of Neurosurgery: Pediatrics,* vol. 107, pp. 474-478, 2007.

[45] B. C. Warf, "Comparison of 1-year outcomes for the Chhabra and Codman-Hakim Micro Precision shunt systems in Uganda: a prospective study in 195 children," *J Neurosurg,* vol. 102, pp. 358-62, May 2005.
[46] B. H. Brown, "Electrical impedance tomography (EIT): a review," *J Med Eng Technol,* vol. 27, pp. 97-108, May-Jun 2003.
[47] J. G. Webster and P. Hua, "Recent North American progress in electrical impedance tomography," *Clin Phys Physiol Meas,* vol. 9 Suppl A, pp. 127-30, 1988.
[48] T. J. Yorkey*, et al.*, "Comparing reconstruction algorithms for electrical impedance tomography," *IEEE Trans Biomed Eng,* vol. 34, pp. 843-52, Nov 1987.
[49] J. Riera*, et al.*, "Electrical impedance tomography in acute lung injury," *Med Intensiva,* vol. 35, pp. 509-517, Nov 2011.
[50] O. Gilad*, et al.*, "Design of electrodes and current limits for low frequency electrical impedance tomography of the brain," *Med Biol Eng Comput,* vol. 45, pp. 621-33, Jul 2007.
[51] A. Morimoto*, et al.*, "Spatial resolution in the electrical impedance tomography for the local tissue," *Conf Proc IEEE Eng Med Biol Soc,* vol. 6, pp. 6638-41, 2005.
[52] E. J. Woo*, et al.*, "A robust image reconstruction algorithm and its parallel implementation in electrical impedance tomography," *IEEE Trans Med Imaging,* vol. 12, pp. 137-46, 1993.
[53] A. A. Linninger*, et al.*, "Rigorous mathematical modeling techniques for optimal delivery of macromolecules to the brain," *IEEE Trans Biomed Eng,* vol. 55, pp. 2303-13, Sep 2008.
[54] A. A. Linninger*, et al.*, "Prediction of convection-enhanced drug delivery to the human brain," *J Theor Biol,* vol. 250, pp. 125-38, Jan 7 2008.
[55] D. S. Tuch*, et al.*, "Conductivity tensor mapping of the human brain using diffusion tensor MRI," *Proc Natl Acad Sci U S A,* vol. 98, pp. 11697-701, Sep 25 2001.
[56] J. Haueisen*, et al.*, "The influence of brain tissue anisotropy on human EEG and MEG," *Neuroimage,* vol. 15, pp. 159-66, Jan 2002.
[57] J. Zhang and R. Patterson, "Non-invasive determination of absolute lung resistivity in adults using electrical impedance tomography," *Physiol Meas,* vol. 31, pp. S45-56, Aug 2010.
[58] H. Wrigge*, et al.*, "Electrical impedance tomography compared with thoracic computed tomography during a slow inflation maneuver in experimental models of lung injury," *Crit Care Med,* vol. 36, pp. 903-9, Mar 2008.
[59] I. G. Bikker*, et al.*, "Electrical impedance tomography measured at two thoracic levels can visualize the ventilation distribution changes at the bedside during a decremental positive end-expiratory lung pressure trial," *Crit Care,* vol. 15, p. R193, Aug 11 2011.
[60] A. Vonk-Noordegraaf, 2nd*, et al.*, "Determination of stroke volume by means of electrical impedance tomography," *Physiol Meas,* vol. 21, pp. 285-93, May 2000.
[61] D. S. Holder, "Detection of cerebral ischaemia in the anaesthetised rat by impedance measurement with scalp electrodes: implications for non-invasive imaging of stroke by electrical impedance tomography," *Clin Phys Physiol Meas,* vol. 13, pp. 63-75, Feb 1992.
[62] V. Cherepenin*, et al.*, "A 3D electrical impedance tomography (EIT) system for breast cancer detection," *Physiol Meas,* vol. 22, pp. 9-18, Feb 2001.
[63] J. Kozlowska*, et al.*, "Electrical impedance tomography. Determination of impedance of tissue in the frequency range 10(-6)-20 MHz: preliminary results," *Clin Phys Physiol Meas,* vol. 13 Suppl A, pp. 73-5, 1992.
[64] B. Blad and B. Baldetorp, "Impedance spectra of tumour tissue in comparison with normal tissue; a possible clinical application for electrical impedance tomography," *Physiol Meas,* vol. 17 Suppl 4A, pp. A105-15, Nov 1996.

[65] Z. Boneva-Asiova and M. Boyanov, "Age-related changes of body composition and abdominal adipose tissue assessed by bio-electrical impedance analysis and computed tomography," *Endocrinol Nutr,* Sep 30 2011.
[66] O. Gilad and D. S. Holder, "Impedance changes recorded with scalp electrodes during visual evoked responses: implications for Electrical Impedance Tomography of fast neural activity," *Neuroimage,* vol. 47, pp. 514-22, Aug 15 2009.
[67] T. Tidswell*, et al.*, "Three-dimensional electrical impedance tomography of human brain activity," *Neuroimage,* vol. 13, pp. 283-94, Feb 2001.
[68] T. Oh*, et al.*, "A novel method for recording neuronal depolarization with recording at 125-825 Hz: implications for imaging fast neural activity in the brain with electrical impedance tomography," *Med Biol Eng Comput,* vol. 49, pp. 593-604, May 2011.
[69] X. L. Xu*, et al.*, "An alternative subspace approach to EEG dipole source localization," *Phys Med Biol,* vol. 49, pp. 327-43, Jan 21 2004.
[70] W. H. Lee*, et al.*, "Influence of white matter anisotropy on EEG source localization: an experimental study," *Conf Proc IEEE Eng Med Biol Soc,* vol. 2009, pp. 2923-5, 2009.
[71] J. Baan*, et al.*, "Continuous measurement of left ventricular volume in animals and humans by conductance catheter," *Circulation,* vol. 70, pp. 812-23, Nov 1984.
[72] C. L. Wei*, et al.*, "Nonlinear conductance-volume relationship for murine conductance catheter measurement system," *IEEE Trans Biomed Eng,* vol. 52, pp. 1654-61, Oct 2005.
[73] C. L. Wei and M. H. Shih, "Calibration capacity of the conductance-to-volume conversion equations for the mouse conductance catheter measurement system," *IEEE Trans Biomed Eng,* vol. 56, pp. 1627-34, Jun 2009.
[74] X. F. Wei and W. M. Grill, "Current density distributions, field distributions and impedance analysis of segmented deep brain stimulation electrodes," *J Neural Eng,* vol. 2, pp. 139-47, Dec 2005.
[75] C. C. McIntyre*, et al.*, "Electric field and stimulating influence generated by deep brain stimulation of the subthalamic nucleus," *Clin Neurophysiol,* vol. 115, pp. 589-95, Mar 2004.
[76] T. Stieglitz*, et al.*, "Brain-computer interfaces: an overview of the hardware to record neural signals from the cortex," *Prog Brain Res,* vol. 175, pp. 297-315, 2009.
[77] C. Thaijiam and T. J. Gale, "The effect of fiber orientation on volume measurement using conductance catheter techniques," *Conf Proc IEEE Eng Med Biol Soc,* vol. 1, pp. 5981-4, 2006.
[78] C. Thaijiam and T. J. Gale, "Investigation of catheter curvature and genetic algorithms in conductance catheter optimization," *Conf Proc IEEE Eng Med Biol Soc,* vol. 2007, pp. 2195-8, 2007.
[79] D. C. Zhu*, et al.*, "Dynamics of lateral ventricle and cerebrospinal fluid in normal and hydrocephalic brains," *J Magn Reson Imaging,* vol. 24, pp. 756-70, Oct 2006.
[80] A. A. Linninger*, et al.*, "Computational methods for predicting drug transport in anisotropic and heterogeneous brain tissue," *J Biomech,* vol. 41, pp. 2176-87, Jul 19 2008.
[81] H. D. Hettiarachchi*, et al.*, "The Effect of Pulsatile Flow on Intrathecal Drug Delivery in the Spinal Canal," *Ann Biomed Eng,* Jul 13 2011.
[82] M. R. Del Bigio and Y. W. Zhang, "Cell death, axonal damage, and cell birth in the immature rat brain following induction of hydrocephalus," *Exp Neurol,* vol. 154, pp. 157-69, Nov 1998.
[83] M. R. Del Bigio*, et al.*, "Chronic hydrocephalus in rats and humans: white matter loss and behavior changes," *Ann Neurol,* vol. 53, pp. 337-46, Mar 2003.
[84] B. J. Gantz*, et al.*, "Evaluation of five different cochlear implant designs: audiologic assessment and predictors of performance," *Laryngoscope,* vol. 98, pp. 1100-6, Oct 1988.
[85] G. E. Loeb*, et al.*, "Design and fabrication of an experimental cochlear prosthesis," *Med Biol Eng Comput,* vol. 21, pp. 241-54, May 1983.

[86] C. R. Butson and C. C. McIntyre, "Role of electrode design on the volume of tissue activated during deep brain stimulation," *J Neural Eng,* vol. 3, pp. 1-8, Mar 2006.
[87] K. C. Iverson*, et al.*, "Cochlear implantation using thin-film array electrodes," *Otolaryngol Head Neck Surg,* vol. 144, pp. 934-9, Jun 2011.
[88] P. J. Rousche*, et al.*, "Flexible polyimide-based intracortical electrode arrays with bioactive capability," *IEEE Trans Biomed Eng,* vol. 48, pp. 361-71, Mar 2001.
[89] P. J. Rousche and R. A. Normann, "Chronic intracortical microstimulation (ICMS) of cat sensory cortex using the Utah Intracortical Electrode Array," *IEEE Trans Rehabil Eng,* vol. 7, pp. 56-68, Mar 1999.
[90] B. Pakkenberg, "Pronounced reduction of total neuron number in mediodorsal thalamic nucleus and nucleus accumbens in schizophrenics," *Arch Gen Psychiatry,* vol. 47, pp. 1023-8, Nov 1990.
[91] P. S. Motta and J. W. Judy, "Multielectrode microprobes for deep-brain stimulation fabricated with a customizable 3-D electroplating process," *IEEE Trans Biomed Eng,* vol. 52, pp. 923-33, May 2005.
[92] S. A. Haddad*, et al.*, "The evolution of pacemakers," *IEEE Eng Med Biol Mag,* vol. 25, pp. 38-48, May-Jun 2006.
[93] S. Schmidt*, et al.*, "Biocompatibility of silicon-based electrode arrays implanted in feline cortical tissue," *J Biomed Mater Res,* vol. 27, pp. 1393-9, Nov 1993.
[94] R. R. Richardson, Jr.*, et al.*, "Polyimides as biomaterials: preliminary biocompatibility testing," *Biomaterials,* vol. 14, pp. 627-35, Jul 1993.
[95] M. Schuettler*, et al.*, "A voltage-controlled current source with regulated electrode bias-voltage for safe neural stimulation," *J Neurosci Methods,* vol. 171, pp. 248-52, Jun 30 2008.
[96] L. E. Thibault*, et al.*, "Biomechanical aspects of a fluid percussion model of brain injury," *J Neurotrauma,* vol. 9, pp. 311-22, Winter 1992.
[97] D. W. Brands*, et al.*, "On the potential importance of non-linear viscoelastic material modelling for numerical prediction of brain tissue response: test and application," *Stapp Car Crash J,* vol. 46, pp. 103-21, Nov 2002.
[98] E. K. Walsh and A. Schettini, "Elastic behavior of brain tissue in vivo," *Am J Physiol,* vol. 230, pp. 1058-62, Apr 1976.
[99] A. Pellicer*, et al.*, "Noninvasive continuous monitoring of the effects of head position on brain hemodynamics in ventilated infants," *Pediatrics,* vol. 109, pp. 434-40, Mar 2002.
[100] G. Schmid*, et al.*, "Dielectric properties of human brain tissue measured less than 10 h postmortem at frequencies from 800 to 2450 MHz," *Bioelectromagnetics,* vol. 24, pp. 423-30, Sep 2003.
[101] M. Kaczmarek*, et al.*, "The hydromechanics of hydrocephalus: steady-state solutions for cylindrical geometry," *Bull Math Biol,* vol. 59, pp. 295-323, Mar 1997.
[102] A. SMILLIE*, et al.*, "A hydroelastic model of hydrocephalus," *Journal of Fluid Mechanics,* vol. 539, pp. 417-443, 2005.
[103] G. A. Bateman, "Vascular compliance in normal pressure hydrocephalus," *AJNR Am J Neuroradiol,* vol. 21, pp. 1574-85, Oct 2000.
[104] G. Nagra*, et al.*, "Impaired lymphatic cerebrospinal fluid absorption in a rat model of kaolin-induced communicating hydrocephalus," *Am J Physiol Regul Integr Comp Physiol,* vol. 294, pp. R1752-9, May 2008.
[105] P. K. Eide and A. Brean, "Cerebrospinal fluid pulse pressure amplitude during lumbar infusion in idiopathic normal pressure hydrocephalus can predict response to shunting," *Cerebrospinal Fluid Res,* vol. 7, p. 5, 2010.
[106] K. Aquilina*, et al.*, "Preliminary evaluation of a novel intraparenchymal capacitive intracranial pressure monitor," *J Neurosurg,* May 27 2011.
[107] S. Chung*, et al.*, "Development of MEMS-based Cerebrospinal Fluid Shunt System," *Biomedical Microdevices,* vol. 5, pp. 311-321, 2003.

[108] J. P. McAllister, 2nd, "Neuronal damage in hydrocephalus," *J Neurosurg,* vol. 104, pp. 297-8; discussion 298, May 2006.
[109] J. P. McAllister, 2nd*, et al.*, "Neuronal effects of experimentally induced hydrocephalus in newborn rats," *J Neurosurg,* vol. 63, pp. 776-83, Nov 1985.
[110] M. R. Del Bigio*, et al.*, "Magnetic resonance imaging and behavioral analysis of immature rats with kaolin-induced hydrocephalus: pre- and postshunting observations," *Exp Neurol,* vol. 148, pp. 256-64, Nov 1997.
[111] U. Meier*, et al.*, "The ICP-dependency of resistance to cerebrospinal fluid outflow: a new mathematical method for CSF-parameter calculation in a model with H-TX rats," *J Clin Neurosci,* vol. 9, pp. 58-63, Jan 2002.
[112] O. H. Khan*, et al.*, "Brain damage in neonatal rats following kaolin induction of hydrocephalus," *Exp Neurol,* vol. 200, pp. 311-20, Aug 2006.
[113] G. Paxinos*, et al.*, "Bregma, lambda and the interaural midpoint in stereotaxic surgery with rats of different sex, strain and weight," *J Neurosci Methods,* vol. 13, pp. 139-43, Apr 1985.
[114] J. D. Mann*, et al.*, "Clearance of macromolecular and particulate substances from the cerebrospinal fluid system of the rat," *J Neurosurg,* vol. 50, pp. 343-8, Mar 1979.
[115] S. R. Herrera*, et al.*, "CT Ventriculography for diagnosis of occult ventricular cysticerci," *Surg Neurol Int,* vol. 1, p. 92, 2010.
[116] J. M. Bland and D. G. Altman, *Statistical methods for assessing agreement between two methods of clinical measurement* vol. 47, 2010.
[117] S. B. Baumann*, et al.*, "The electrical conductivity of human cerebrospinal fluid at body temperature," *IEEE Trans Biomed Eng,* vol. 44, pp. 220-3, Mar 1997.
[118] M. R. Del Bigio*, et al.*, "Monoamine neurotransmitters and their metabolites in the mature rabbit brain following induction of hydrocephalus," *Neurochem Res,* vol. 23, pp. 1379-86, Nov 1998.
[119] K. Higashi*, et al.*, "Cerebral blood flow and metabolism in experimental hydrocephalus," *Neurol Res,* vol. 8, pp. 169-76, Sep 1986.
[120] G. Grasso*, et al.*, "Assessment of human brain water content by cerebral bioelectrical impedance analysis: a new technique and its application to cerebral pathological conditions," *Neurosurgery,* vol. 50, pp. 1064-72; discussion 1072-4, May 2002.
[121] S. Cetinkunt, *Mechatronics*. Hoboken, NJ: John Wiley, 2007.
[122] P. K. Eide and W. Sorteberg, "Association among intracranial compliance, intracranial pulse pressure amplitude and intracranial pressure in patients with intracranial bleeds," *Neurol Res,* vol. 29, pp. 798-802, Dec 2007.
[123] A. Linninger*, et al.*, "An impedance sensor to monitor and control cerebral ventricular volume," *Med Eng Phys,* vol. 31, pp. 838-45, Sep 2009.
[124] K. M. Boje, "In vivo measurement of blood-brain barrier permeability," *Curr Protoc Neurosci,* vol. Chapter 7, p. Unit 7 19, Aug 2001.

APPENDIX A - SENSOR SPECIFICATIONS

This appendix is intended to provide the specifications of a human impedance sensor for monitoring cerebral ventricular volume. The design for a human and rat animal model is presented. Also presented are the specifications of the instrumentation required to operate the sensor.

Sensor Parameter	Human	Hydrocephalic Rat
Catheter Length *The catheter length is defined from the tip of the shunt to the connection with the instrumentation.*	10 cm	2 cm
Shunt Diameter *The shunt diameter is an average VP shunt diameter.*	2 mm	0.3 mm
Electrode Surface Area *The surface area reduces the current density while distributing the electric field in a larger spatial domain.*	15.7 mm^2	2.4 mm^2
Inter-Measurement Electrode Distance *The voltage potential difference is greater when the measurement electrodes are further spaced apart.*	5 mm	1.5 mm
Inter-Excitatory Electrode Distance *The length of the frontal horn of the lateral ventricles limits the distribution of the electric field.*	9 mm	3 mm

Instrumentation Parameter	Human	Hydrocephalic Rat
Voltage Magnitude *This value represents the maximum potential difference recorded in the fluid-filled region*	1 mV	6.5 mV
Applied Current Density *The current density must remain below the threshold of neuronal stimulation of 0.1 A/m^2 [50].*	0.06 A/m^2	0.4 A/m^2
Signal Frequency *The excitation frequency must remain below threshold of neuronal stimulation [50].*	100 Hz	100 Hz
Signal Noise Ratio *The gain applied by the instrumentation amplifier is 1000 with a common mode rejection ratio of 130.*	10:1	50:1
Duty Cycle *Battery life is increased 1000 fold with a duty cycle of 10 %.*	10%	10%
RF Transmitter Frequency *FCC approved frequency bands for medical devices.*	400 Mhz	434 Mhz

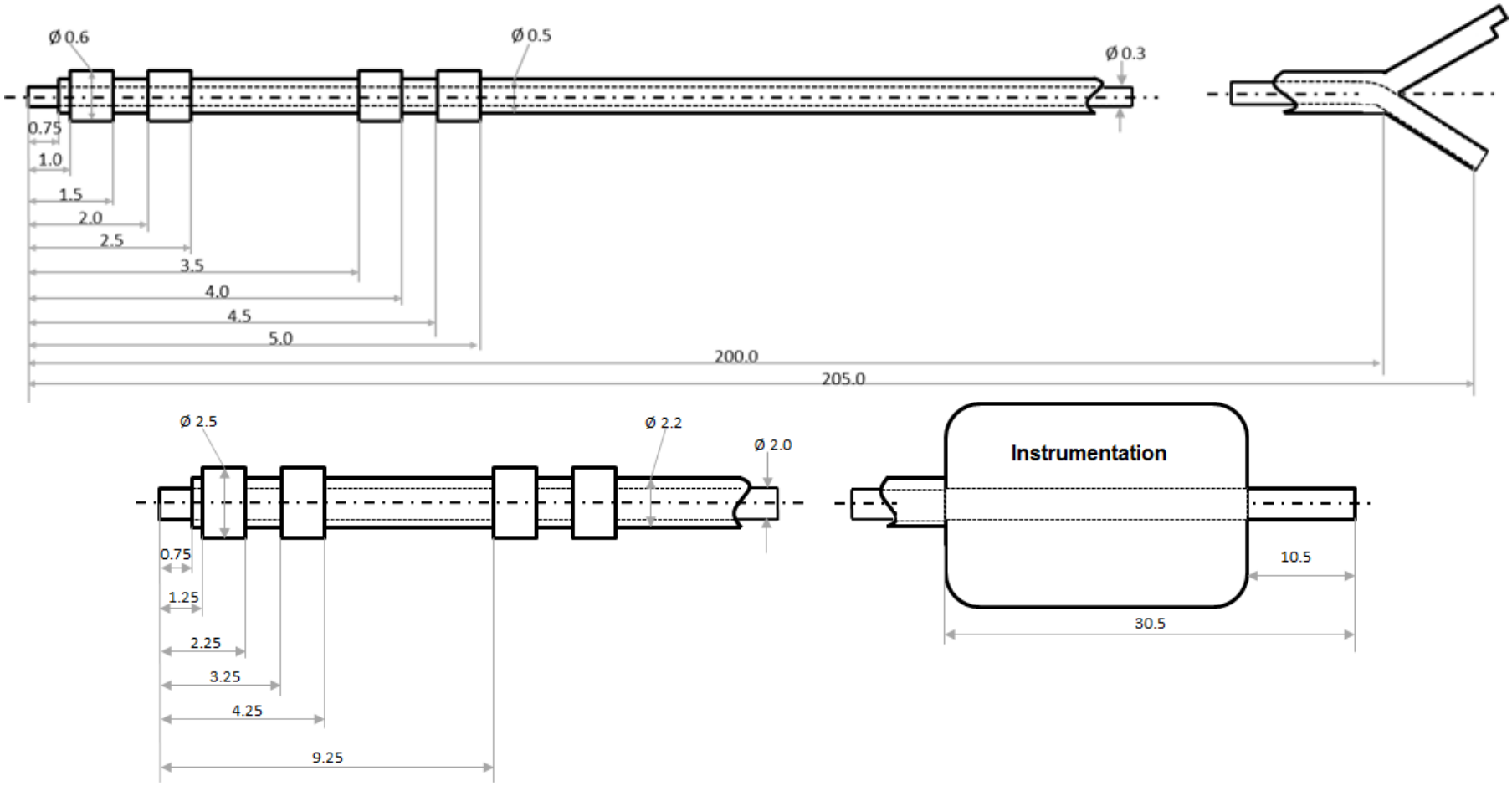

Figure 33. Size specifications for CSF volume sensor and instrumentation. The top image shows a hydrocephalic rat design with a distal y connector while the bottom shows a clinical design with distal implantable electronics and shunt leading to peritoneal cavity. Specifications are provided in millimeters.

APPENDIX B - MICROCONTROLLER CODE

The following code was programmed for a PIC12683 using MicroChip MPLAB v8.53. Comments are shown on the right side of the code.

```
//=======================================
//        Analog/Digital Conversion and Serial Data Communication
//                LED lights up when data is sent
//                Sukhi Basati 9/31/10
//=======================================

#include <htc.h>
__CONFIG(MCLREN & UNPROTECT & BORDIS & WDTEN & PWRTEN & INTIO);

#define Vcc             GPIO5                   /* positive power on*/
#define Vci             GPIO1                   /* negative power on*/
#define XTAL            4000000
//baudrate
#define BRATE                   2400
#define SCALER                  820000 //600000
#define ITIME           4*SCALER/XTAL       /* Instruction cycle */
#define DLY                     8//9                    /* cycles per null loop */
#define TX_OHEAD    6                               /* overhead cycles per loop */
#define DELAY(ohead)(((SCALER/BRATE)-(ohead*ITIME))/(DLY*ITIME))
```

```
#define LED1   GPIO0  //LED on pin 7 lights when data is sent


void measure_send();
void synch_out(unsigned char);
void ser_out(unsigned char);
void delay_ms(char);


void main()
{


//initialization
        TRISIO = 0b001100;        //configure GP0,GP1,GP4,and GP5 as output
        OPTION = 0b11001111;          //set WDT timeout: prescaler assigned to WDT (PSA=1)
                                                // WDT timeout = 2.3 s
        WDTCON = 0b01101;             // watchdog timer period select bits
                                                // 0000 = 1:1024
        CMCON0 = 7;                             //disable comparators
        ANSEL  = 0b00010100;//GP2 is only analog (pin 5)
        ADCON0 = 0b00001001;          // in ANSEL, put 001 in ADCS<2:0> bit for conversion clock
                                                //put in ADCON0 register CHS<1:0> : read from AN2:
10
                                                // in ADCON0 change ADFM (bit 7) to left justified : 0
                                                // so most significant eight bits of data is in ADRESH
                                                // change VCFG (bit 6) in ADCON0 (reference voltage)
to 0
                                                // and change ADON to 1 in (bit 0) of ADCON0 register
```

```
                                                    // so ADCON0 should look like: 00001001
        for (;;) {
                Vcc = 1;                            // SB 4/2011 turn on power control using optoisolator
                Vci = 1;
        measure_send();     // sub-function for A/D conversion and serial out
                Vcc = 0;                            // turn optoisolators off
                Vci = 0;
                SLEEP();                            // turn electronics off
        }
}


void measure_send() {
        char j;
        for (j=0;j<50;j++) {        // perform 50 measurements
                LED1 = 1;                           // indicator LED
                delay_ms(4);
                GODONE = 1;                         // start conversion
                while (GODONE)                      // wait until done
                        ;
                synch_out(85);              // send synchronization 'U' out sub-function
                delay_ms(1);
                ser_out(ADRESH);        // send measurement out sub-function
                LED1 = 0;
                delay_ms(12);
        }
}
```

```
void synch_out(unsigned char c)
{
        //Serial out Pin 3
        #define TxData          GPIO4

        unsigned char   bitno;
        unsigned char   dly;

        TxData = 1;                             /* start spike lasts 4 uS*/

        bitno = 10;                             // number of bits allowed in signal

do {
                dly = DELAY(TX_OHEAD);  /* wait one bit time */
                do
                        /* waiting in delay loop */ ;
                while(--dly);
                if (bitno==10) {
                        TxData = 0;
} else {
                if(c & 1)
                        TxData = 1;
                if(!(c & 1))
                        TxData = 0;
                c = (c >> 1);
};
```

```
        } while(--bitno);
NOP();
}

void ser_out(unsigned char a)
{
        //Serial out Pin 3
        #define TxData          GPIO4

        unsigned char   bitnot;
        unsigned char   dly1;
        TxData = 1;                     /* start spike lasts 4 uS*/
        bitnot = 9; // number of bits allowed in signal
        do {
                dly1 = DELAY(TX_OHEAD);  /* wait one bit time */

                do
                        /* waiting in delay loop */ ;
                while(--dly1);
                if (bitnot==10) {
                        TxData = 0;
                        } else {
                if(a & 1)
                        TxData = 1;
                if(!(a & 1))
                        TxData = 0;
```

```
                    a = (a >> 1);
            }
            } while(--bitnot);
NOP();
}

void delay_ms(char x)
{
   //char variable
   char y, z;
   //Couple for loops to cause a specific delay.
   for ( ; x > 0 ; x--)
      for ( y = 0 ; y < 3 ; y++)
         for ( z = 0 ; z < 56 ; z++); //136
}
```

Figure 34. Microcontroller code for a PIC12F683. Functionality includes duty cycling under sleep mode, A/D conversion, and serial data communications with an RF transmitter.

APPENDIX C - SENSOR AND PRESSURE MEASUREMENTS

The properties of the model were observed during the silicone balloon experiments. When volume was controlled with a syringe pump at a rate of 30 µL/min, the dynamics of pressure were observed. Figure 35 may indicate observable compliance of the silicone balloon.

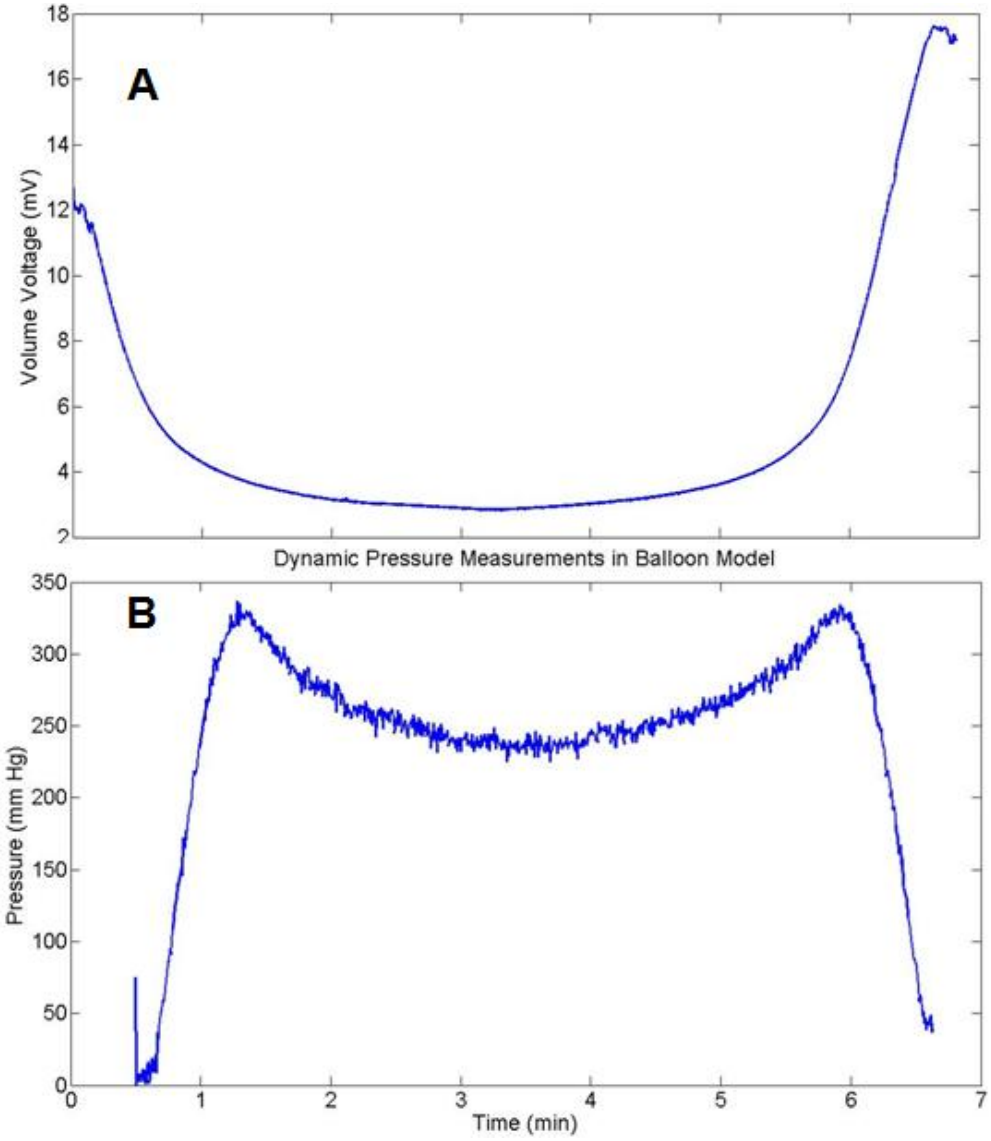

Figure 35. Dynamic voltage and pressure measurements with the silicone balloon model. The reduction in sensor voltage implies that volume increases. Pressure also increases albeit with a slight drop. These measurements may be an indication of dynamic compliance of the silicone wall boundary.

APPENDIX D - BENCH-TOP MEASUREMENT VARIABILITY

Additional experiments were performed using the rat-size sensor in the agarose bench-top model. The measured potential was higher in deeper cavities shown in frame A, which may be due to the overall salt content. Frame B shows that the salt content of the saline in the cavity matches that of rat CSF.

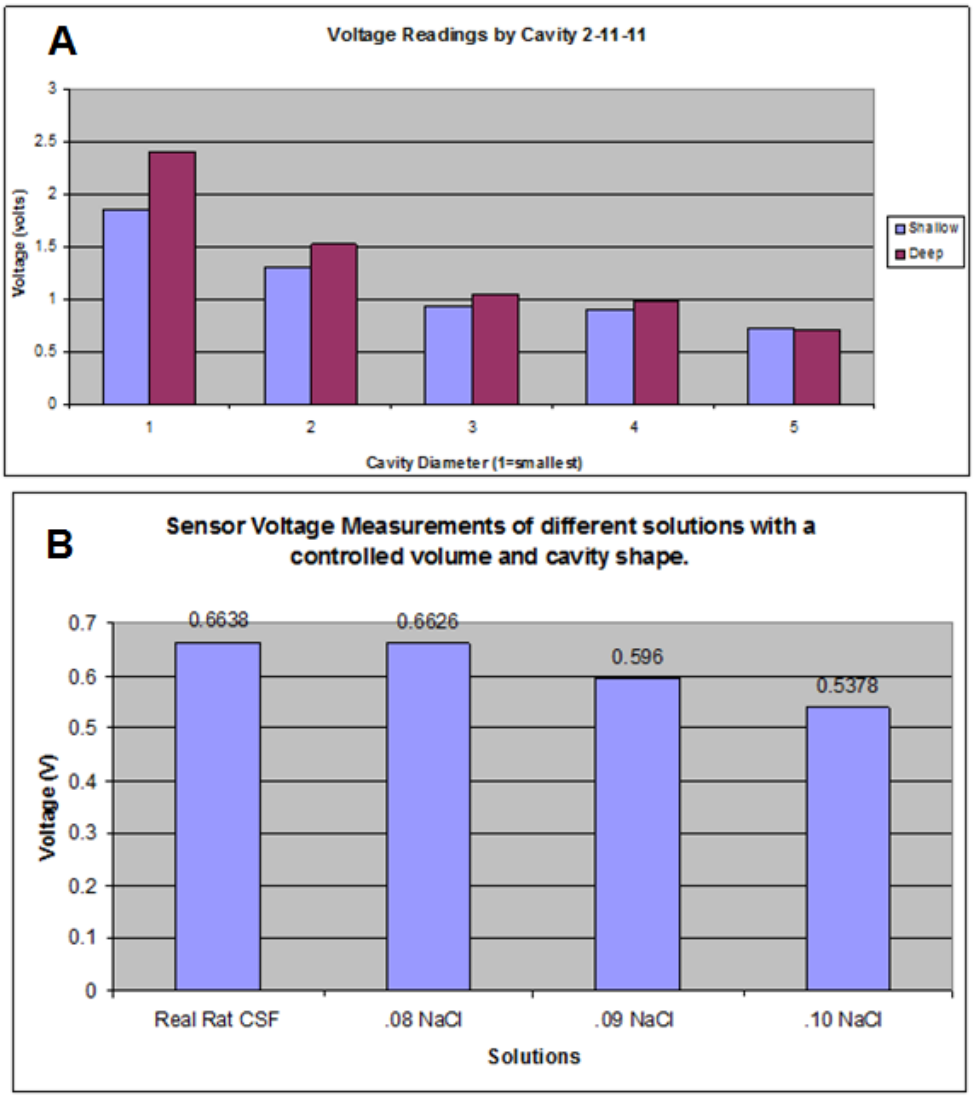

Figure 36. Agarose bench-top variability. Frame A shows measurements due to varying the depth of the cavity, while frame B compares salt content of saline compared to rat CSF.

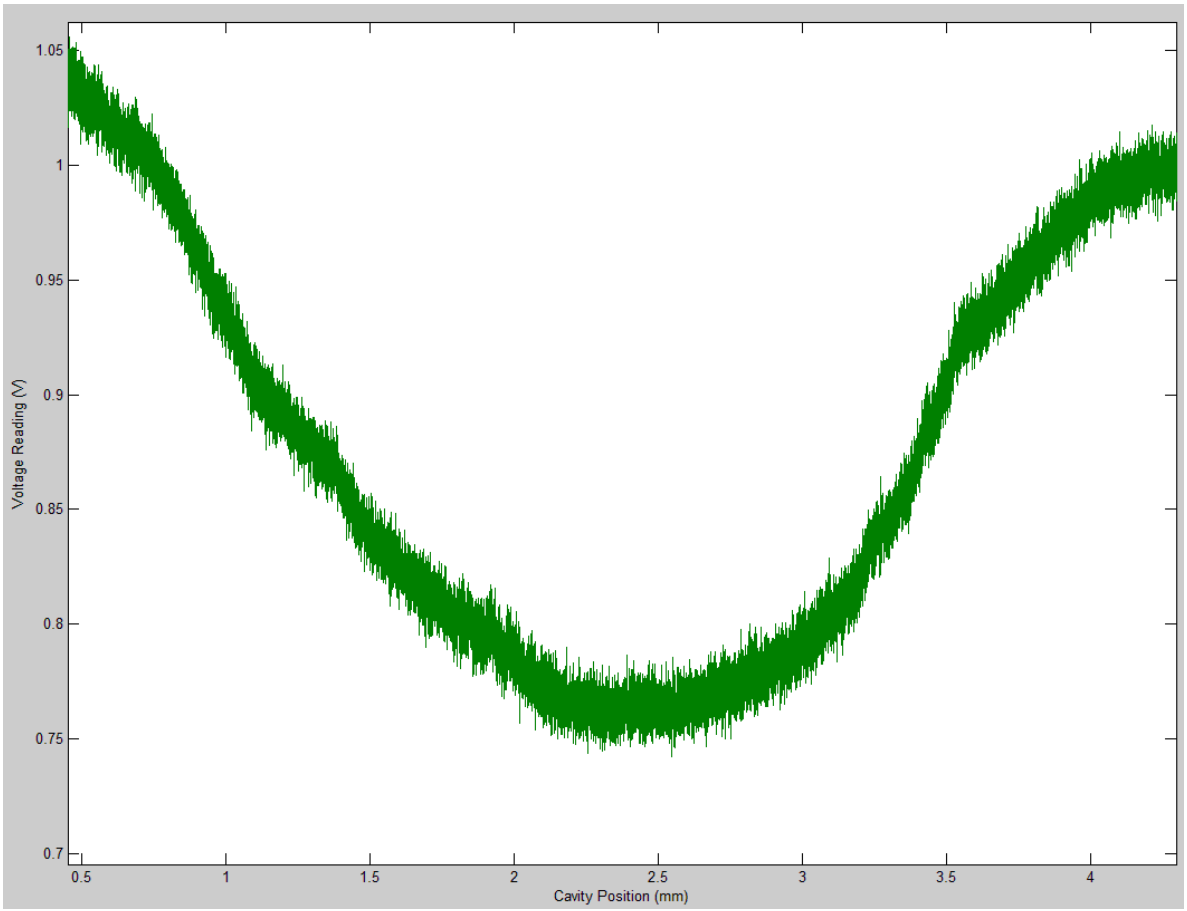

Figure 37. Positional dependence in agarose model. The sensor was placed near the wall and swept across. The lowest measurement occurs when the sensor is in the middle of the cavity. A 20% signal increase occurs as the sensor is moved closer to the boundary.

APPENDIX E - HYDROCEPHALIC RAT MEASUREMENT PROTOCOL

The purpose of this protocol was to test a novel volume sensor that measures the fluid volume within the brain. The first procedure was to induce hydrocephalus in the juvenile rats. On the day of the hydrocephalus induction, rats were anesthetized via isoflurane. A mask compatible with a stereotactic frame to continuously deliver the anesthetic was used. Once the animal was under deep anesthesia, up to 0.02 mL of a 25% w/v sterile kaolin suspension was prepared for injection. The injection was a percutaneous injection into the cisterna magna. The injection was quick and did not need additional surgery. The location was verified by observing a puncture of the atlanto-occipital membrane [124]. Once the injection was complete, the animal was allowed to wake from anesthesia. The animal will be monitored until fully recumbent.

Inspection for unusual behavior or lassitude, indicative of pain or intracranial pressure, was performed. Incisions were checked for bleeding or inflammation. The animals were inspected twice during the day immediately after surgery. They were weighed 3x weekly thereafter. For severely hydrocephalic animals, full inspection was made at least 3x weekly including weighings, to make sure they were still able to feed and drink adequately.

The second full surgery was performed two weeks after injection of kaolin. At 28 days after hydrocephalus induction, a sensor with an internal shunt to withdraw fluid was implanted. On the day of the experiment, rats were anesthetized deeply. Once under isoflurane induced deep anesthesia, a craniectomy was performed via stereotactic surgery. Superficial material was removed by scraping and/or wiping with a sterile Q-tip so that a dry cranial surface is obtained and landmarks (lambda etc) can be identified. Puncture of the dura was performed by puncture with a 27-gauge needle. Small volume of CSF leakage is typical in hydrocephalic rats.

Figure 38 shows an incision made in the hydrocephalic rat. The thin skull is easily identifiable. A burr hole was drilled to implant the sensor into the enlarged cerebral ventricles. Gap space was sealed using dental acrylic. Sequential shunting and infusing were performed to validate volume measurements. After the experiment was performed, the animal was sacrificed and the brain was fixed in formalin.

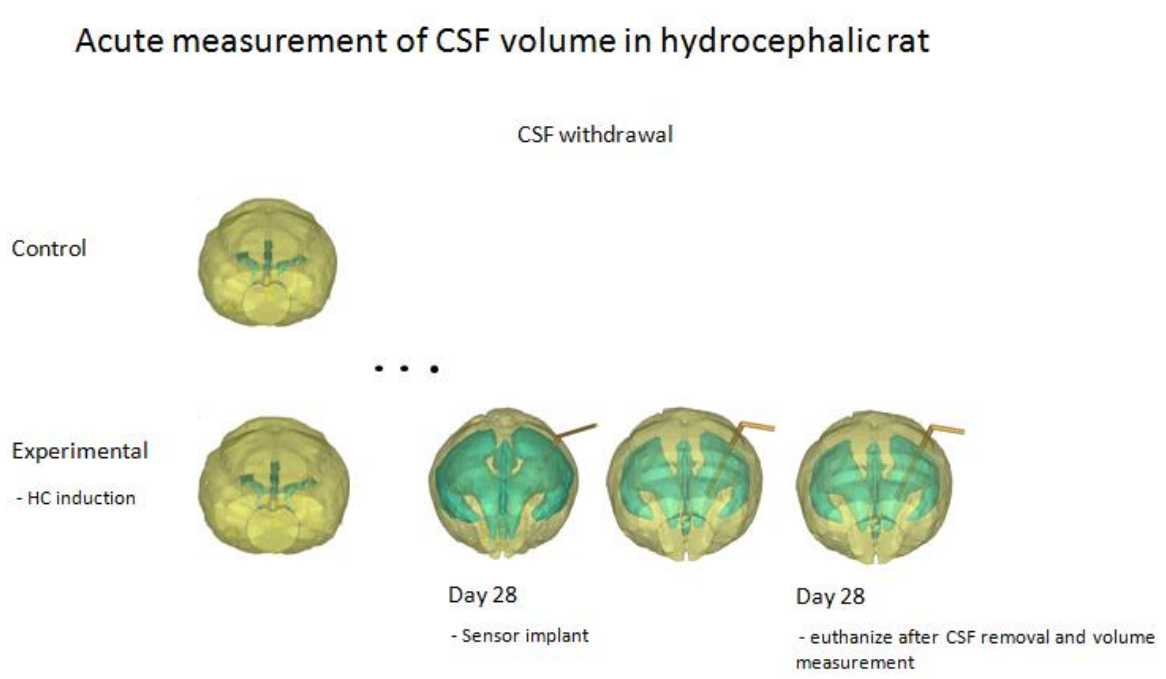

Figure 38. Surgical implantation of sensor in hydrocephalic rat. The protocol is illustrated on the left via three dimensional models.

APPENDIX F - MATLAB CODE TO GENERATE BLAND ALTMAN PLOT

```
%% Sukhi Basati Bland Altman Plot
% code modified from www.mathworks.com/matlabcentral 2011

 average_volu_t1=abs(average_vol_t1);
 volu_actual_t1=abs(vol_actual_t1);
 data=zeros(82,1); %first column of identifiers
 data (:, 2) = average_volu_t1; %second column of measured data
 data (:, 3) = volu_actual_t1; %third column of actual data

% Array funxy contains the Cartesian coordinates of Bland Altman function,

funxy(:,1) = (data(:,2) + data(:,3))/2;  %poin mean between two methods
funxy(:,2) = data (:,2) - data (:,3);    %point difference between two methods

disp ('Bland Altman Plot');

funxy(any(isnan(funxy),2),:) = [ ];

%Calculate mean of differences
diffmean = mean (funxy (:, 2))

%Calculate standard deviation of difference
sdev = std(funxy(:,2), 1);
twosdev = sdev * 1.96;

%Calculate max value of the mean
maxx = max (funxy (:, 1));

%Calculate max value of the difference
maxy = max (funxy (:, 2));

if (maxy < twosdev)
    maxy = twosdev;
end

%Add 1 sd to optimize graph
maxy = maxy + sdev;

%Min value of difference
miny = min (funxy (:, 2));

if (miny > -twosdev)
    miny = -twosdev;
end

%Subtract 1 sd to optimize graph
```

```
miny = miny - sdev;

% scatterplot of funxy
figure (1);
scatter (funxy(:,1), funxy(:,2));
axis ([0 maxx miny maxy]);
axis on;
hold on;

%Title and axis titles
title ('Bland-Altman plot');

xlabel ('Average');
ylabel ('Difference (Sensor Volume - Pump Controlled Volume)');

%Draw 2*sdev line
line ([0 maxx], [(twosdev+diffmean) (twosdev+diffmean)],'LineStyle','--');

line ([0 maxx], [(diffmean-twosdev) (diffmean-twosdev)], 'LineStyle','--');

%Draw line as mean of differences
line ([0 maxx], [diffmean diffmean],'LineStyle','-', 'LineWidth', 2);

%Add text 'mean'
text (maxx, diffmean, ' mean', 'Color', 'b' , 'FontSize', 14);% 'FontWeight',
'bold');

clear funxy miny maxy maxx twosdev;
```

Figure 39. MATLAB code to generate Bland-Altman plot for data analysus.

VITA

NAME:	Sukhraaj Basati
EDUCATION:	1. PhD candidate, Biomedical Engineering, University of Illinois at Chicago, August 2007 – current 2. BS, Biomedical Engineering, University of Illinois at Chicago, Awarded December 2005
AWARDS:	1. Student Presenter Award, Graduate College, 2010 2. Student Research Award, Honorable Mention, 2010 3. Student Research Award, 2nd place, 2009 4. Deiss Biomedical Endowment Award , Graduate College, 2008
PAPERS IN REFEREED JOURNALS:	1. S. Basati, B. Desai, A. Alaraj, F. Charbel, and A. Linninger. *Validation of cerebrospinal fluid volume sensors for hydrocephalus.* (in preparation) 2. R. Penn, S. Basati, B. Sweetman, X. Guo, and A. Linninger. *Ventricular wall movements and cerebrospinal fluid flow in hydrocephalus*. J. Neurosurgery. January 28, 2011. 3. S. Basati. T. Harris, A. Linninger. *Dynamic brain phantom for intracranial volume measurements*. IEEE Trans Biomed Engr., 58(5):1450-55, 2011. 4. Linninger, S. Basati, R. Dawe, R. Penn. *An impedance sensor to monitor and control cerebral ventricular volume*. Medical engineering & physics. 31(7):838-45, 2009. 5. F. Despa, S. Basati, Z. Zhang, J. D'Andrea, J. Reilly, E. Bodnar, R. Lee, *Electromuscular Incapacitation Results From Stimulation of Spinal Reflexes*. Bioelectromagnetics. 30(5):411-21, 2009. 6. F. Despa, S. Basati, X. Tang, R.C. Lee. *Uncoordinated Muscular Response to Microsecond Electrical Pulses is a Manifestation of Simulataneous Multiple Spinal Reflexes*. Molecular and Cellular Biomechanics. 3 (4): 193-194, 2006.
PROCEEDINGS PAPERS:	1. S. Basati, T. Harris, and A. Linninger, Optimal Sensor Design Using Subject Specific Images, *Proc. Of the 2010 Design of Medical Devices Conference*, Minneapolis MN, April13-15th 2010. 2. B. Sweetman, S. Basati, M. Iyer and Andreas A. Linninger. Modeling and design of distributed systems; methods and algorithms, *Proc. 10th International Symposium on Process Systems Engineering, PSE'09,* Salvador-Bahia-Brazil, August 16–20, 2009. 3. B. Sweetman, S. Basati, M. Iyer and A. Linninger. Mathematical Modeling-Knowledge Acquisition About Brain Physics. *Proc. 7th International Conference on Foundations of Computer-Aided Process Design*, pp 805-813, CRC Press, Taylor and Francis, 2009.
INVITED LECTURES:	1. Cerebrospinal Fluid Volume Monitoring for Hydrocephalus Therapy", Design of Medical Devices 2011 Conference, "*Advances in Imaging and Monitoring*", Minneapolis, MN, April 14th, 2011. 2. "An Implantable System for Intracranial Volume Measurements", *Neuroscience Brown Bag Meeting*, University of Illinois at Chicago, January 26th, 2011.

POSTER PRESENTATIONS:	1. S. Basati, B. Sweetman, J. Lancaster, and A. Linninger, *Intracranial Dynamics and its Role in Hydrocephalus Treatment*, Midwest Bioengineering Career Conference, April 1, 2011. 2. S. Basati, M. LaRiviere, R. Penn, and A. Linninger, *Cerebrospinal Fluid Volume Monitoring for Hydrocephalus Therapy",* Design of Medical Devices Conference, Minneapolist, MN, April 12-14th, 2011. 3. S. Basati, M. LaRiviere, T. Harris, R. Penn, and A. Linninger, *Development of Improved Treatment Options for Hydrocephalic Patients*, UIC Student Research Forum, Chicago, IL, April 20, 2010. 4. S. Basati, T. Harris, and A. Linninger, *Optimal Sensor Design Using Subject Specific Images*, Design of Medical Devices Conference, Minneapolis MN, April13-15th, 2010. 5. S. Basati, T. Harris, and A. Linninger, *Optimal Sensor Design and Fabrication*, UIC Student Research Forum, Chicago, IL, April 17, 2009. 6. B. Sweetman, S. Basati, M. Iyer and A. Linninger, *Modeling and Design of Distributed Systems; Methods and Algorithms*, Proc. 10th International Symposium on Process Systems Engineering, PSE'09, Salvador-Bahia-Brazil, August 16–20, 2009. 7. N. Sindhwani, O. Ivanchenko, B. Sweetman, S. Basati and A. Linninger. *Stress Analysis in Porous Media During Convection Enhanced Delivery*, 10th US National Congress on Computational Mechanics (USNCCM 2009), Columbus, OH, July 16, 2009. 8. S. Basati, B. Sweetman and A. Linninger, *An Impedance Sensor to Monitor Cerebral Ventricular Volume*, BMES 2008 Annual Fall Meeting, St. Louis, MO, October 2-4th, 2008. 9. A. Linninger, M.S. Iyer, S. Basati M.B. Somayiji, and A. Politis, *Computational Approach for Predicting Transport of Macromolecules in the Brain Interstitium*, Computational Biology Track, BMES 2008 Annual Fall Meeting, St. Louis, MO, October 2-4th, 2008. 10. A. Linninger, S. Basati and R. Penn, *A Novel Impedance Sensor to Monitor and Control Ventricular Size*, Hydrocephalus Congress 2008, Paper O.096, Hannover, Germany, September 17-20th, 2008. 11. S. Basati, M.S. Iyer, B. Sweetman, and A. Linninger, *An Impedance Sensor to Monitor Cerebral Ventricular Volume*, Student Poster Session; Poster 11, Midwest Biomedical Engineering Conference, Illinois Institute of Technology, Chicago, IL, April 4, 2008.
TEACHING EXPERIENCE:	1. Department of Biomedical Engineering, University of Illinois at Chicago, Illinois: Biological Systems Analysis, BioE 310, Fall 2008.